Journal of Theoretical Biology

A mathematical model of signalling molecule-mediated processes during regeneration of osteochondral defects after chondrocyte implantation

--Manuscript Draft--

Manuscript Number:	JTB-D-23-00814R1
Article Type:	Regular paper
Keywords:	osteochondral defect; cartilage defect; Mathematical modelling; reaction-diffusion model; endochondral ossification
Corresponding Author:	Jan-Herman Kuiper, MSc, PhD Keele University Oswestry, Shropshire UNITED KINGDOM
First Author:	Kelly Campbell, PhD
Order of Authors:	Kelly Campbell, PhD
	Shailesh Dr. Naire, PhD
	Jan-Herman Kuiper, MSc, PhD
Abstract:	Treating bone-cartilage defects is a fundamental clinical problem. The ability of damaged cartilage to self-repair is limited due to its avascularity. Left untreated, these defects can lead to osteoarthritis. Details of osteochondral defect repair are elusive, but animal models indicate healing occurs via an endochondral ossification-like process, similar to that in the growth plate. In the growth plate, the signalling molecules parathyroid hormone-related protein (PTHrP) and Indian Hedgehog (Ihh) form a feedback loop regulating chondrocyte hypertrophy, with Ihh inducing and PTHrP suppressing hypertrophy. To better understand this repair process and to explore the regulatory role of signalling molecules on the regeneration process, we formulate a mathematical model of osteochondral defect regeneration after chondrocyte implantation. The drivers of healing are assumed to be chondrocytes and osteoblasts, and their interaction via signalling molecules. We model cell proliferation, migration and chondrocyte hypertrophy, and matrix production and conversion, spatially and temporally. We further model nutrient and signalling molecule diffusion and their interaction with the cells. We consider the PTHrP-Ihh feedback loop as the backbone mechanisms but the model is flexible to incorporate extra signalling mechanisms if needed. Our mathematical model is able to represent repair of osteochondral defects, starting with cartilage formation throughout the defect. This is followed by chondrocyte hypertrophy, matrix calcification and bone formation deep inside the defect, while cartilage at the surface is maintained and eventually separated from the deeper bone by a thin layer of calcified cartilage. The complete process requires around 48 months. A key highlight of the model demonstrates that the PTHrP-Ihh loop alone is insufficient and an extra mechanism is required to initiate chondrocyte hypertrophy, represented by a critical cartilage density. A parameter sensitivity study reveals that the timing of the repair process crucially depends on parameters, such as the critical cartilage density, and those describing the actions of PTHrP to suppress hypertrophy, such as its diffusion coefficient, threshold concentration and degradation rate.
Response to Reviewers:	Reply to Reviewers We thank the reviewers for their careful reading of the manuscript and the insightful comments and suggestions they have provided. This has led to the manuscript being thoroughly revised both in the content and structure. The main revisions made are as follows. These are referred to by the corresponding section numbers and page numbers in the revised manuscript. 1. The Introduction (section 1) and Discussion (Section 5) are now more focused on the main goals and objectives of the paper based on the suggestions by Reviewer 1. 2. We have slightly modified the equation for the rate of change of hypertrophy-suppressing signalling molecule, gHS (Eq. 15). This is related to the production term (third term on the right-hand-side of Eq. 15)) which is proportional to the product of

gHM and CC. The explanation for this is provided below Eq. 15.

3. We have conducted a more extensive literature search on parameters related to the suppressing and modulating signalling molecules. This has resulted in small changes to the boundary and initial conditions (Sections 2.2 and 2.3), non-dimensionalization of gHM and gHS and dimensionless equation (Section 3) and related dimensional and dimensionless parameters in Tables 1 and 2, respectively. These changes are highlighted in yellow in the corresponding text.

4. We have revised Section 4.2 – Sensitivity of parameters by adding plots that gives a quantitative measure of model sensitivity related to the biologically important parameters as well as some of the “guessed” parameters. We have removed Table 3 and embedded the results and explanations within the text in Section 4.2.

5. We have improved the quality of all the figures in the manuscript and provided requested details in the captions.

6. We have revised the Discussion such that we clearly address the main aim and two specific questions.

We now provide replies to each of the reviewer’s comments.

Reply to Reviewer 1

1. My only concern about this work is that the mathematical formulation is mainly based on reaction-diffusion equations. Therefore, the solution of these equations are normally mesh dependent. Have the authors performed some analysis of the effect of the mesh size?

Reply: Yes, we have performed a formal error and convergence analysis based on reducing the mesh size systematically and measuring the error in the solution. We do not show the formal analysis here as the focus is more on the biology. However, we have added a paragraph at the beginning of Section 3.1 – Implementation and simulated case, explaining this.

2. I think initial and boundary conditions should be represented in one figure, or even it could be included in figure 2b.
Reply: We think this is going to be very difficult to represent in one figure which would make it too crowded and difficult to synthesize. We have decided to keep as it is in Sections 2.2 and 2.3.

Reply to Reviewer 2

Thank you once again for your helpful and extensive comments. We have grouped the points 1.1 to 1.4 in our response.

1.It was not clear exactly what the authors main objectives were with this paper.

1.1In the introduction the author stated they were using the model to address 2 questions: ‘(a) How does the PTHrP-Ihh feedback loop control endochondral ossification in the healing process, and (b) Which key parameters most influence the healing process, controlling the thickness of the articular cartilage in the repaired defect?’.
However, both of these aims had only the briefest mentions in the discussion, so I am not sure if these were in fact the aim?

1.2The beginning of the discussion implied the aim was to produce a model that was comparable to animal experiments from Lydon et al.? If this is the goal of the model, rather than the questions mentioned in 1.1), it needs to be stated early on in the paper, and a more explicit comparison of the model to the animal results (either quantitative or qualitative) is required in both results and discussion.
Summarize 1.1 and 1.2, I would suggest that the authors provide a discussion that explicitly addresses the aims of the paper that they have stated in the introduction, whether these be one the two aims listed above or otherwise.

1.3As detailed in 1.1 it is not fully clear to me what the aims and hence the conclusion of this study is. It is essential that this is clarified in the manuscript.

1.4Related to 1.2), at the beginning of the discussion the authors state they use extensive insights from an animal model from Lydon et al. However minimal comparison is made between the data/results from that paper and the model to support model results. If it is purely a qualitative comparison the authors need to make this clear and more comprehensive, otherwise the comparison data should be included in the results and an interpretation of the comparison between the model and the data should be added to the discussion. If the animal model was used primarily in model development this needs to be made clearer in the model formulation. In this case, I would also question that there were no parameters derived from the animal model? if there is quantitative data available from the animal model in Lydon et al, this paper would benefit from a comprehensive comparison to the data. This would also help justify the parameters used and add credibility to the model results.

Reply: Re-reading the Introduction and Discussion in light of your comments 1.1-1.4, we entirely agree, to the point where we ask ourselves why we hadn't noticed this ourselves. As indicated in the Introduction, our starting point was the suggestion from animal experiments (including those by Lydon et al.) that healing of osteochondral defects seems to recapitulate processes that occur in the growth plate. Our main aim was therefore indeed to address the two questions you also noted in the Introduction, namely:
(a) How does the PTHrP-Ihh feedback loop control endochondral ossification in the healing process, and (b) Which key parameters most influence the healing process, controlling the thickness of the articular cartilage in the repaired defect?
We did have access to more data from Lydon et al. and wanted to make an extensive quantitative comparison, but we never got to a position we could do this. An important reason for this is that assessing PTHrP gene expression levels in tissue is very difficult because the levels are so low. Current knowledge around the PTHrP-Ihh loop comes from genetically engineered mouse lines that use a reporter construct to show these levels. Whereas this is relatively straightforward with mice, doing this in a large animal model is currently not possible. However, since a mouse is so much smaller than a human, one important question is whether the PTHrP-Ihh loop can even work on the scale of an adult human. Knowing that in principle it can work would give a motivation to perform targeted experiments or use novel spatial transcriptomics techniques such as single-molecule fluorescence in situ hybridization (smFISH) that can assess low-level expression levels. Therefore, a better pair of questions is:
(a) Can the PTHrP-Ihh feedback loop control endochondral ossification in the healing process, and (b) Which key parameters most influence the healing process, in particular controlling the thickness of the articular cartilage in the repaired defect?
We have now amended these questions in the Introduction, and explicitly answer them in the Discussion. The answer to our second question about the key parameters is now more extensive in response to your comment 1.9 below. We have removed the sentence in the Discussion referring to an extensive comparison with the sheep model from Lydon et al.

1.5The discussion provides a comprehensive description of results and limitations, but I found it lacking in interpretation of the results. The discussion would benefit for some from some further interpretation of the implications of the model results on the disease and treatment modelled.

Reply: Thank you for your suggestion. As we explain above, an important question is whether the feedback loop can work at all on the human scale. We have now amended the discussion to include this, and provide some implications for further research.

1.6If one of the main goals is the addition of the PTHrP-Ihh feedback loop control in the model, the discussion could benefit from a more concise statement of the advantages of the addition of the feedback loop in relation to the results shown including the feedback loop compared to previous results without this feedback loop.

Reply: As explained above, the aim was not so much to implement the feedback loop, but rather to find if it might work on the scale of a large animal. We think we have

answered this affirmatively, so the next step would be to follow the suggestions that you asked for under 1.5 above and 1.7 below.

1.7The authors have addressed the limitations of the model in relation to simplification of the biology. However, the manuscript could benefit from some discussion on the limitations of the model from a mathematical perspective, namely parameter identification.

Reply: The reviewer is right: our model is probably too simplified to try a best fit to an experiment. As we explain above, this was our initial plan, but we quickly realised we did not know enough about the basic building blocks of a suitable model. We therefore decided to start simple and explore whether the PTHrP-Ihh feedback loop could play a role in endochondral defect healing. We think we are now at a stage where a geometrically more realistic model could be made and fitted to experiments – perhaps starting modestly with a rodent model. We have now added some discussion in the limitations of our model in this sense.

1.8I found most of the manuscript to be well structured, but the discussion could be more concise. This may improve with clarification of the aims of the paper, potentially using subheadings in the discussion section to make it clearer, and some editing of text to clarify the message of each paragraph.

Reply: We have tried to do what you suggested, hopefully we have managed.

1.9The second concern was related to parameterization of the model. A large number of the parameters used in the model were listed as a 'guess'. Note, this is not in and of itself a major issue, I appreciate that it is difficult to find sufficient data to parameterize such a model, my concern is that this was not addressed in the manuscript and no analysis was presented on the sensitivity of the results due to these parameter guesses. Consequently, it is difficult to know how credible the results presented are. Though some sensitivity analysis was performed, it was presented from a biological standpoint and did not directly address the issue of unknown parameters. I would recommend a formal analysis to investigate the sensitivity of the model, and consequently the results presented in this paper, to the unknown parameters in particular.

Reply: Section 4.2 has now been revised to include a sensitivity analysis of both the biologically important parameters as well as some of the “guessed” parameters. This comment also prompted us to re-check the literature hoping to reduce the number of guessed parameters, which we managed. The additional references (and adjusted values) are indicated in Table 1.

Minor
1.1.The authors have provided all equations and parameters needed to reproduce the model. However, I would strongly suggest the authors provide their model code alongside the paper (see research data section of the authors guide for the journal).

Reply: Thank you for this very good suggestion. We will provide the MATLAB codes for the model with appropriate documentation.

1.2.Figure 1: needs more detail in the caption, such as supplying the colour scheme for the cells in the diagram and an explanation of what the arrows indicate.

Reply: Our apologies, we should have done this in the first place. We have now modified the caption to explain the meaning of the colours and arrows.

1.3.Figure 3: diagram would benefit from changing some of the fill colours, it is difficult to see the black text on the blue and brown background. Additionally, the text and next to the arrows was quite low resolution in my version of the manuscript.

Reply: This has been done now.

1.4.The manuscript could benefit from a diagram of the spatial dynamics of the system in addition to the signalling interactions shown in Figure 3.

	Reply: We hope that our improved Figure 3, in combination with Fig. 1, addresses this comment. 1.5.Figures 4-9: please use colours that are easier to see against a white background and also consider a different aspect ratio to widen plots. Reply: We have now improved the quality of all the figures in the manuscript. 1.6.Figures 5-9: please put the legend in each figure for which the colour scheme is used. Reply: This has been done now. 1.7.Table 1: consider putting references/justifications of parameters values in a third column. Also note error in cite command for p8. Reply: We have tried this but the columns become too wide and difficult to format. We have decided to keep it as it is. We thank the reviewer for pointing out this error which has been corrected along with a few other typos. 1.8.Table 3: rather than presenting these results as a table containing paragraphs of text, I would consider the use of symbols or numbers in a table, or plots. Note, this relates to my comments on the sensitivity analysis which may result in modifications to this table. I would strongly recommend adding a plot that gives some quantitative measure of model sensitivity to enable readers to easily interpret these results. Reply: We have now removed Table 3 and embedded within the text in Section 4.2. We have also added plots to give some quantitative measure of all the model parameters, where possible. 1.9.I would consider mentioning the specific modelling approach taken in the abstract and possibly also in keywords. Reply: Definitely a good idea, we have now added reaction-diffusion to the abstract and keywords. 1.10.I found the equations to have bad readability, specifically equations 2, 3, 5, 7, 20 and 22. I believe this is related to placing multiple equations next to each other on one line. Potentially also excessive use of intermediate functions, such that many functions required combinations of multiple equations (e.g. I think the formula for dC_C required putting together 5 equations), which made it difficult to understand the model formulation. Reply: Unfortunately, we cannot think of any better way to formulate the equations. As for readability, our reasons to place multiple equations on a single line was to save space and facilitate getting an overview. We have now tried to improve readability by (1) increasing the line spacing between subsequent lines, and (2) using a “long space” between each equation instead of a comma. These two changes improve the separation between neighbouring equations and hopefully improves readability.

Dr. Akira Sasaki
Co-Chief Editor
Journal of Theoretical Biology

Oswestry, 12 April 2024

Dear Dr Asaki

Re: Revision of JTB-D-23-00814 (A mathematical model of signalling molecule-mediated processes during regeneration of osteochondral defects after chondrocyte implantation)

Please find enclosed the revised version of our manuscript, plus our responses to the reviewers' comments. We would like to thank you again for the opportunity to revise our manuscript, the extra time you gave us, and hope this version addresses the reviewers' concerns.

With kind regards, Jan Herman Kuiper

This piece of the submission is being sent via mail.

Reply to Reviewers

We thank the reviewers for their careful reading of the manuscript and the insightful comments and suggestions they have provided. This has led to the manuscript being thoroughly revised both in the content and structure. The main revisions made are as follows. These are referred to by the corresponding section numbers and page numbers in the revised manuscript.

1. The Introduction (section 1) and Discussion (Section 5) are now more focused on the main goals and objectives of the paper based on the suggestions by Reviewer 1.

2. We have slightly modified the equation for the rate of change of hypertrophy-suppressing signalling molecule, g_{HS} (Eq. 15). This is related to the production term (third term on the right-hand-side of Eq. 15)) which is proportional to the product of g_{HM} and C_C. The explanation for this is provided below Eq. 15.

3. We have conducted a more extensive literature search on parameters related to the suppressing and modulating signalling molecules. This has resulted in small changes to the boundary and initial conditions (Sections 2.2 and 2.3), non-dimensionalization of g_{HM} and g_{HS} and dimensionless equation (Section 3) and related dimensional and dimensionless parameters in Tables 1 and 2, respectively. These changes are highlighted in yellow in the corresponding text.

4. We have revised *Section 4.2 – Sensitivity of parameters* by adding plots that gives a quantitative measure of model sensitivity related to the biologically important parameters as well as some of the "guessed" parameters. We have removed Table 3 and embedded the results and explanations within the text in Section 4.2.

5. We have improved the quality of all the figures in the manuscript and provided requested details in the captions.

6. We have revised the Discussion such that we clearly address the main aim and two specific questions.

We now provide replies to each of the reviewer's comments.

Reply to Reviewer 1

1. *My only concern about this work is that the mathematical formulation is mainly based on reaction-diffusion equations. Therefore, the solution of these equations are normally mesh dependent. Have the authors performed some analysis of the effect of the mesh size?*

Reply: Yes, we have performed a formal error and convergence analysis based on reducing the mesh size systematically and measuring the error in the solution. We do not show the formal analysis here as the focus is more on the biology. However, we have added a paragraph at the beginning of *Section 3.1 – Implementation and simulated case*, explaining this.

2. *I think initial and boundary conditions should be represented in one figure, or even it could be included in figure 2b.*

Reply: We think this is going to be very difficult to represent in one figure which would make it too crowded and difficult to synthesize. We have decided to keep as it is in Sections 2.2 and 2.3.

Reply to Reviewer 2

Thank you once again for your helpful and extensive comments. We have grouped the points 1.1 to 1.4 in our response.

1. *It was not clear exactly what the authors main objectives were with this paper.*
   1.1 In the introduction the author stated they were using the model to address 2 questions: '(a) How does the PTHrP-Ihh feedback loop control endochondral ossification in the healing process, and (b) Which key parameters most influence the healing process, controlling the thickness of the articular cartilage in the repaired defect?'.
   However, both of these aims had only the briefest mentions in the discussion, so I am not sure if these were in fact the aim?

   1.2 The beginning of the discussion implied the aim was to produce a model that was comparable to animal experiments from Lydon et al.? If this is the goal of the model, rather than the questions mentioned in 1.1), it needs to be stated early on in the paper, and a more explicit comparison of the model to the animal results (either quantitative or qualitative) is required in both results and discussion.

Summarize 1.1 and 1.2, I would suggest that the authors provide a discussion that explicitly addresses the aims of the paper that they have stated in the introduction, whether these be one the two aims listed above or otherwise.

   1.3 As detailed in 1.1 it is not fully clear to me what the aims and hence the conclusion of this study is. It is essential that this is clarified in the manuscript.

   1.4 Related to 1.2), at the beginning of the discussion the authors state they use extensive insights from an animal model from Lydon et al. However minimal comparison is made between the data/results from that paper and the model to support model results. If it is purely a qualitative comparison the authors need to make this clear and more comprehensive, otherwise the comparison data should be included in the results and an interpretation of the comparison between the model and the data should be added to the discussion. If the animal model was used primarily in model development this needs to be made clearer in the model formulation. In this case, I would also question that there were no parameters derived from the animal model? if there is quantitative data available from the animal model in Lydon et al, this paper would benefit from a comprehensive comparison to the data. This would also help justify the parameters used and add credibility to the model results.

Reply: Re-reading the Introduction and Discussion in light of your comments 1.1-1.4, we entirely agree, to the point where we ask ourselves why we hadn't noticed this ourselves. As indicated in the Introduction, our starting point was the suggestion from animal experiments (including those by Lydon et al.) that healing of osteochondral defects seems to recapitulate processes that occur in the growth plate. Our main aim was therefore indeed to address the two questions you also noted in the Introduction, namely:

(a) How does the PTHrP-Ihh feedback loop control endochondral ossification in the healing process, and (b) Which key parameters most influence the healing process, controlling the thickness of the articular cartilage in the repaired defect?

We did have access to more data from Lydon et al. and wanted to make an extensive quantitative comparison, but we never got to a position we could do this. An important reason for this is that assessing PTHrP gene expression levels in tissue is very difficult because the levels are so low. Current knowledge around the PTHrP-Ihh loop comes from genetically engineered mouse lines that use a reporter construct to show these levels. Whereas this is relatively straightforward with mice, doing this in a large animal model is currently not possible. However, since a mouse is so much smaller than a human, one important question is whether the PTHrP-Ihh loop can even work on the scale of an adult human. Knowing that in principle it can work would give a motivation to perform targeted experiments or use novel spatial transcriptomics techniques such as single-molecule fluorescence in situ hybridization (smFISH) that can assess low-level expression levels. Therefore, a better pair of questions is:

(a) Can the PTHrP-Ihh feedback loop control endochondral ossification in the healing process, and (b) Which key parameters most influence the healing process, in particular controlling the thickness of the articular cartilage in the repaired defect?

We have now amended these questions in the Introduction, and explicitly answer them in the Discussion. The answer to our second question about the key parameters is now more extensive in response to your comment 1.9 below. We have removed the sentence in the Discussion referring to an extensive comparison with the sheep model from Lydon et al.

1.5 The discussion provides a comprehensive description of results and limitations, but I found it lacking in interpretation of the results. The discussion would benefit for some from some further interpretation of the implications of the model results on the disease and treatment modelled.

Reply: Thank you for your suggestion. As we explain above, an important question is whether the feedback loop can work at all on the human scale. We have now amended the discussion to include this, and provide some implications for further research.

1.6 If one of the main goals is the addition of the PTHrP-Ihh feedback loop control in the model, the discussion could benefit from a more concise statement of the advantages of the addition of the feedback loop in relation to the results shown including the feedback loop compared to previous results without this feedback loop.

Reply: As explained above, the aim was not so much to implement the feedback loop, but rather to find if it might work on the scale of a large animal. We think we have answered this affirmatively, so the next step would be to follow the suggestions that you asked for under 1.5 above and 1.7 below.

1.7 The authors have addressed the limitations of the model in relation to simplification of the biology. However, the manuscript could benefit from some discussion on the

limitations of the model from a mathematical perspective, namely parameter identification.

Reply: The reviewer is right: our model is probably too simplified to try a best fit to an experiment. As we explain above, this was our initial plan, but we quickly realised we did not know enough about the basic building blocks of a suitable model. We therefore decided to start simple and explore whether the PTHrP-Ihh feedback loop could play a role in endochondral defect healing. We think we are now at a stage where a geometrically more realistic model could be made and fitted to experiments – perhaps starting modestly with a rodent model. We have now added some discussion in the limitations of our model in this sense.

1.8 I found most of the manuscript to be well structured, but the discussion could be more concise. This may improve with clarification of the aims of the paper, potentially using subheadings in the discussion section to make it clearer, and some editing of text to clarify the message of each paragraph.

Reply: We have tried to do what you suggested, hopefully we have managed.

1.9 The second concern was related to parameterization of the model. A large number of the parameters used in the model were listed as a 'guess'. Note, this is not in and of itself a major issue, I appreciate that it is difficult to find sufficient data to parameterize such a model, my concern is that this was not addressed in the manuscript and no analysis was presented on the sensitivity of the results due to these parameter guesses. Consequently, it is difficult to know how credible the results presented are. Though some sensitivity analysis was performed, it was presented from a biological standpoint and did not directly address the issue of unknown parameters. I would recommend a formal analysis to investigate the sensitivity of the model, and consequently the results presented in this paper, to the unknown parameters in particular.

Reply: Section 4.2 has now been revised to include a sensitivity analysis of both the biologically important parameters as well as some of the “guessed” parameters. This comment also prompted us to re-check the literature hoping to reduce the number of guessed parameters, which we managed. The additional references (and adjusted values) are indicated in Table 1.

Minor

1.1. The authors have provided all equations and parameters needed to reproduce the model. However, I would strongly suggest the authors provide their model code alongside the paper (see research data section of the authors guide for the journal).

Reply: Thank you for this very good suggestion. We will provide the MATLAB codes for the model with appropriate documentation.

1.2. Figure 1: needs more detail in the caption, such as supplying the colour scheme for the cells in the diagram and an explanation of what the arrows indicate.

Reply: Our apologies, we should have done this in the first place. We have now modified the caption to explain the meaning of the colours and arrows.

1.3. *Figure 3: diagram would benefit from changing some of the fill colours, it is difficult to see the black text on the blue and brown background. Additionally, the text and next to the arrows was quite low resolution in my version of the manuscript.*
Reply: This has been done now.

1.4. *The manuscript could benefit from a diagram of the spatial dynamics of the system in addition to the signalling interactions shown in Figure 3.*

We hope that our improved Figure 3, in combination with Fig. 1, addresses this comment.

1.5. *Figures 4-9: please use colours that are easier to see against a white background and also consider a different aspect ratio to widen plots.*

Reply: We have now improved the quality of all the figures in the manuscript.

1.6. *Figures 5-9: please put the legend in each figure for which the colour scheme is used.*

Reply: This has been done now.

1.7. *Table 1: consider putting references/justifications of parameters values in a third column. Also note error in cite command for p8.*

Reply: We have tried this but the columns become too wide and difficult to format. We have decided to keep it as it is. We thank the reviewer for pointing out this error which has been corrected along with a few other typos.

1.8. *Table 3: rather than presenting these results as a table containing paragraphs of text, I would consider the use of symbols or numbers in a table, or plots. Note, this relates to my comments on the sensitivity analysis which may result in modifications to this table. I would strongly recommend adding a plot that gives some quantitative measure of model sensitivity to enable readers to easily interpret these results.*

Reply: We have now removed Table 3 and embedded within the text in Section 4.2. We have also added plots to give some quantitative measure of all the model parameters, where possible.

1.9. *I would consider mentioning the specific modelling approach taken in the abstract and possibly also in keywords.*

Reply: Definitely a good idea, we have now added reaction-diffusion to the abstract and keywords.

1.10. *I found the equations to have bad readability, specifically equations 2, 3, 5, 7, 20 and 22. I believe this is related to placing multiple equations next to each other on one line. Potentially also excessive use of intermediate functions, such that many*

functions required combinations of multiple equations (e.g. I think the formula for dC_C required putting together 5 equations), which made it difficult to understand the model formulation.

Reply: Unfortunately, we cannot think of any better way to formulate the equations. As for readability, our reasons to place multiple equations on a single line was to save space and facilitate getting an overview. We have now tried to improve readability by (1) increasing the line spacing between subsequent lines, and (2) using a “long space” between each equation instead of a comma. These two changes improve the separation between neighbouring equations and hopefully improves readability.

A mathematical model of signalling molecule-mediated processes during regeneration of osteochondral defects after chondrocyte implantation

Kelly Campbell[a], Shailesh Naire[a], Jan-Herman Kuiper[b,c,*]

[a] *School of Computing and Mathematics, Keele University, Keele, ST5 5BG, U.K.*

[b] *School of Pharmacy and Bioengineering, Keele University, Keele, ST5 5BG, U.K.*

[c] *Robert Jones and Agnes Hunt Orthopaedic & District Hospital NHS Trust, Oswestry, SY10 7AG, U.K.*

Abstract

Treating bone-cartilage defects is a fundamental clinical problem. The ability of damaged cartilage to self-repair is limited due to its avascularity. Left untreated, these defects can lead to osteoarthritis. Details of osteochondral defect repair are elusive, but animal models indicate healing occurs via an endochondral ossification-like process, similar to that in the growth plate. In the growth plate, the signalling molecules parathyroid hormone-related protein (PTHrP) and Indian Hedgehog (Ihh) form a feedback loop regulating chondrocyte hypertrophy, with Ihh inducing and PTHrP suppressing hypertrophy. To better understand this repair process and to explore the regulatory role of signalling molecules on the regeneration process, we formulate a reaction-diffusion mathematical model of osteochondral defect regeneration after chondrocyte implantation. The drivers of healing are assumed to be chondrocytes and osteoblasts, and their interaction via signalling molecules. We model cell proliferation, migration and chondrocyte hypertrophy, and matrix production and conversion, spatially and temporally. We further model nutrient and signalling molecule diffusion and their interaction with the cells. We consider the PTHrP-Ihh feedback loop as the backbone mechanisms but the model is flexible to incorporate extra signalling mechanisms if needed. Our mathematical model is able to represent repair of osteochondral defects, starting with cartilage formation throughout the defect. This is followed by chondrocyte hypertrophy, matrix calcification and bone formation deep inside the defect, while cartilage at the surface is maintained and eventually separated from the deeper bone by a thin layer of calcified cartilage. The complete process requires around 48 months. A key highlight of the model demonstrates that the PTHrP-Ihh loop alone is insufficient and an extra mechanism is required to initiate chondrocyte hypertrophy, represented by a critical cartilage density. A parameter sensitivity study reveals that the timing of the repair process crucially depends on parameters, such as the critical cartilage density, and those describing the actions of PTHrP to suppress hypertrophy, such as its diffusion coefficient, threshold concentration and degradation rate.

Keywords: osteochondral defect, cartilage defect, mathematical modelling, reaction-diffusion model, endochondral ossification

*Corresponding author: School of Pharmacy and Bioengineering, Keele University, email:j.h.kuiper@keele.ac.uk

1. Introduction

Chondral and osteochondral defects are both a cause and result of osteoarthritis, a degenerative condition that causes the joints to become painful and stiff, primarily in patients over 50 years old (Falah et al. (2010); Moyad (2011); Allen et al. (2022)). Osteochondral defects of the knee can occur through acute trauma, natural wear and tear of the joint, and underlying disease of the bone (Madry et al. (2010); Williams et al. (1998)). General understanding of osteochondral defect healing has clinical significance, but little experimental data in humans is available and reliable treatment strategies are lacking. Once a joint with an osteochondral defect is osteoarthritic, repair is problematic and treatment options are limited (Gomoll et al. (2012)). Some treatment options for osteochondral defects include autologous chondrocyte implantation (ACI), osteochondral autograft transfer (OAT), osteochondral allograft transplantation surgery (OATS) and microfracture (Brittberg (2008); Dahmen et al. (2018); de Windt and Saris (2014)). Of these, ACI and the two graft procedures are able to achieve the hyaline-type cartilage needed for long-term clinical benefit and are the treatments most used in clinical practice, with ACI determined to be an effective treatment strategy (Biant et al. (2014); Brittberg (2008); De Bari and Roelofs (2018)). ACI is a two-stage surgical procedure: in stage one healthy chondrocytes (cartilage cells) are harvested from a non-weight-bearing area of the joint, to be cultured to appropriate cell numbers. Approximately two weeks later, in a second procedure, these cells are implanted into the chondral or osteochondral defect and sealed with a periosteal patch or collagen membrane, or alternatively seeded first in a biodegradable scaffold which is then placed in the defect (Brittberg (2008)). Long-term outcomes of this procedure are very good, with ACI not only the gold standard treatment for chondral defects, but also showing good outcomes in osteochondral lesions of the knee (Biant et al. (2014)).

Natural osteochondral defect healing can occur spontaneously but the underlying mechanism driving tissue regeneration is elusive. The quality of naturally regenerated tissue is unpredictable and can often be primarily fibrous, resulting in subsequent degradation. When an osteochondral defect forms, damaged blood vessels located within bone at the site of the defect produce blood which coagulates and forms a fibrous clot. Within this clot there are thought to be cartilage and bone precursors, such as mesenchymal stem cells (MSCs), along with a fibrin net that acts as a scaffold for cells to travel along (Madry et al. (2010)). The precursor cells are thought to move into the defect and differentiate into chondrocytes, fibroblasts or osteoblasts, which synthesize new tissue from the base of the defect. The tissue resulting from natural healing is generally of poor quality overall: although the defect may fill it is typically with fibro-cartilaginous tissue which is not the hyaline-type needed for long-term withstanding of the compressive forces across weight-bearing joints (Guo et al. (2004); Jackson et al. (2001)). Generally, this fibro-cartilage tissue will degrade and the original symptoms of pain and discomfort will return, putting the patient at increased risk of developing osteoarthritis (Wakitani et al. (1994)).

Lydon et al. (2019), using an ovine model, demonstrated that healing of osteochondral defects in large mammals involves endochondral ossification. They showed that healing begins with cartilage formation first occurring along the edges of the defect, filling from the sides inwards and upwards until the defect fills and forms a cartilage model. Once this process has completed, chondrocytes undergo hypertrophy and ossification takes place, with a layer of cartilage remaining along the articular surface of the defect. Other earlier studies using smaller mammals found a similar healing mechanism, such as those using the Göttingen minipig (GMP) model that show defects located in

the trochlear groove of the knee heal via endochondral ossification (Gotterbarm et al. (2008); Jung et al. (2009)). Shapiro et al. (1993) also observed an endochondral sequence starting from the base of osteochondral defects in rabbit models.

The occurrence of endochondral ossification during healing of osteochondral defects suggests that the process may be similar to processes in the growth plate (Mariani et al. (2014)). In the growth plate, the signalling molecules parathyroid hormone-related protein (PTHrP) and Indian Hedgehog (Ihh) form a negative feedback loop regulating chondrocyte hypertrophy, with Ihh produced by pre- and early-hypertrophic chondrocytes stimulating production of PTHrP, which in its turn suppresses chondrocyte hypertrophy (Figure 1; Kronenberg (2003); Mariani et al. (2014)). Indian hedgehog (Ihh) stimulates chondrocyte proliferation, along with chondrocyte and osteoblast differentiation

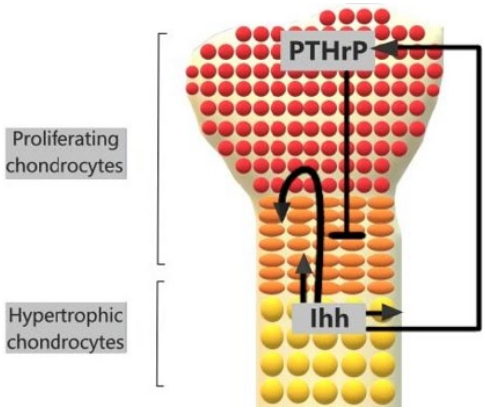

Figure 1: Schematic of the PTHrP-Ihh feedback loop that occurs during endochondral ossification. Adapted from Kronenberg (2003). Red circles represent proliferating chondrocytes, orange ovals pre-hypertrophic chondrocytes and yellow circles hypertrophic chondrocytes. Lines ending with an arrow head indicate stimulation, lines ending with a horizontal line indicate suppression.

(Kronenberg (2003)). Indian hedgehog is secreted when chondrocytes are exiting their proliferative state to undergo hypertrophy, whereas parathyroid hormone-related protein (PTHrP) is secreted by proliferating chondrocytes in the growth plate and surface zone chondrocytes in articular cartilage, the latter under the influence of mechanical loading (Jiang et al. (2008); Zhang et al. (2012)). PTHrP keeps chondrocytes in their proliferative state, inhibiting chondrocyte hypertrophy and therefore production of Ihh, thus forming a negative feedback loop (Kronenberg (2003); Zhang et al. (2012)).

Various authors have reported the need for an additional local or external signaling molecule for chondrocytes to progress from proliferative to hypertrophic state, thereby initiating the endochondral ossification process. Kerkhofs et al. (2012) explore the chondrocyte gene network controlling endochondral ossification in the growth plate, and identify a self-regulated sequential process that does however need external switching of PTHrP and Ihh levels to initiate state transitions, including that from proliferation to hypertrophy. The additional signaling molecule could be a systemic factor, such as thyroid hormone (TH, see Mackie et al. (2011) but also a local regulator, for instance a critical minimum cartilage density as implemented by Geris et al. (2008) and Carlier et al. (2016) to initiate chondrocyte hypertrophy in their bio-regulatory computer models of fracture healing. This concept of a minimum cartilage density is based on observations by Einhorn (1998) in a rat model of fracture healing that cartilage mineralisation occurs in the abundance of cartilage, similar to a critical density being achieved. Kozhemyakina

et al. (2015) describe pathways regulating the conversion of chondrocytes from a proliferative to a hypertrophic state within the growth plate, and argue that C-type natriuretic peptide (CNP) is a key regulator involved in the initiation of hypertrophy. CNP is produced by proliferative and pre-hypertrophic chondrocytes and hypertrophy is initiated when the local CNP concentration is high enough. CNP might thus underlie both Einhorn's observations and the critical cartilage density hypothesis used in fracture healing models: a regulator outside the PTHrP-Ihh loop initiating the conversion from proliferation to hypertrophy in chondrocytes.

As indicated above, the direct evidence for the role of the PTHrP-Ihh feedback loop in endochondral bone formation comes from small animal (mouse and rat) models. This is related to the fact that the gene expression levels for the two proteins are low, requiring the use of transgenic mice and reporter genes (Chen et al. (2008)). However, in these animals cartilage thickness is small. A widely cited paper argues that intercellular communication distances are restricted to around 250 µm (Francis and Palsson (1997)), which would be reasonable for mice. However, an osteochondral defect can be over 10 mm deep in adult humans (Nizak et al. (2017)) and it is therefore not clear if this feedback loop can work in humans. Mathematical models can help to address such a question. Moreover, these models can also explain and explore the complex interactions between the cell types and signalling molecules that contribute to osteochondral defect repair and mediate the endochondral ossification process. The aim of this study is to formulate a mathematical model to describe the osteochondral defect healing process as occurs in large animals after ACI. The model aims to incorporate the main characteristics of healing as described above, focusing on healing via the endochondral ossification pathway. ~~The model will address two key questions: (*a*) How does the PTHrP-Ihh feedback loop control endochondral ossification in the healing process, and (*b*) Which key parameters most influence the healing process, controlling the thickness of the articular cartilage in the repaired defect?~~

Current mathematical models of osteochondral defect repair are primarily concerned with mechanical stimuli, exploring the properties of relevant scaffolds used in defect repair (Kelly and Prendergast (2006)) and mechanical influence on mesenchymal stem cell differentiation within a defect (Kelly and Prendergast (2005)). Though these models explore some aspects of the healing process, our study will develop a mathematical model to depict the key mechanisms of osteochondral defect healing via endochondral ossification.

In previous work, we formulated a series of reaction-diffusion type mathematical models exploring the processes involved in chondral defect healing after cell therapy. Lutianov et al. (2011) simulated cartilage regeneration following ACI or autologous stem cell implantation (ASCI), an ACI-like therapy where mesenchymal stem cells are implanted instead of chondrocytes. The simulations compared healing patterns between the two cell therapies, concluding there was no difference in overall healing time while highlighting differences in cell behaviour and healing evolution. Following on from this work, the effects of two signalling molecules were incorporated into this model to simulate the interactions between chondrocytes and mesenchymal stem cells in a co-implantation cell therapy procedure (Campbell et al. (2019a,b)). This work highlighted the importance to chondral healing of cell-to-cell interactions between mesenchymal stem cells and chondrocytes. Specifically, it built on an in vitro model by Wu (2013) and demonstrated how the co-implantation of these two cell types led to a growth-factor mediated trophic effect on healing at early times, though there was no difference in overall healing time.

Mathematical models relevant to our approach study bone fracture healing and include Bailón-Plaza and Van-der Meulen (2001), who proposed a modelling framework for fracture healing, primarily focused on the role of signalling molecules on the healing process. Their model includes the process of endochondral ossification regulated by extracellular matrix density (ECM). Geris et al. (2006) formulated a mathematical model of fracture healing in mice to validate experimental data; their model utilised modelling principles similar to Bailón-Plaza and Van-der Meulen (2001), and achieved results similar to those of the experimental data in murine models, along with a bio-regulatory model for bone fracture healing that utilised an endochondral ossification process including a critical density to regulate chondrocyte hypertrophy (Geris et al. (2008)).

We follow the modelling approaches undertaken in our work so far, combined with those in Bailón-Plaza and Vander Meulen (2001), Geris et al. (2006) and Geris et al. (2008), and apply them to our aim of formulating a reaction-diffusion mathematical model to describe the osteochondral defect healing process after ACI. The model will address two key questions: (*a*) Can the PTHrP-Ihh feedback loop control endochondral ossification in the healing process in large animals, and (*b*) Which key parameters most influence the healing process, in particular controlling the thickness of the articular cartilage in the repaired defect? The plan of the paper is as follows. In §2 we describe the basic model and the assumptions made, the boundary and initial conditions used, estimates of the parameter values and the scalings used to non-dimensionalise the equations. The results of our simulations are discussed in §4, where a sensitivity analysis is undertaken in §4.2 to validate our parameters and highlight those most sensitive to change within the model. Finally, in §5 we explore the implications of the model and suggest future work.

2. Mathematical model

2.1. Model formulation

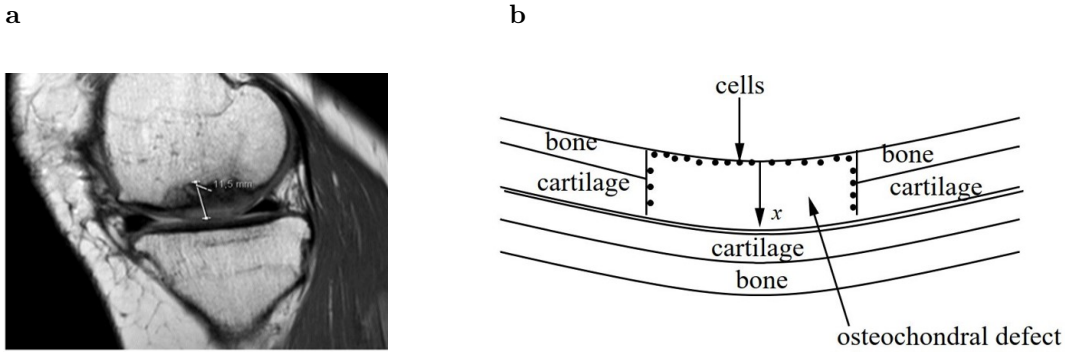

Figure 2: (a) Magnetic Resonance (MR) image of an 11.5mm deep osteochondral defect in the knee (Nizak et al. (2017)); (b) Schematic cross-section of the defect shown in (a). The axis denoted by x in (b) is along the depth of the defect. After debridement of the defect, chondrocytes are seeded along the defect boundaries.

A typical osteochondral defect has small aspect ratio, i.e., its length and width are much larger than its depth, see Fig. 2a. Hence, cell growth along the width of the defect can be assumed negligible compared to that along its depth. This is valid in the middle section of the defect, away from the walls. This assumption enables us to simplify to a one-dimensional problem where we model cell growth along the defect depth only, shown as the x direction in Fig. 2b.

Our model assumes a regenerating osteochondral defect can be populated by three cell types, namely chondrocytes, hypertrophic chondrocytes and osteoblasts, which each produce their specific matrix: cartilage, calcified cartilage or bone, respectively. Depending on cell type, the cells are able to migrate non-directed (random diffusion), proliferate via the uptake of nutrients, differentiate, undergo hypertrophy and deposit matrix via nutrient uptake. In order to explore our central hypothesis that the PTHrP-Ihh feedback loop, important in endochondral ossification, also controls the healing of osteochondral defects, we include a particular mechanism representing the signaling molecules in this feedback loop and their stimulative and suppressive influence on chondrocyte hypertrophy. We do not include mechanobiological signals, known to influence bone resorption and remodelling as well as patterns of endochondral ossification, even though they may play a role in the repair process. We also do not explicitly include chemotaxis (directed motility). As with the model formulated in Campbell et al. (2019a,b), cell motility (assumed to occur through diffusion) is modelled proportional to nutrient concentration, with cell proliferation and differentiation ceasing when nutrient levels are low. At these levels, cell motility is the driving force of changing cell densities, with cells migrating towards locations of higher nutrient concentration. We now develop a mathematical model for the evolution of each species in time, t, and space, x, where x is measured along the depth of the defect (see Fig. 2b). Much of the model formulation follows from our previous models of chondral defect regeneration (Campbell et al. (2019a,b); Lutianov et al. (2011)).

The variables in our model are three cell densities (chondrocyte density C_C, mature (or hypertrophied) chondrocyte density C_H and osteoblast density C_B, all expressed as cells/mm^3), four matrix densities (total matrix density m, which is made up of cartilage matrix density m_C, bone matrix density m_B and calcified cartilage density m_{Ca}, all expressed in g/mm^3), the nutrient concentration n (moles/mm^3) and three signaling molecules (hypertrophy-inducing molecule concentration g_{HI}, hypertrophy-suppressing molecule concentration g_{HS} and hypertrophy modulating molecule concentration g_{HM}, all expressed in moles/mm^3).

Osteochondral defect repair follows a sequential healing process, with the defect first filling entirely with cartilage, before chondrocyte hypertrophy and eventual conversion into bone occurs (Lydon et al. (2019)). We focus here on formulating the cartilage-to-calcified cartilage and calcified cartilage-to-bone transitions in the endochondral ossification pathway and the role of signaling molecules, in particular PTHrP and Ihh, and other factors such as cartilage matrix density mediating these. We assume three signaling molecules regulate these stages, represented in the model by g_{HI} , g_{HM}, g_{HS}. Here, we use g_{HI} to represent a locally produced molecule that induces hypertrophy. Once hypertrophic chondrocytes are being produced, a modulating molecule g_{HM} is released that acts as an intermediate step within the signalling pathway. This factor g_{HM} represents Ihh which stimulates chondrocytes to produce a hypertrophy-suppressing signalling molecule g_{HS}, representing effects similar to PTHrP, and suppressing hypertrophy by keeping chondrocytes proliferating (Kerkhofs et al. (2012)). Figure 3 shows a schematic of the signalling feedback loop.

We also include a local regulator that allows chondrocytes to switch from a proliferative to a hypertrophic state, namely the critical cartilage density $m_{C,crit}$. Once $m_{C,crit}$ is reached, cartilage can begin conversion into calcified matrix which is subsequently remodelled to bone as seen in bone fracture healing (Carlier et al. (2016); Geris et al. (2008)). This conversion of cartilage to calcified matrix can only occur at locations where m_C reaches $m_{C,crit}$ by

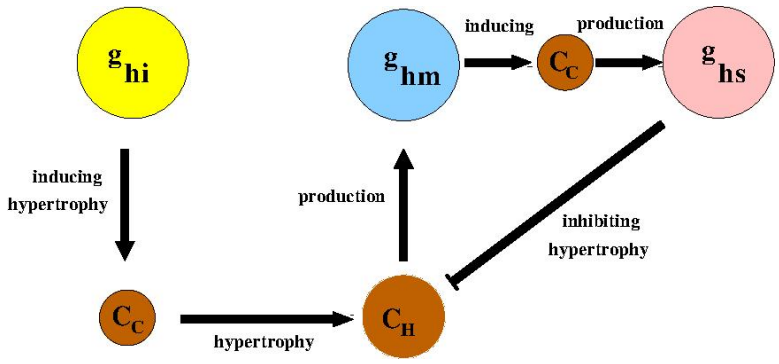

Figure 3: Schematic of signaling molecule feedback loop of endochondral ossification with inducing (g_{HI}), modulating (g_{HM}) and suppressing signalling molecules (g_{HS}). PTHrP and Ihh are the prototype suppressing and modulating signalling molecules, respectively, whereas several candidates exist for the inducing molecule. Solid black lines with arrows indicate inducing and without arrows represent inhibiting. C_C and C_H represent chondrocytes and hypertrophic chondrocytes, respectively.

allowing chondrocytes to convert from a proliferative to a hypertrophic state. Below we describe in detail how the above mechanisms are incorporated in our model.

Chondrocytes proliferate by uptake of nutrients, they can migrate and can undergo hypertrophy. Based on these processes, the rate of change of chondrocyte density is modelled as:

$$\begin{aligned}\frac{\partial C_C}{\partial t} = \frac{\partial}{\partial x}\left(D_{C_C}(m)\frac{\partial C_C}{\partial x}\right) + p_5\left(m, \frac{C_C}{C_{C,max}(m)}\right)C_C\frac{n}{n+n_0}H\left(n-n_1\right) \\ - p_6 C_C H\left(g_{HI}-g_{HI_0}\right)H\left(g_{HS_0}-g_{HS}\right)H\left(m_C-m_{C,crit}\right) - p_7 C_c H\left(n_1-n\right).\end{aligned} \tag{1}$$

The first term on the right of Eq. (1) represents random chondrocyte migration, modelled as a diffusion process, with an effective chondrocyte diffusion coefficient, D_{C_C}. This coefficient is assumed to depend on the total matrix density, m, where $m = m_C + m_B + m_{Ca}$. This is based on the argument that cells can only migrate by attaching to a substrate (in this case, matrix). We use a density-weighted formula for the effective chondrocyte diffusion coefficient, D_{C_C}, based on the diffusivity through cartilage, $D_{C_{C,C}}$, calcified cartilage, $D_{C_{C,Ca}}$, and bone matrix, $D_{C_{C,B}}$, using a mixtures rule (analogous to the total circuit resistance of parallel resistors in an electrical circuit). We follow Olsen et al. (1997) and Bailón-Plaza and Vander Meulen (2001) in choosing expressions for $D_{C_{C,C}}$, $D_{C_{C,Ca}}$ and $D_{C_{C,B}}$.

$$\begin{aligned}&\frac{1}{D_{C_C}(m)} = \left(\frac{m_C}{m}\right)^\alpha \frac{1}{D_{C_{C,C}}(m_C)} + \left(\frac{m_B}{m}\right)^\alpha \frac{1}{D_{C_{C,B}}(m_B)} + \left(\frac{m_{Ca}}{m}\right)^\alpha \frac{1}{D_{C_{C,Ca}}(m_{Ca})}, \quad \alpha \geq 2 \\ &D_{C_{C,C}}(m_C) = D_{C_{C,C_0}}\frac{m_C}{m_C^2 + m_{C,1}^2} \qquad D_{C_{C,B}}(m_B) = D_{C_{C,B_0}}\frac{m_B}{m_B^2 + m_{B,1}^2} \\ &D_{C_{C,Ca}}(m_{Ca}) = D_{C_{C,Ca_0}}\frac{m_{Ca}}{m_{Ca}^2 + m_{Ca,1}^2}\end{aligned} \tag{2}$$

where $(D_{C_{C,C_0}}, D_{C_{C,B_0}}, D_{C_{C,Ca_0}})$ are reference diffusion ratios of chondrocytes, cartilage, bone and calcified cartilage, respectively, and $(m_{C,1}, m_{B,1}, m_{Ca,1})$ are reference matrix densities. The exponent $\alpha \geq 2$ is chosen so that we mimic the low motility of cells for the limiting cases when there is no cartilage (or bone) present and for large cartilage (or bone) matrix densities.

The second term on the right of Eq. (1) represents chondrocyte proliferation. Cell proliferation is assumed to be proportional to the chondrocyte density and the nutrient concentration. This process is assumed to start only when the nutrient concentration exceeds a critical value, n_1 (or, alternatively, cell proliferation is switched-off when the nutrient concentration falls below this critical value). This is modelled by the Heaviside function, $H(n-n_1)$, which takes the unit value when $n > n_1$ and zero otherwise. The chondrocyte proliferation rate is given by p_5. The proliferation rate is assumed to depend on both the chondrocyte and total matrix densities. We choose

$$
\begin{aligned}
& p_5\left(m, \frac{C_C}{C_{C,max}(m)}\right) = p_{5,m}\left(1 - \frac{C_C}{C_{C,max}(m)}\right) \\
& \frac{1}{p_{5,m}(m)} = \left(\frac{m_{C_{tot}}}{m}\right)^{\alpha} \frac{1}{p_{5,C}(m_{C_{tot}})} + \left(\frac{m_B}{m}\right)^{\alpha} \frac{1}{p_{5,B}(m_B)}, \quad \alpha \geq 2 \\
& p_{5,C}(m_{C_{tot}}) = p_{5,C_0} \frac{m_{C_{tot}}}{m_{C_{tot}}^2 + m_{C,2}^2} \qquad p_{5,B}(m_B) = p_{5,B_0} \frac{m_B}{m_B^2 + m_{B,2}^2} \\
& C_{C,max}(m) = C_{C,max0}\left(1 - \frac{m}{m_{max}}\right).
\end{aligned}
\tag{3}
$$

The dependence of p_5 on the total matrix density is represented by $p_{5,m}(m)$. A density-weighted formula (similar to the effective cell migration/diffusion coefficient) is used to model the effective proliferation rate based on the cell proliferation rate in the presence of cartilage (represented by $p_{5,C}$) and bone (represented by $p_{5,B}$). The dependence of $(p_{5,C}, p_{5,B})$ on the matrix density $(m_{C_{tot}}, m_B)$ are chosen so that $(p_{5,C}, p_{5,B}) = 0$ when $(m_{C_{tot}}, m_B) = 0$, $(p_{5,C}, p_{5,B}) \to 0$ for large $(m_{C_{tot}}, m_B)$ and $(p_{5,C}, p_{5,B})$ attain a maximum at some intermediate matrix density, $(m_{C_{tot}}, m_B) = (m_{C,2}, m_{B,2})$. The coefficients, (p_{5,C_0}, p_{5,B_0}), represent chondrocyte proliferation rates in the presence of cartilage and bone, respectively. We assume that $p_{5,C}$ depends on the total cartilage matrix density, $m_{C_{tot}} = m_C + m_{Ca}$ and not on the cartilage type, i.e., whether regular or calcified cartilage. The dependence of p_5 on the chondrocyte density is assumed to follow a logistic growth model with the proliferation rate decreasing as the chondrocyte density approaches its maximum value, $C_{C,max}$. This maximum chondrocyte density is assumed to decrease linearly with total matrix density, m, because the presence of matrix will limit the space for cells. C_{C,max_0} is a reference maximum chondrocyte density.

The third term on the right of Eq. (1) models chondrocyte maturation (hypertrophic state). This is assumed to be proportional to the chondrocyte density and is regulated by the hypertrophy-inducing and suppressing signaling molecules g_{HI} and g_{HS}, respectively, and the critical cartilage density $m_{C,crit}$. The maturation rate is p_6 and assumed constant. The dependence on these signaling molecule concentrations is modelled using the Heaviside function, $H(g_{HI} - g_{HI_0})$ and $H(g_{HS_0} - g_{HS})$, where g_{HI_0} and g_{HS_0} are a threshold hypertrophy-inducing and suppressing molecule concentration, respectively. The first Heaviside function promotes hypertrophy once the hypertrophy-inducing signaling molecule concentration exceeds its threshold value, g_{HI_0}, and the second suppresses hypertrophy once the hypertrophy-suppressing signaling molecule concentration exceeds its threshold value, g_{HS_0}. The Heaviside function, $H(m_C - m_{C,crit})$, initiates chondrocyte hypertrophy only if $m_C > m_{C,crit}$ at any location in the defect.

The last term in Eq. (1) represents cell death due to lack of adequate nutrients. This process starts when the nutrient concentration falls below the critical value, n_1, and is modelled using the Heaviside function, $H(n_1 - n)$,

which takes the unit value when $n < n_1$ and zero otherwise. The cell death rate is p_7, and is assumed constant.

The rate of change of mature hypertrophic chondrocyte density is modelled as:

$$\frac{\partial C_H}{\partial t} = \frac{\partial}{\partial x}\left(D_{C_H}(m)\frac{\partial C_H}{\partial x}\right) - p_8 C_H + p_6 C_C H\left(g_{HI} - g_{HI_0}\right) H\left(g_{HS_0} - g_{HS}\right) H\left(m_C - m_{C,crit}\right), \tag{4}$$

where D_{C_H} is the migration (diffusion) coefficient and p_8 is the death rate. We use similar expressions as in Eq. (2) for

$$\begin{aligned}
&\frac{1}{D_{C_H}(m)} = \left(\frac{m_C}{m}\right)^{\alpha}\frac{1}{D_{C_{H,C}}(m_C)} + \left(\frac{m_B}{m}\right)^{\alpha}\frac{1}{D_{C_{H,B}}(m_B)} + \left(\frac{m_{Ca}}{m}\right)^{\alpha}\frac{1}{D_{C_{H,Ca}}(m_{Ca})}, \quad \alpha \geq 2 \\
&D_{C_{H,C}}(m_C) = D_{C_{H,C_0}}\frac{m_C}{m_C^2 + m_{C,1}^2} \qquad D_{C_{H,B}}(m_B) = D_{C_{H,B_0}}\frac{m_B}{m_B^2 + m_{B,1}^2} \\
&D_{C_{H,Ca}}(m_{Ca}) = D_{C_{H,Ca_0}}\frac{m_{Ca}}{m_{Ca}^2 + m_{Ca,1}^2},
\end{aligned} \tag{5}$$

where $(D_{C_{H,C_0}}, D_{C_{H,B_0}}, D_{C_{H,Ca_0}})$ are reference diffusion rates of hypertrophic chondrocytes through cartilage, bone and calcified cartilage, respectively. The last term in Eq. (4) models formation of hypertrophic chondrocytes modulated by the hypertrophy-inducing and suppressing signaling molecule concentrations, and the critical cartilage densiyt, $m_{C,crit}$.

The rate of change of osteoblast density is modelled as:

$$\begin{aligned}
\frac{\partial C_B}{\partial t} = &\frac{\partial}{\partial x}\left(D_{C_B}(m)\frac{\partial C_B}{\partial x}\right) + p_9\left(m, \frac{C_B}{C_{B,max}(m)}\right) C_B \frac{n}{n + n_0} H\left(n - n_1\right) \\
&- p_{10} C_B H\left(n_1 - n\right),
\end{aligned} \tag{6}$$

where D_{C_B} is the osteoblast migration (diffusion) coefficient, p_9 is the osteoblast proliferation rate and p_{10} is the osteoblast death rate. We use similar expressions as in Eqs. (2,3,5) for the matrix-dependent osteoblast diffusion and proliferation coefficients, given by

$$\begin{aligned}
&\frac{1}{D_{C_B}(m)} = \left(\frac{m_C}{m}\right)^{\alpha}\frac{1}{D_{C_{B,C}}(m_C)} + \left(\frac{m_B}{m}\right)^{\alpha}\frac{1}{D_{C_{B,B}}(m_B)} + \left(\frac{m_{Ca}}{m}\right)^{\alpha}\frac{1}{D_{C_{B,Ca}}(m_{Ca})}, \quad \alpha \geq 2 \\
&D_{C_{B,C}}(m_C) = D_{C_{B,C_0}}\frac{m_C}{m_C^2 + m_{C,1}^2} \qquad D_{C_{B,B}}(m_B) = D_{C_{B,B_0}}\frac{m_B}{m_B^2 + m_{B,1}^2} \\
&D_{C_{B,Ca}}(m_{Ca}) = D_{C_{B,Ca_0}}\frac{m_{Ca}}{m_{Ca}^2 + m_{Ca,1}^2} \qquad p_9\left(m, \frac{C_B}{C_{B,max}(m)}\right) = p_{9,m}\left(1 - \frac{C_B}{C_{B,max}(m)}\right) \\
&\frac{1}{p_{9,m}(m)} = \left(\frac{m_{C_{tot}}}{m}\right)^{\alpha}\frac{1}{p_{9,C}(m_{C_{tot}})} + \left(\frac{m_B}{m}\right)^{\alpha}\frac{1}{p_{9,B}(m_B)}, \quad \alpha \geq 2 \\
&p_{9,C}(m_{C_{tot}}) = p_{9,C_0}\frac{m_{C_{tot}}}{m_{C_{tot}}^2 + m_{C,2}^2} \qquad p_{9,B}(m_B) = p_{9,B_0}\frac{m_B}{m_B^2 + m_{B,2}^2} \\
&C_{B,max}(m) = C_{B,max0}\left(1 - \frac{m}{m_{max}}\right),
\end{aligned} \tag{7}$$

where $(D_{C_{B,C_0}}, D_{C_{B,B_0}}, D_{C_{B,Ca_0}})$ are reference osteoblast migration rates through cartilage, bone and calcified cartilage, respectively, and (p_{9,C_0}, p_{9,B_0}) are reference osteoblast proliferation rates in the presence of cartilage and bone, respectively. The maximum osteoblast density, $C_{B,max}$, is assumed to decrease linearly with total matrix

density, m. C_{B,max_0} is a reference maximum osteoblast density. We choose the reference maximum stem cell, normal and mature chondrocyte and osteoblast densities, C_{S,max_0}, C_{C,max_0}, C_{H,max_0}, C_{B,max_0}, respectively, such that $C_{S,max_0} + C_{C,max_0} + C_{H,max_0} + C_{B,max_0} = C_{total,max_0}$, where C_{total,max_0} is a reference maximum total cell density. Hence, using the expressions for $C_{S,max}$, $C_{C,max}$ and $C_{B,max}$ in Eqs. (2,7) gives, $(C_{S,max} + C_{C,max} + C_{B,max})(m) = (C_{total,max_0} - C_{H,max_0})(1 - m/m_{max})$.

The rate of change of cartilage matrix density is modelled as:

$$\frac{\partial m_C}{\partial t} = D_{m_C}\frac{\partial^2 m_C}{\partial x^2} + p_{11}(m_C)\frac{n}{n+n_0}C_C - p_{12}(m_C)C_H, \tag{8}$$

where D_{m_C} is the cartilage matrix diffusion coefficient (assumed constant), p_{11} is the cartilage matrix synthesis rate and p_{12} is the rate of localized cartilage matrix degradation. We choose

$$p_{11}(m_C) = p_{11_0} - p_{11_1}m_C, \tag{9}$$

where p_{11_0} is a cartilage matrix production rate and p_{11_1} is its degradation rate. This assumes that the cartilage matrix synthesis rate decreases linearly with increasing cartilage matrix density (Olsen et al. (1997), Bailón-Plaza and Vander Meulen (2001)). The last term in Eq. (8) models localized degradation of cartilage matrix and is assumed to be proportional to the hypertrophic chondrocyte density. We choose

$$p_{12}(m_C) = p_{12_0}m_C, \tag{10}$$

where p_{12_0} is a cartilage matrix degradation rate. This assumes that the degradation is proportional to the cartilage matrix density. We allow cartilage degradation to occur once $\bar{m}_C$ has reached the critical density $m_{C_{crit}}$ and to cease when m_{Ca} and m_B have reached the maximum matrix density.

The rate of change of calcified cartilage matrix density is modelled as:

$$\frac{\partial m_{Ca}}{\partial t} = p_{12}(m_C)C_H - p_{20}m_{Ca}C_B. \tag{11}$$

The first term on the right of Eq. (11) describes the formation of calcified cartilage as the cartilage matrix degrades in the presence of hypertrophic chondrocytes. This term is switched on only when m_C has reached the critical density $m_{C_{crit}}$. The second term describes degradation of calcified cartilage matrix and is assumed to be proportional to its density and the osteoblast density, and p_{20} the degradation rate. Here, we do not distinguish between osteoblasts and osteoclasts which are responsible for converting calcified cartilage into bone.

The rate of change of bone matrix density is modelled as:

$$\frac{\partial m_B}{\partial t} = D_{m_B}\frac{\partial^2 m_B}{\partial x^2} + p_{13}(m_B)\frac{n}{n+n_0}C_B + p_{20}m_{Ca}C_B, \tag{12}$$

where D_{m_B} is the bone matrix diffusion coefficient (assumed constant) and p_{13} is the bone matrix synthesis rate. We choose

$$p_{13}(m_B) = p_{13_0} - p_{13_1}m_B, \tag{13}$$

where p_{13_0} is a bone matrix production rate and p_{13_1} is its degradation rate. The last term in Eq. (12) models bone matrix formation from calcified cartilage matrix.

The rate of change of hypertrophy-inducing signaling molecule concentration is modelled as:

$$\frac{\partial g_{HI}}{\partial t} = D_{g_{HI}} \frac{\partial^2 g_{HI}}{\partial x^2} - p_{25} g_{HI}, \tag{14}$$

where $D_{g_{HI}}$ is the hypertrophy-inducing signaling molecule diffusion coefficient (assumed constant) and p_{25} is the rate of degradation (assumed constant).

The rate of change of hypertrophy-suppressing signaling molecule concentration is modelled as:

$$\frac{\partial g_{HS}}{\partial t} = D_{g_{HS}} \frac{\partial^2 g_{HS}}{\partial x^2} + p_{21} C_C H\left(x - 90\%d\right) + p_{15} g_{HM} C_C H\left(x - 90\%d\right) - p_{22} g_{HS}, \tag{15}$$

where $D_{g_{HS}}$ is the hypertrophy-suppressing signaling molecule diffusion coefficient (assumed constant), p_{21} is the production rate by surface chondrocytes, p_{15} represents its production rate, and p_{22} is the degradation rate (assumed constant). The second term in Eq. (15) models the production of a hypertrophy-suppressing signalling molecule from chondrocytes and is assumed to be proportional to the chondrocyte density. We assume here that this signalling molecule is produced only by the chondrocytes at the upper 10% of the defect (denoted by $x = 90\%d$). The third term models the production of hypertrophy-suppressing signalling molecule via the stimulation of chondrocytes by the hypertrophy-modulating signalling molecule, and is assumed to be proportional to hypertrophy-modulating signalling molecule concentration and the chondrocyte density (only chondrocytes in the upper 10% of the defect). The fourth term represents the degradation of this signalling molecule (assumed to be proportional to the hypertrophy-suppressing signalling molecule concentration).

The rate of change of hypertrophy-modulating signalling molecule concentration is modelled as:

$$\frac{\partial g_{HM}}{\partial t} = D_{g_{HM}} \frac{\partial^2 g_{HM}}{\partial x^2} + p_{23} C_H - p_{26} g_{HM}, \tag{16}$$

where $D_{g_{HM}}$ is the hypertrophy-modulating signalling molecule diffusion coefficient (assumed constant), p_{23} is the production rate by hypertrophic chondrocytes, and p_{26} represents its degradation rate (assumed constant). The production of the hypertrophy-modulating molecule is assumed to be proportional to the hypertrophic chondrocyte density (second term in Eq. (16)).

Finally, the rate of change of nutrient concentration is modelled as

$$\frac{\partial n}{\partial t} = D_n \frac{\partial^2 n}{\partial x^2} - \frac{n}{n + n_0} \left(p_{17} C_C + p_{18} C_B + p_{19} C_H\right), \tag{17}$$

where D_n is the nutrient diffusion coefficient (assumed constant), p_{17}, p_{18} and p_{19} represent the nutrient uptake rate by chondrocytes, osteoblasts and mature chondrocytes, respectively (assumed constant).

2.2. Boundary conditions

We need to specify two boundary conditions for each species (except m_{Ca}, which does not require spatial boundary conditions). These are specified at either end of the defect domain. We assume $x = 0$ at the subchondral bone interface ("base" of the defect) and $x = d$ at the interface with the opposing normal cartilage ("top" of the defect, see Fig. 2b). The boundary conditions chosen at $x = 0$ are:

$$\begin{gathered} -D_{C_C}(m)\frac{\partial C_C}{\partial x} = -D_{C_H}(m)\frac{\partial C_H}{\partial x} = -D_{m_C}\frac{\partial m_C}{\partial x} = -D_{m_B}\frac{\partial m_B}{\partial x} = 0 \\ C_B = C_{B_0} \qquad n = N_0 \qquad g_{HI} = g_{HI_1} \qquad g_{HS} = g_{HS_1} \qquad g_{HM} = g_{HM_1} \end{gathered} \tag{18}$$

The first four boundary conditions represent no flux of chondrocytes, hypertrophic chondrocytes, cartilage matrix and osteoblasts from the subchondral bone. We assume that a reservoir of osteoblasts from the underlying intact bone, with uniform cell density, C_{B_0}, and nutrients from the underlying vascular network, with uniform concentration, N_0, are always available at this end. This is represented by the sixth and seventh boundary conditions, respectively. The last three boundary conditions represent a constant supply of hypertrophy-inducing, suppressing and modulating signalling molecules from the underlying vascular network, with uniform concentration, g_{HI_1}, g_{HS_1} and g_{HM_1}, respectively.

At $x = d$, we impose:

$$
\begin{aligned}
&-D_{C_C}(m)\frac{\partial C_C}{\partial x} = -D_{C_B}(m)\frac{\partial C_B}{\partial x} = -D_{C_H}(m)\frac{\partial C_H}{\partial x} = -D_{m_C}\frac{\partial m_C}{\partial x} = -D_{m_B}\frac{\partial m_B}{\partial x} = 0 \\
&n = N_1 \qquad g_{HI} = g_{HI_2} \qquad -D_{g_{HS}}\frac{\partial g_{HS}}{\partial x} = \gamma_1(g_{HS} - g_{HS_2}) \qquad -D_{g_{HM}}\frac{\partial g_{HM}}{\partial x} = \gamma_2(g_{HM} - g_{HM_2})
\end{aligned}
\tag{19}
$$

The first four boundary conditions represent no flux of chondrocytes, osteoblasts, hypertrophic chondrocytes and matrix, respectively, from the normal cartilage interface. We assume that a reservoir of nutrients with uniform concentration, N_1, is always available at this end. A constant supply of hypertrophy-inducing signalling molecule, with uniform concentration, g_{HI_2} is available at this boundary. We allow the hypertrophy-suppressing and modulating molecules to permeate (diffuse) through this boundary, represented by the eight and ninth boundary conditions, respectively, with the diffusive flux proportional to the signalling molecule concentration, and constant of proportionality $\gamma_{1,2}$, respectively (assumed constant). Here, g_{HS_2,HM_2} represent the concentrations of the hypertrophy-suppressing and modulating signalling molecules in the overlying articular cartilage (assumed constant)

2.3. Initial conditions

We need to prescribe profiles for each species at time $t = 0$. We are interested in one implantation scenario, related to Autologous Chondrocyte Implantation (ACI). Initially, chondrocytes are implanted into a nutrient-filled defect with a small amount of matrix present. The initial conditions chosen for this case are:

$$
\begin{aligned}
&C_C = C_C^{(0)}h(x) \qquad C_B = C_{B_0}h_1(x) \qquad C_H = 0 \qquad n = N_0 - (N_0 - N_1)\frac{x}{d} \qquad m_C = m_{C,3} \\
&m_B = m_{B,3} \qquad m_{Ca} = 0 \qquad g_{HI} = g_{HI_1} - (g_{HI_1} - g_{HI_2})\frac{x}{d} \qquad g_{HS} = g_{HS_1} \qquad g_{HM} = g_{HM_1}
\end{aligned}
\tag{20}
$$

Here, $C_C^{(0)}$, $h(x)$ and $h_1(x)$ are an initial chondrocyte density, and specified initial spatial profiles for chondrocytes and osteoblasts, respectively.

There are several parameters appearing in the model. Their estimated values and the references from which they are obtained are provided in Table 1. All approximated parameters are disclosed in this table and references are provided where available.

dimensional parameters	estimated value
defect depth d	3-5 mm - 1-2 mm cartilage, 2-3 mm bone (Ahern et al. (2009) for

maximum chondrocyte migration (or diffusion) coefficient in cartilage, $D_{C_{C,C}}$	3.6×10^{-4} mm^2/hr Obradovic et al. (2000), in silico
maximum chondrocyte migration (or diffusion) coefficient in bone, $D_{C_{C,B}}$	3.6×10^{-4} mm^2/hr (assumed same as $D_{C_{C,C}}$)
maximum chondrocyte migration (or diffusion) coefficient in calcified cartilage, $D_{C_{C,Ca}}$	3.6×10^{-4} mm^2/hr (assumed same as $D_{C_{C,C}}$)
maximum mature chondrocyte migration (or diffusion) coefficient in cartilage, $D_{C_{H,C}}$	10^{-5} mm^2/hr (guess)
maximum mature chondrocyte migration (or diffusion) coefficient in bone, $D_{C_{H,B}}$	10^{-5} mm^2/hr (assumed same as $D_{C_{H,C}}$)
maximum mature chondrocyte migration (or diffusion) coefficient in calcified cartilage, $D_{C_{H,Ca}}$	10^{-5} mm^2/hr (assumed same as $D_{C_{H,C}}$)
maximum osteoblast migration (or diffusion) coefficient in cartilage, $D_{C_{B,C}}$	10^{-6} - 10^{-5} mm^2/hr (guess)
maximum osteoblast migration (or diffusion) coefficient in bone, $D_{C_{B,B}}$	10^{-4} - 10^{-3} mm^2/hr (guess)
maximum osteoblast migration (or diffusion) coefficient in calcified cartilage, $D_{C_{B,Ca}}$	10^{-4} - 10^{-3} mm^2/hr (guess)
chondrocyte migration (or diffusion) coefficient, $D_{C_{C,C_0}} = 2m_{C,1}D_{C_{C,C}}$	7.2×10^{-9} (mm^2/hr) (g/mm^3) (assuming $m_{C,1} = 10^{-5}$ g/mm^3)
chondrocyte migration (or diffusion) coefficient, $D_{C_{C,B_0}} = 2m_{B,1}D_{C_{C,B}}$	7.2×10^{-9} (mm^2/hr) (g/mm^3) (assuming $m_{B,1} = 10^{-5}$ g/mm^3)
chondrocyte migration (or diffusion) coefficient, $D_{C_{C,Ca_0}} = 2m_{Ca,1}D_{C_{C,Ca}}$	7.2×10^{-9} (mm^2/hr) (g/mm^3) (assuming $m_{Ca,1} = 10^{-5}$ g/mm^3)
mature chondrocyte migration (or diffusion) coefficient, $D_{C_{H,C_0}} = 2m_{C,1}D_{C_{H,C}}$	10^{-10} (mm^2/hr) (g/mm^3) (assuming $m_{C,1} = 10^{-5}$ g/mm^3)
mature chondrocyte migration (or diffusion) coefficient, $D_{C_{H,B_0}} = 2m_{B,1}D_{C_{H,B}}$	10^{-10} (mm^2/hr) (g/mm^3) (assuming $m_{B,1} = 10^{-5}$ g/mm^3)
mature chondrocyte migration (or diffusion) coefficient, $D_{C_{H,Ca_0}} = 2m_{Ca,1}D_{C_{H,Ca}}$	10^{-10} (mm^2/hr) (g/mm^3) (assuming $m_{Ca,1} = 10^{-5}$ g/mm^3)
osteoblast migration (or diffusion) coefficient, $D_{C_{B,C_0}} = 2m_{C,1}D_{C_{B,C}}$	10^{-11} - 10^{-10} (mm^2/hr) (g/mm^3) (assuming $m_{C,1} = 10^{-5}$ g/mm^3)
osteoblast migration (or diffusion) coefficient, $D_{C_{B,B_0}} = 2m_{B,1}D_{C_{B,B}}$	10^{-9} (mm^2/hr) (g/mm^3) (assuming $m_{B,1} = 10^{-5}$ g/mm^3)
osteoblast migration (or diffusion) coefficient, $D_{C_{B,Ca_0}} = 2m_{Ca,1}D_{C_{B,Ca}}$	10^{-9} (mm^2/hr) (g/mm^3) (assuming $m_{Ca,1} = 10^{-5}$ g/mm^3)

nutrient diffusion coefficient, D_n	4.6 mm^2/hr Zhou et al. (2004), mathematical model
cartilage matrix diffusion coefficient, D_{m_C}	0-2.5 $\times 10^{-5}$ mm^2/hr Obradovic et al. (2000), in silico
bone matrix diffusion coefficient, D_{m_B}	0-10^{-6} mm^2/hr (guess)
hypertrophy-inducing signalling molecule diffusion coefficient, $D_{g_{HI}}$	0.8 mm^2/hr Williams et al. (2007), in vitro, in vivo
hypertrophy-suppressing signalling molecule diffusion coefficient, $D_{g_{HS}}$	0.18 mm^2/hr Fasano et al. (2010), mathematical model, in vivo
hypertrophy-modulating signalling molecule diffusion coefficient, $D_{g_{HM}}$	0.18 mm^2/hr Fasano et al. (2010), mathematical model, in vivo
maximum chondrocyte proliferation rate in cartilage, $p_{5,C}$	2×10^{-4}/hr (guess)
maximum chondrocyte proliferation rate in bone, $p_{5,B}$	2×10^{-4}/hr (assumed same as $p_{5,C}$)
chondrocyte proliferation rate, $p_{5_{C,0}} = 2m_{C,2}p_{5,C}$	4×10^{-9} g/mm^3/hr (assuming $m_{C,2} = 10^{-5}$ g/mm^3)
chondrocyte proliferation rate, $p_{5_{B,0}} = 2m_{B,2}p_{5,B}$	4×10^{-9} g/mm^3/hr (assuming $m_{B,2} = 10^{-5}$ g/mm^3)
chondrocyte hypertrophic differentiation rate, p_6	2×10^{-2}/hr Wilsman et al. (1996), in vivo
chondrocyte death rate, p_7	3.75×10^{-3}/hr (guess)
mature chondrocyte death rate, p_8	6×10^{-3}/hr Wilsman et al. (1996), in vivo
maximum osteoblast proliferation rate in cartilage, $p_{9,C}$	(10^{-3}-10^{-2})/hr (guess)
maximum osteoblast proliferation rate in bone, $p_{9,B}$	(10^{-3}-10^{-2})/hr (assumed same as $p_{9,C}$)
osteoblast proliferation rate, $p_{9,C_0} = 2m_{C,2}p_{9,C}$	$2 \times$ (10^{-8}-10^{-7}) g/mm^3/hr (assuming $m_{C,2} = 10^{-5}$ g/mm^3)
osteoblast proliferation rate, $p_{9,B_0} = 2m_{B,2}p_{9,B}$	$2 \times$ (10^{-8}-10^{-7}) g/mm^3/hr (assuming $m_{B,2} = 10^{-5}$ g/mm^3)
osteoblast death rate, p_{10}	10^{-3}/hr (guess)
cartilage matrix production rate, p_{11_0}	3.75×10^{-13}(g/mm^3)/((N_C/mm^3) hr) Obradovic et al. (2000), in silico
cartilage matrix degradation rate, p_{11_1}	3.75×10^{-9}/((N_C/mm^3) hr) Obradovic et al. (2000), in silico
cartilage matrix degradation rate by hypertrophic chondrocytes, p_{12_0}	4×10^{-5} /((N_C/mm^3) hr) Wilsman et al. (1996), in vivo
bone matrix production rate, p_{13_0}	5×10^{-12} (g/mm^3)/((N_C/mm^3) hr)
bone matrix degradation rate, p_{13_1}	10^{-12}/((N_C/mm^3) hr) (guess)
nutrient uptake rate by chondrocytes, p_{17}	1.5×10^{-14} mol/(N_C hr) Zhou et al. (2004), mathematical model
nutrient uptake rate by osteoblasts, p_{18}	1.5×10^{-14} mol/(N_C hr) (assumed same as p_{17})
nutrient uptake rate by mature chondrocytes, p_{19}	1.5×10^{-14} mol/(N_C hr) (assumed same as p_{17})
calcified cartilage matrix degradation rate, p_{20}	$8 \times$ (10^{-3}-10^{-2})/((N_C/mm^3) hr)

	Bailón-Plaza and Vander Meulen (2001), mathematical model
hypertrophy-inducing signalling molecule degradation rate, p_{25}	5.78×10^{-2} /hr (assuming half-life 12 hours, Rayon et al. (2020))
hypertrophy-suppressing signalling molecule production rate by surface chondrocytes, p_{21}	3.3×10^{-22} mol/(N_C hr) Garzón-Alvarado et al. (2009), mathematical model
hypertrophy-suppressing signalling molecule production rate by proliferating chondrocytes, p_{15}	10^{-6}/((N_C/mm^3) hr) (guess)
hypertrophy-suppressing signalling molecule degradation rate, p_{22}	5.78×10^{-2} /hr (assuming half-life 12 hours, Rayon et al. (2020))
hypertrophy-modulating signalling molecule production rate, p_{23}	2.6×10^{-21} mol/(N_C hr) Garzón-Alvarado et al. (2009) mathematical model
hypertrophy-modulating signalling molecule degradation rate, p_{26}	5.78×10^{-2} /hr (assuming half-life 12 hours, Rayon et al. (2020))
maximum total cell density, C_{total,max_0}	10^6 N_C/mm^3 (assuming $10\mu m$ cell diameter)
maximum chondrocyte density, C_{C,max_0}	$0 - 10^6$ N_C/mm^3
maximum mature chondrocyte density, C_{H,max_0}	$0 - 10^6$ N_C/mm^3
maximum osteoblast density, C_{B,max_0}	$0 - 10^6$ N_C/mm^3
maximum cartilage matrix density, $m_{C,max}$	10^{-4} g/mm^3 Bailón-Plaza and Vander Meulen (2001), mathematical model
maximum bone matrix density, $m_{B,max}$	1×10^{-3} g/mm^3 (based on density of cortical bone)
maximum calcified cartilage matrix density, $m_{Ca,max}$	$(1 - 2) \times 10^{-3}$ g/mm^3 (assumed same as $m_{B,max}$)
maximum matrix density, $m_{max} = m_{C,max} + m_{B,max} + m_{Ca,max}$	$(2.1 - 4.1) \times 10^{-3}$ g/mm^3
maximum total cartilage matrix density, $m_{C_{tot,max}} = m_{C,max} + m_{Ca,max}$	$(1.1 - 2.1) \times 10^{-3}$ g/mm^3
initial chondrocyte cell density, $C_C^{(0)}$	2.5×10^5 N_C/mm^3 (based on 10^6 cells in 20mm x 20mm x 10μm volume)
reference cartilage matrix density, $m_{C,1}$	10^{-5} g/mm^3 (assumed $m_{max}/100$)
intermediate cartilage matrix density, $m_{C,2}$	10^{-5} g/mm^3 (assumed $m_{max}/100$)
reference calcified cartilage density, $m_{Ca,1}$	10^{-5} g/mm^3 (assumed $m_{max}/100$)
reference bone matrix density, $m_{B,1}$	10^{-5} g/mm^3 (assumed $m_{max}/100$)
intermediate bone matrix density, $m_{B,2}$	10^{-5} g/mm^3 (assumed $m_{max}/100$)
initial cartilage/bone matrix density, $m_{C,3}$,$m_{B,3}$	10^{-8} g/mm^3 (assumed $m_{max}/10^5$)
initial nutrient concentration, N_1	(2.85 - 9.5) $\times$ 10^{-11} mol/mm^3 (3-10% oxygen tension) Zhou et al. (2004), mathematical model
initial nutrient concentration, N_0	9.5 $\times$ 10^{-11} mol/mm^3 (Kiaer et al. (1989), human

threshold nutrient concentration, n_0	2.3×10^{-11} mol/mm^3 Zhou et al. (2004), mathematical model
critical nutrient concentration, n_1	9.5×10^{-12} mol/mm^3 (assumed $N_0/10$)
threshold hypertrophy-inducing signalling molecule concentration, g_{HI_0}	$(0.5 - 1) \times 10^{-15}$ mol/mm^3
threshold hypertrophy-suppressing signalling molecule concentration, g_{HS_0}	40×10^{-18} mol/mm^3 (guess)
initial hypertrophy-inducing signalling molecule concentration, g_{HI_1}	2×10^{-15} mol/mm^3 Rovensky et al. (2005)
initial hypertrophy-inducing signalling molecule concentration, g_{HI_2}	2×10^{-15} mol/mm^3 Rovensky et al. (2005)
hypertrophy-suppressing signalling molecule concentration, g_{HS_1}	2×10^{-18} mol/mm^3 Okano et al. (1995)
hypertrophy-suppressing signalling molecule concentration, g_{HS_2}	2×10^{-18} mol/mm^3 Okano et al. (1995)
hypertrophy-modulating signalling molecule concentration, g_{HM_1}	3×10^{-16} mol/mm^3 Zhang et al. (2014)
hypertrophy-modulating signalling molecule concentration, g_{HM_2}	3×10^{-16} mol/mm^3 Zhang et al. (2014)
initial osteoblast cell density, C_{B_0}	9×10^3 N$_C$/mm^3 Martin and Burr (1984), human
hypertrophy-suppressing signalling molecule flux parameter, γ_1	0 mm/hr (no flux - guess)
hypertrophy-modulating signalling molecule flux parameter, γ_2	0 mm/hr (no flux - guess)
critical cartilage density, $m_{C,crit}$	95% $m_{C,max}$

Table 1: Estimated values of dimensional parameters. In the above, N_C represents number of cells.

3. Non-dimensionalisation of model equations, boundary and initial conditions

It is instructive to non-dimensionalise (make dimensionless) the above equations, boundary and initial conditions. One can then compare (or measure) the variables against their corresponding characteristic quantities. We introduce

the following dimensionless variables based on characteristic quantities for each variable:

$$\bar{x} = x/d \qquad \bar{t} = t(p_{11_0} C_{total,max_0}/m_{C,max}) \qquad (\bar{C}_C, \bar{C}_H, \bar{C}_B) = (C_C, C_H, C_B)/C_{total,max_0}$$

$$(\bar{m}, \bar{m}_C, \bar{m}_{Ca}, \bar{m}_B, \bar{m}_{C_{tot}}) = (m/m_{max}, m_C/m_{C,max}, m_{Ca}/m_{Ca,max}, m_B/m_{B,max}, m_{C_{tot}}/m_{C_{tot,max}}) \tag{21}$$

$$\bar{n} = n/N_1 \qquad \bar{g}_{HI} = g_{HI}/g_{HI_1} \qquad \bar{g}_{HM} = g_{HM}/g_{HM_1} \qquad \bar{g}_{HS} = g_{HS}/g_{HS_1},$$

where the overbars represent dimensionless quantities. The characteristic quantities used to measure the spatial variable, x, cell densities, matrix densities, nutrient concentration and the hypertrophy-inducing, suppressing and modulating signalling molecule concentrations are the defect depth, d, the reference maximum total cell density, C_{total,max_0}, the maximum cartilage and bone matrix densities, $m_{C,max}$, $m_{Ca,max}$, $m_{B,max}$, respectively, the total matrix density, $m_{max} = m_{C,max} + m_{Ca,max} + m_{B,max}$, the total cartilage matrix density, $m_{C_{total},max} = m_{C,max} + m_{Ca,max}$, the initial nutrient concentration at $x = d$, N_1, and the initial hypertrophy-inducing, suppressing and modulating signalling molecule concentrations at $x = 0$, g_{HI_1}, g_{HS_1} and g_{HM_1}, respectively. We choose to measure time, t, based on the cartilage matrix production time scale, $m_{C,max}/(p_{11_0} C_{total,max_0})$. Using the parameter values in Table 1, we estimate this time scale to be approximately 11 days (a unit of time corresponds to approximately 11 days).

Using the above dimensionless variables, the non-dimensional equations can be written as:

$$\frac{\partial \bar{C}_C}{\partial \bar{t}} = \frac{\partial}{\partial \bar{x}}\left(\bar{D}_{C_C}(\bar{m})\frac{\partial \bar{C}_C}{\partial \bar{x}}\right) + \bar{p}_5\left(\bar{m}, \frac{\bar{C}_C}{\bar{C}_{C,max}(\bar{m})}\right)\frac{\bar{n}}{\bar{n}+\bar{n}_0}\bar{C}_C H(\bar{n}-\bar{n}_1)$$

$$- \bar{p}_6 \bar{C}_C H(\bar{g}_{HI} - \bar{g}_{HI_0}) H(\bar{g}_{HS_0} - \bar{g}_{HS}) H(\bar{m}_C - \bar{m}_{C,crit}) - \bar{p}_7 \bar{C}_C H(\bar{n}_1 - \bar{n}) \tag{22a}$$

$$\frac{\partial \bar{C}_H}{\partial \bar{t}} = \frac{\partial}{\partial \bar{x}}\left(\bar{D}_{C_H}(\bar{m})\frac{\partial \bar{C}_H}{\partial \bar{x}}\right) + \bar{p}_6 \bar{C}_C H(\bar{g}_{HI} - \bar{g}_{HI_0}) H(\bar{g}_{HS_0} - \bar{g}_{HS}) H(\bar{m}_C - \bar{m}_{C,crit}) - \bar{p}_8 \bar{C}_H \tag{22b}$$

$$\frac{\partial \bar{C}_B}{\partial \bar{t}} = \frac{\partial}{\partial \bar{x}}\left(\bar{D}_{C_B}(\bar{m})\frac{\partial \bar{C}_B}{\partial \bar{x}}\right) + \bar{p}_9\left(\bar{m}, \frac{\bar{C}_B}{\bar{C}_{B,max}(\bar{m})}\right)\frac{\bar{n}}{\bar{n}+\bar{n}_0}\bar{C}_B H(\bar{n}-\bar{n}_1) - \bar{p}_{10}\bar{C}_B H(\bar{n}_1 - \bar{n}) \tag{22c}$$

$$\frac{\partial \bar{m}_C}{\partial \bar{t}} = \bar{D}_{m_C}\frac{\partial^2 \bar{m}_C}{\partial \bar{x}^2} + \bar{p}_{11}(\bar{m})\frac{\bar{n}}{\bar{n}+\bar{n}_0}\bar{C}_C - \bar{p}_{12}(\bar{m}_C)\bar{C}_H \tag{22d}$$

$$\frac{\partial \bar{m}_{Ca}}{\partial \bar{t}} = \frac{\bar{p}_{12}}{\Gamma_1}(\bar{m}_C)\bar{C}_H - \bar{p}_{20}\bar{m}_{Ca}\bar{C}_B \tag{22e}$$

$$\frac{\partial \bar{m}_B}{\partial \bar{t}} = \bar{D}_{m_B}\frac{\partial^2 \bar{m}_B}{\partial \bar{x}^2} + \bar{p}_{13}(\bar{m})\frac{\bar{n}}{\bar{n}+\bar{n}_0}\bar{C}_B + \bar{p}_{20}\frac{\Gamma_1}{\Gamma}\bar{m}_{Ca}\bar{C}_B \tag{22f}$$

$$\frac{\partial \bar{g}_{HI}}{\partial \bar{t}} = \bar{D}_{g_{HI}}\frac{\partial^2 \bar{g}_{HI}}{\partial \bar{x}^2} - \bar{p}_{25}\bar{g}_{HI} \tag{22g}$$

$$\frac{\partial \bar{g}_{HS}}{\partial \bar{t}} = \bar{D}_{g_{HS}}\frac{\partial^2 \bar{g}_{HS}}{\partial \bar{x}^2} + \left(\bar{p}_{21}\bar{C}_C + \bar{p}_{15}\bar{g}_{HM}\bar{C}_C\right) H\left(\bar{x} - 0.9\right) - \bar{p}_{22}\bar{g}_{HS} \tag{22h}$$

$$\frac{\partial \bar{g}_{HM}}{\partial \bar{t}} = \bar{D}_{g_{HM}}\frac{\partial^2 \bar{g}_{HM}}{\partial \bar{x}^2} + \bar{p}_{23}\bar{C}_H - \bar{p}_{26}\bar{g}_{HM} \tag{22i}$$

$$\frac{\partial \bar{n}}{\partial \bar{t}} = \bar{D}_n\frac{\partial^2 \bar{n}}{\partial \bar{x}^2} - \frac{\bar{n}}{\bar{n}+\bar{n}_0}\left(\bar{p}_{17}\bar{C}_C + \bar{p}_{18}\bar{C}_B + \bar{p}_{19}\bar{C}_H\right), \tag{22j}$$

where

$$\bar{p_5}\left(\bar{m}, \frac{\bar{C}_C}{\bar{C}_{C,max}(\bar{m})}\right) = \bar{p}_{5,m}(\bar{m})\left(1 - \frac{\bar{C}_C}{\bar{C}_{C,max}(\bar{m})}\right) \qquad \bar{C}_{C,max}(\bar{m}) = \bar{C}_{C,max_0}(1-\bar{m})$$

$$\frac{1}{\bar{p}_{5,m}(\bar{m})} = (\beta+\epsilon)^\alpha \left(\frac{\bar{m}_{C_{total}}}{\bar{m}}\right)^\alpha \frac{1}{\bar{p}_{5,C}(\bar{m}_{C_{total}})} + \eta^\alpha \left(\frac{\bar{m}_B}{\bar{m}}\right)^\alpha \frac{1}{\bar{p}_{5,B}(\bar{m}_B)}, \;\; \alpha \geq 2$$

$$\bar{p}_{5,C}(\bar{m}_{C_{total}}) = \bar{p}_{5,C_0}\frac{\bar{m}_{C_{total}}}{\bar{m}^2_{C_{total}} + \bar{m}^2_{C,2}} \qquad \bar{p}_{5,B}(\bar{m}_B) = \bar{p}_{5,B_0}\frac{\bar{m}_B}{\bar{m}^2_B + \bar{m}^2_{B,2}}$$

$$\bar{p_9}\left(\bar{m}, \frac{\bar{C}_B}{\bar{C}_{B,max}(\bar{m})}\right) = \bar{p}_{9,m}(\bar{m})\left(1 - \frac{\bar{C}_B}{\bar{C}_{B,max}(\bar{m})}\right) \qquad \bar{C}_{B,max}(\bar{m}) = \bar{C}_{B,max_0}(1-\bar{m})$$

$$\frac{1}{\bar{p}_{9,m}(\bar{m})} = (\beta+\epsilon)^\alpha \left(\frac{\bar{m}_{C_{total}}}{\bar{m}}\right)^\alpha \frac{1}{\bar{p}_{9,C}(\bar{m}_{C_{total}})} + \eta^\alpha \left(\frac{\bar{m}_B}{\bar{m}}\right)^\alpha \frac{1}{\bar{p}_{9,B}(\bar{m}_B)}, \;\; \alpha \geq 2$$

$$\bar{p}_{9,C}(\bar{m}_{C_{total}}) = \bar{p}_{9,C_0}\frac{\bar{m}_{C_{total}}}{\bar{m}^2_{C_{total}} + \bar{m}^2_{C,2}} \qquad \bar{p}_{9,B}(\bar{m}_B) = \bar{p}_{9,B_0}\frac{\bar{m}_B}{\bar{m}^2_B + \bar{m}^2_{B,2}}$$

$$\bar{p}_{11}(\bar{m}_C) = 1 - \bar{p}_{11_1}\bar{m}_C \qquad \bar{p}_{12}(\bar{m}_C) = \bar{p}_{12_0}\bar{m}_C \qquad \bar{p}_{13}(\bar{m}_B) = \bar{p}_{13_0} - \bar{p}_{13_1}\bar{m}_B$$

$$\bar{D}_{C_{C,C}}(\bar{m}_C) = \bar{D}_{C_{C,C_0}}\frac{\bar{m}_C}{\bar{m}^2_C + \bar{m}^2_{C,1}} \qquad \bar{D}_{C_{C,B}}(\bar{m}_B) = \bar{D}_{C_{C,B_0}}\frac{\bar{m}_B}{\bar{m}^2_B + \bar{m}^2_{B,1}} \tag{23}$$

$$\bar{D}_{C_{C,Ca}}(\bar{m}_{Ca}) = \bar{D}_{C_{C,Ca_0}}\frac{\bar{m}_{Ca}}{\bar{m}^2_{Ca} + \bar{m}^2_{Ca,1}}$$

$$\frac{1}{\bar{D}_{C_H}(\bar{m})} = \beta^\alpha \left(\frac{\bar{m}_C}{\bar{m}}\right)^\alpha \frac{1}{\bar{D}_{C_{H,C}}(\bar{m}_C)} + \eta^\alpha \left(\frac{\bar{m}_B}{\bar{m}}\right)^\alpha \frac{1}{\bar{D}_{C_{H,B}}(\bar{m}_B)} + \epsilon^\alpha \left(\frac{\bar{m}_{Ca}}{\bar{m}}\right)^\alpha \frac{1}{\bar{D}_{C_{H,Ca}}(\bar{m}_{Ca})}$$

$$\bar{D}_{C_{H,C}}(\bar{m}_C) = \bar{D}_{C_{H,C_0}}\frac{\bar{m}_C}{\bar{m}^2_C + \bar{m}^2_{C,1}} \qquad \bar{D}_{C_{H,B}}(\bar{m}_B) = \bar{D}_{C_{H,B_0}}\frac{\bar{m}_B}{\bar{m}^2_B + \bar{m}^2_{B,1}}$$

$$\bar{D}_{C_{H,Ca}}(\bar{m}_{Ca}) = \bar{D}_{C_{H,Ca_0}}\frac{\bar{m}_{Ca}}{\bar{m}^2_{Ca} + \bar{m}^2_{Ca,1}}$$

$$\frac{1}{\bar{D}_{C_B}(\bar{m})} = \beta^\alpha \left(\frac{\bar{m}_C}{\bar{m}}\right)^\alpha \frac{1}{\bar{D}_{C_{B,C}}(\bar{m}_C)} + \eta^\alpha \left(\frac{\bar{m}_B}{\bar{m}}\right)^\alpha \frac{1}{\bar{D}_{C_{B,B}}(\bar{m}_B)} + \epsilon^\alpha \left(\frac{\bar{m}_{Ca}}{\bar{m}}\right)^\alpha \frac{1}{\bar{D}_{C_{B,Ca}}(\bar{m}_{Ca})}$$

$$\bar{D}_{C_{B,C}}(\bar{m}_C) = \bar{D}_{C_{B,C_0}}\frac{\bar{m}_C}{\bar{m}^2_C + \bar{m}^2_{C,1}} \qquad \bar{D}_{C_{B,B}}(\bar{m}_B) = \bar{D}_{C_{B,B_0}}\frac{\bar{m}_B}{\bar{m}^2_B + \bar{m}^2_{B,1}}$$

$$\bar{D}_{C_{B,Ca}}(\bar{m}_{Ca}) = \bar{D}_{C_{B,Ca_0}}\frac{\bar{m}_{Ca}}{\bar{m}^2_{Ca} + \bar{m}^2_{Ca,1}} \qquad \bar{C}_{C,max_0} + \bar{C}_{B,max_0} = 1 - \bar{C}_{H,max_0}$$

The non-dimensional boundary and initial conditions are:

$$-\bar{D}_{C_C}(\bar{m})\frac{\partial \bar{C}_C}{\partial \bar{x}} = -\bar{D}_{C_H}(\bar{m})\frac{\partial \bar{C}_H}{\partial \bar{x}} = -\bar{D}_{m_C}\frac{\partial \bar{m}_C}{\partial \bar{x}} = -\bar{D}_{m_B}\frac{\partial \bar{m}_B}{\partial \bar{x}} = 0 \tag{24a}$$

$$\bar{C}_B = \bar{C}_{B_0} \qquad \bar{n} = \bar{N}_0 \qquad \bar{g}_{HI} = 1 \qquad \bar{g}_{HS} = \bar{g}_{HM} = 1 \qquad \text{at } \bar{x} = 0$$

$$-\bar{D}_{C_C}(\bar{m})\frac{\partial \bar{C}_C}{\partial \bar{x}} = -\bar{D}_{C_H}(\bar{m})\frac{\partial \bar{C}_H}{\partial \bar{x}} = -\bar{D}_{C_B}(\bar{m})\frac{\partial \bar{C}_C}{\partial \bar{x}} = -\bar{D}_{m_C}\frac{\partial \bar{m}_C}{\partial \bar{x}} = -\bar{D}_{m_B}\frac{\partial \bar{m}_B}{\partial \bar{x}} = 0 \tag{24b}$$

$$\bar{n} = 1 \qquad \bar{g}_{HI} = \bar{g}_{HI_2} \qquad -\bar{D}_{g_{HS}}\frac{\partial \bar{g}_{HS}}{\partial \bar{x}} = \bar{\gamma}_1(\bar{g}_{HS} - \bar{g}_{HS_2})$$

$$-\bar{D}_{g_{HM}}\frac{\partial \bar{g}_{HM}}{\partial \bar{x}} = \bar{\gamma}_2(\bar{g}_{HM} - \bar{g}_{HM_2}) \qquad \text{at } \bar{x} = 1$$

$$\bar{C}_C = \bar{C}_C^{(0)}\bar{h}(\bar{x}) \qquad \bar{C}_B = \bar{C}_{B_0}\bar{h}_1(\bar{x}) \qquad \bar{C}_H = 0 \tag{24c}$$

$$\bar{n} = \bar{N}_0 - (\bar{N}_0 - 1)\bar{x} \qquad \bar{m}_C = \bar{m}_{C,3} \qquad \bar{m}_B = \bar{m}_{B,3} \qquad \bar{m}_{Ca} = 0$$

$$\bar{g}_{HI} = 1 - (1 - \bar{g}_{HI_2})\bar{x} \qquad \bar{g}_{HS} = \bar{g}_{HM} = 1 \qquad \text{at } \bar{t} = 0.$$

The dimensionless parameters and their estimated values are provided in Table 2.

dimensionless parameters		estimated value
chondrocyte migration (or diffusion) coefficient (cartilage)	$\bar{D}_{C_{C,C_0}} = D_{C_{C,C_0}}/(p_{11_0}C_{total,max_0}d^2)$	10^{-3}
chondrocyte migration (or diffusion) coefficient (bone)	$\bar{D}_{C_{C,B_0}} = D_{C_{C,B_0}}/(p_{11_0}C_{total,max_0}d^2\Gamma)$	10^{-3}
chondrocyte migration (or diffusion) coefficient (calcified cartilage)	$\bar{D}_{C_{C,Ca_0}} = D_{C_{C,Ca_0}}/(p_{11_0}C_{total,max_0}d^2\Gamma_1)$	10^{-3}
hypertrophic chondrocyte migration (or diffusion) coefficient (cartilage)	$\bar{D}_{C_{H,C_0}} = D_{C_{H,C_0}}/(p_{11_0}C_{total,max_0}d^2)$	10^{-5}
hypertrophic chondrocyte migration (or diffusion) coefficient (bone)	$\bar{D}_{C_{H,B_0}} = D_{C_{H,B_0}}/(p_{11_0}C_{total,max_0}d^2\Gamma)$	10^{-5}
hypertrophic chondrocyte migration (or diffusion) coefficient (calcified cartilage)	$\bar{D}_{C_{H,Ca_0}} = D_{C_{H,Ca_0}}/(p_{11_0}C_{total,max_0}d^2\Gamma_1)$	10^{-5}
osteoblast migration (or diffusion) coefficient (cartilage)	$\bar{D}_{C_{B,C_0}} = D_{C_{B,C_0}}/(p_{11_0}C_{total,max_0}d^2)$	10^{-6}
osteoblast migration (or diffusion) coefficient (bone)	$\bar{D}_{C_{B,B_0}} = D_{C_{B,B_0}}/(p_{11_0}C_{total,max_0}d^2\Gamma)$	10^{-4}
osteoblast migration (or diffusion) coefficient (calcified cartilage)	$\bar{D}_{C_{B,Ca_0}} = D_{C_{B,Ca_0}}/(p_{11_0}C_{total,max_0}d^2\Gamma_1)$	10^{-4}
cartilage matrix diffusion	$\bar{D}_{m_C} = D_{m_C}m_{C,max}/(p_{11_0}C_{total,max_0}d^2)$	10^{-3}

coefficient		
bone matrix diffusion coefficient	$\bar{D}_{m_B} = D_{m_B} m_{C,max}/(p_{11_0} C_{total,max_0} d^2)$	10^{-5}
nutrient diffusion coefficient	$\bar{D}_n = D_n m_{C,max}/(p_{11_0} C_{total,max_0} d^2)$	100
hypertrophy-inducing signalling molecule diffusion coefficient	$\bar{D}_{g_{HI}} = D_{g_{HI}} m_{C,max}/(p_{11_0} C_{total,max_0} d^2)$	2
hypertrophy-suppressing signalling molecule diffusion coefficient	$\bar{D}_{g_{HS}} = D_{g_{HS}} m_{C,max}/(p_{11_0} C_{total,max_0} d^2)$	0.5
hypertrophy-modulating signalling molecule diffusion coefficient	$\bar{D}_{g_{HM}} = D_{g_{HM}} m_{C,max}/(p_{11_0} C_{total,max_0} d^2)$	0.5
chondrocyte proliferation rate (cartilage)	$\bar{p}_{5,C_0} = p_{5,C_0}/(p_{11_0} C_{total,max_0}/\tau)$	10^{-3}
chondrocyte proliferation rate (bone)	$\bar{p}_{5,B_0} = p_{5,B_0}/(p_{11_0} C_{total,max_0} \Gamma)$	10^{-3}
chondrocyte hypertrophic differentiation rate	$\bar{p}_6 = p_6 m_{C,max}/(p_{11_0} C_{total,max_0})$	5
chondrocyte death rate	$\bar{p}_7 = p_7 m_{C,max}/(p_{11_0} C_{total,max_0})$	1
hypertrophic chondrocyte death rate	$\bar{p}_8 = p_8 m_{C,max}/(p_{11_0} C_{total,max_0})$	1.6
osteoblast proliferation rate (cartilage)	$\bar{p}_{9,C_0} = p_{9,C_0}/(p_{11_0} C_{total,max_0}/\tau)$	5.3×10^{-2}
osteoblast proliferation rate (bone)	$\bar{p}_{9,B_0} = p_{9,B_0}/(p_{11_0} C_{total,max_0} \Gamma)$	5.3×10^{-2}
osteoblast death rate	$\bar{p}_{10} = p_{10} m_{C,max}/(p_{11_0} C_{total,max_0})$	0.2
cartilage matrix degradation rate	$\bar{p}_{11_1} = p_{11_1} m_{C,max}/p_{11_0}$	1
cartilage matrix degradation rate	$\bar{p}_{12_0} = p_{12_0} m_{C,max}/p_{11_0}$	10^4
bone matrix production rate	$\bar{p}_{13_0} = p_{13_0}/(p_{11_0} \eta)$	13
bone matrix degradation rate	$\bar{p}_{13_1} = p_{13_1} m_{C,max}/p_{11_0}$	3×10^{-4}
nutrient uptake rate by chondrocytes	$\bar{p}_{17} = p_{17} m_{C,max}/(p_{11_0} N_1)$	10^4
nutrient uptake rate by osteoblasts	$\bar{p}_{18} = p_{18} m_{C,max}/(p_{11_0} N_1)$	10^4
nutrient uptake rate by hypertrophic chondrocytes	$\bar{p}_{19} = p_{19} m_{C,max}/(p_{11_0} N_1)$	10^4
calcified cartilage matrix degradation rate	$\bar{p}_{20} = p_{20} m_{C,max}/p_{11_0}$	10^5
hypertrophy-suppressing signalling molecule production rate by surface chondrocytes	$\bar{p}_{21} = p_{21} m_{C,max}/(p_{11_0} g_{HS_1})$	4×10^4
hypertrophy-suppressing signalling molecule production rate by hypertrophy-modulating signalling molecule	$\bar{p}_{15} = p_{15} m_{C,max} g_{HM_1}/(p_{11_0} g_{HS_1})$	4×10^4
hypertrophy-suppressing signalling molecule	$\bar{p}_{22} = p_{22} m_{C,max}/(p_{11_0} C_{total,max_0})$	15.47

degradation rate		
hypertrophy-modulating signalling molecule production rate by hypertrophic chondrocytes	$\bar{p}_{23} = p_{23} m_{C,max}/(p_{11_0} g_{HM_1})$	2.3×10^3
hypertrophy-modulating signalling molecule degradation rate	$\bar{p}_{26} = p_{26} m_{C,max}/(p_{11_0} C_{total,max_0})$	15.47
hypertrophy-inducing signalling molecule degradation rate	$\bar{p}_{25} = p_{25} m_{C,max}/(p_{11_0} C_{total,max_0})$	15.47
maximum mature chondrocyte density	$\bar{C}_{H,max_0} = C_{H,max_0}/C_{total,max_0}$	0-1
maximum osteoblast density	$\bar{C}_{B,max_0} = C_{B,max_0}/C_{total,max_0}$	0-1
initial chondrocyte density	$\bar{C}_C^{(0)} = C_C^{(0)}/C_{total,max_0}$	0.25
initial nutrient concentration	$\bar{N}_0 = N_0/N_1$	1-3
threshold nutrient concentration	$\bar{n}_0 = n_0/N_1$	0.24-0.81
critical nutrient concentration	$\bar{n}_1 = n_1/N_1$	0.1
reference cartilage matrix density	$\bar{m}_{C,1} = m_{C,1}/m_{C,max}$	0.1
intermediate cartilage matrix density	$\bar{m}_{C,2} = m_{C,2}/m_{C_{tot},max}$	0.1
reference calcified cartilage density	$\bar{m}_{Ca,1} = m_{Ca,1}/m_{Ca,max}$	0.1
reference bone matrix density	$\bar{m}_{B,1} = m_{B,1}/m_{B,max}$	10^{-2}
intermediate bone matrix density	$\bar{m}_{B,2} = m_{B,2}/m_{B,max}$	10^{-2}
initial cartilage matrix density	$\bar{m}_{C,3} = m_{C,3}/m_{C,max}$	10^{-5}
initial bone matrix density	$\bar{m}_{B,3} = m_{B,3}/m_{B,max}$	10^{-5}
threshold hypertrophy-inducing signalling molecule concentration	$\bar{g}_{HI_0} = g_{HI_0}/g_{HI_1}$	0.5
threshold hypertrophy-suppressing signalling molecule concentration	$\bar{g}_{HS_0} = g_{HS_0}/g_{HS_1}$	20
initial hypertrophy-inducing signalling molecule concentration	$\bar{g}_{HI_2} = g_{HI_2}/g_{HI_1}$	1
hypertrophy-suppressing signalling molecule concentration	$\bar{g}_{HS_2} = g_{HS_2}/g_{HS_1}$	1
hypertrophy-modulating signalling molecule concentration	$\bar{g}_{HM_2} = g_{HM_2}/g_{HM_1}$	1
initial osteoblast density	$\bar{C}_{B_0} = C_{B_0}/C_{total,max_0}$	10^{-2}
maximum cartilage matrix density	$\beta = m_{C,max}/m_{max}$	0.1
maximum bone matrix density	$\eta = m_{B,max}/m_{max}$	1
maximum calcified matrix density	$\epsilon = m_{Ca,max}/m_{max}$	1
ratio maximum bone to cartilage density	$\Gamma = m_{B,max}/m_{C,max}$	10
ratio maximum calcified cartilage to cartilage density	$\Gamma_1 = m_{Ca,max}/m_{C,max}$	10
ratio maximum calcified cartilage	$\tau = m_{Ca,max}/m_{C_{tot,max}}$	1

to total cartilage density		
exponent	α	2
hypertrophy-suppressing signalling molecule flux parameter	$\bar{\gamma}_1 = \gamma_1 d/D_{g_{HS}}$	0
hypertrophy-modulating signalling molecule flux parameter	$\bar{\gamma}_2 = \gamma_2 d/D_{g_{HM}}$	0
critical cartilage matrix density	$\bar{m}_{C,crit}/m_{C,max}$	0.95

Table 2: Estimated values of dimensionless parameters.

3.1. Implementation and simulated case

We use a second order accurate finite-difference discretisation scheme to discretise the spatial variable x in Eqs. 22-24, keeping the time derivative t continuous. The resulting ordinary differential equations are solved in MATLAB (Release 2013a, The MathWorks, Inc., Natick, Massachusetts, United States) using the stiff ODE solver ode15s. The time step was controlled within the solver to maintain the stability of the numerical solutions. The accuracy and convergence of the numerical scheme are formally checked by systematically reducing the mesh size Δx and measuring the error in the solution. Based on this, we choose the mesh size $\Delta x = 5 \times 10^{-3}$ (200 mesh points) to present the numerical solutions below. We confirm that for this choice of Δx the solutions are an accurate reflection of the evolution process and also practical with respect to the computational time taken to run simulations to time equivalent to 48 months.

The dimensionless parameters and their estimated baseline values are provided in Table 2. Initially we have a population of chondrocytes, $\bar{C}_C^{(0)}$, implanted at the base of the defect at the subchondral bone interface ($\bar{x} = 0$), corresponding to an ACI procedure (Lutianov et al. (2011); Campbell et al. (2019a,b)). The initial chondrocyte cell density spatial profile is $\bar{C}_C(x, 0) = \bar{C}_C^{(0)}[1 - \tanh(A(\bar{x} - \bar{x}_0))]/2$, with $A = 10^4$ and $\bar{x}_0 = 0.1$. We also include an initial population of bone cells, $\bar{C}_{B_0}$, assumed to be constant at the subchondral bone interface. The bone cell density spatial profile is $\bar{C}_B(x, 0) = \bar{C}_{B_0}[1 - \tanh(A(\bar{x} - \bar{x}_1))]/2$, with $A = 10^4$ and $\bar{x}_1 = 10^{-3}$. Dimensionally, this corresponds to a chondrocyte density, 2.5×10^5 cells/mm^3, seeded within a region of thickness 500μm near $x = 0$, and zero everywhere else. The initial bone cell density corresponds to 9×10^3 cells/mm^3 present within a region of thickness 5nm near $x = 0$, and zero everywhere else.

We simulate the evolution of chondrocytes, C_C, hypertrophic chondrocytes, C_H, bone cells, C_B, cartilage matrix, m_C, calcified matrix, m_{Ca}, bone matrix, m_B, and nutrients, n, along with signalling molecules, $g_{HS,HM}$.

4. Results and parameter sensitivity analysis

4.1. Numerical results

Figures 4-6 show the evolution of osteochondral defect healing following an ACI procedure, for time ranging from 1 month to 48 months post implantation. As early as 1 month chondrocytes produce cartilage matrix, m_C, and

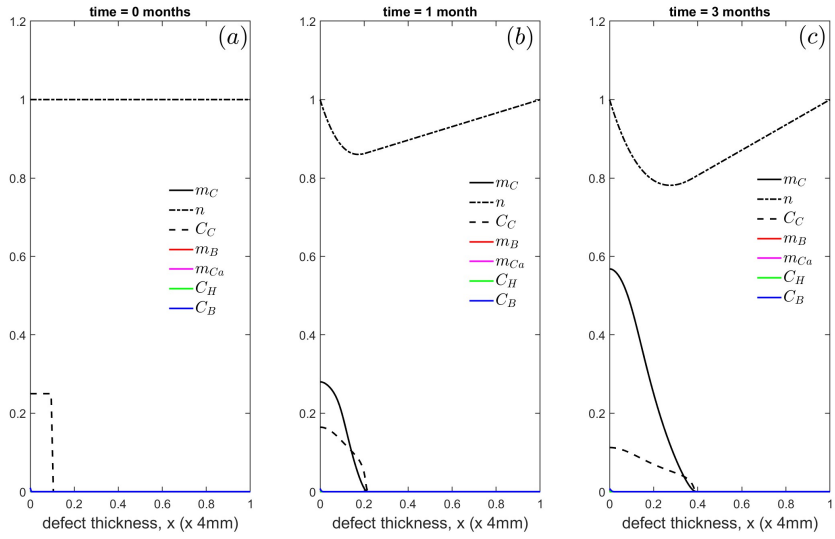

Figure 4: Evolution of cell and matrix densities, and nutrient concentration at (a) t =0 days, (b) $t = 1$ month and (c) $t = 3$ months, following implantation of chondrocytes.

migrate through the matrix towards the top of the defect (Lutianov et al. (2011)). Due to the low proliferation rate of chondrocytes ($\bar{p}_{5,C_0} = 10^{-3}$), migration is their main means of evolution and by 3 months they have extended and deposited cartilage matrix in the bottom half of the defect. These results replicate those of our previous chondral regeneration model, with evolution of cartilage deposition occurring at a fast pace due to high availability of nutrients (Lutianov et al. (2011)). During this initial stage of the regeneration process, a purely chondral regeneration mechanism takes place. At 6 months, m_C is steadily increasing from the base of the defect, with chondrocyte hypertrophy and matrix calcification not yet initiated. As time progresses to 12 months, we observe the defect continuing to fill, with chondrocytes and new cartilage matrix having reached the top of the defect and with a cartilage density over 90% at the defect base (Fig. 5(b)). At the defect base, the critical cartilage matrix density, assumed 95%, is reached at 18 months (Fig. 5(c)). The chondrocytes here start to convert from a proliferative to a hypertrophic state, converting cartilage matrix into calcified matrix, ready to initiate bone production via endochondral ossification (Fig. 5(c)). The hypertrophic chondrocytes convert cartilage matrix at the defect base entirely into calcified matrix, m_{Ca}. Osteoblasts at the defect base further convert this matrix to bone matrix, m_B. The conversion rate of m_C to m_{Ca} and m_{Ca} to m_B is very rapid owing to the large values of $\bar{p}_{12_0} = 10^4$ and $\bar{p}_{20} = 10^5$, therefore m_{Ca} levels observed are very low. This signifies the end of cartilage formation at this location and the beginning of the endochondral ossification process. The modulating and suppressing signalling molecules regulate chondrocyte hypertrophy and cartilage calcification from this time on. At 24 months, our simulations show an upward moving narrow zone where chondrocytes are undergoing hypertrophy and converting cartilage matrix into calcified matrix (Fig. 6(a)). The base of the defect is filled with bone matrix, m_B, with a narrow middle zone of calcified cartilage and a top layer of cartilage that has not yet reached its full density across the top of the defect. As bone matrix was deposited from the defect base, bone cells such as osteoblasts and osteoclasts are able to migrate within this matrix towards the top of the defect. At 36 months, more of the defect has been filled with m_B (Fig.

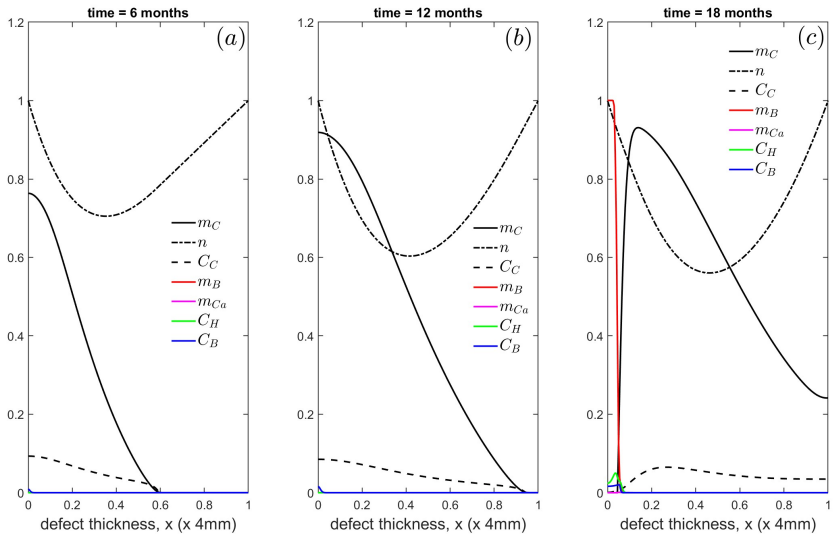

Figure 5: Evolution of cell and matrix densities, and nutrient concentration at (a) $t = 6$ months, (b) $t = 12$ months and (c) $t = 18$ months.

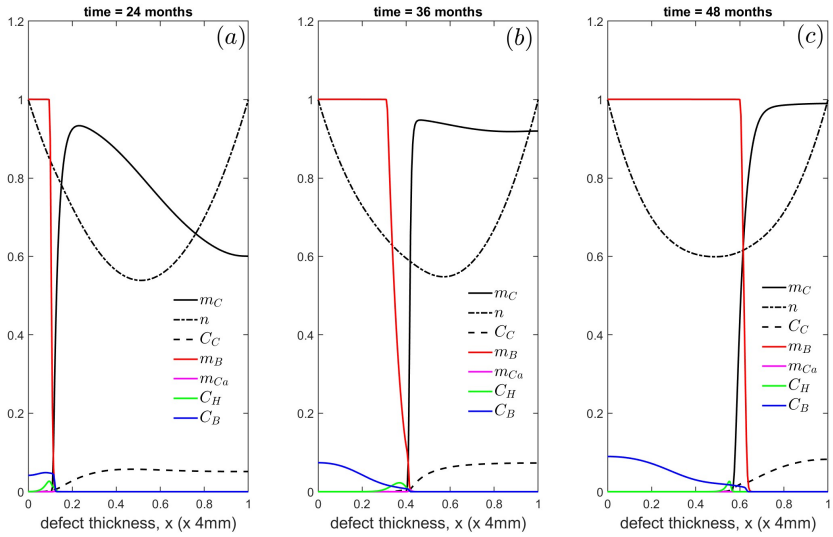

Figure 6: Evolution of cell and matrix densities, and nutrient concentration at (a) $t = 24$ months, (b) $t = 36$ months and (c) $t = 48$ months.

6(b)). The middle zone of active endochondral ossification has moved towards the top, with m_C being remodelled into m_{Ca}, ready for conversion into m_B where bone cells are present (Fig. 6(b)). At the top of the defect, there is a section of cartilage that has not calcified (Fig. 6(b)). This is due to a flux of hypertrophy-suppressing signalling molecule, g_{HS}, diffusing downwards from the top of the defect where it is produced by the surface chondrocytes, both directly and through g_{HM} stimulation of these cells.

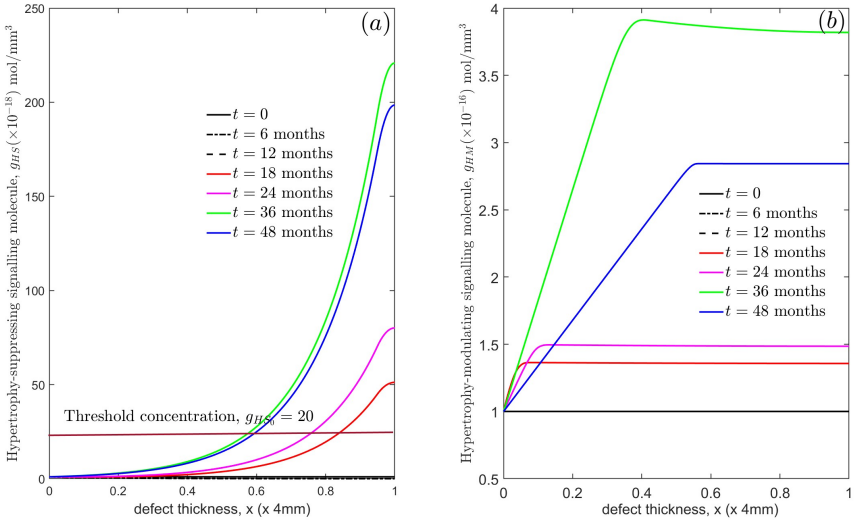

Figure 7: Evolution of the concentration of (a) hypertrophy-suppressing, g_{HS} and (b) hypertrophy-modulating, g_{HM}, signalling molecules from $t = 0 - 48$ months.

Throughout the simulation ($t = 0 - 48$ months), the hypertrophy-inducing molecule g_{HI} concentration remains constant ($g_{HI} = 1$) along the defect height, above its threshold value $\bar{g}_{HI_0} = 0.5$. Hypertrophy is nevertheless suppressed until $t = 18$ months because the cartilage matrix density is below its critical level $m_{Ccrit} = 0.95$, combined with the activity of hypertrophy modifying and suppressing signalling molecules $g_{HS,HM}$ at later times. Figure 7(a, b) show the evolution of $g_{HS,HM}$. The threshold g_{HS} concentration above which hypertrophy is suppressed is $\bar{g}_{HS_0} = 20$, and we assume no-flux of signalling molecules out of the top of the defect ($\bar{\gamma}_1 = \bar{\gamma}_2 = 0$). We observe a progressive build-up of g_{HS} at the top of the defect which diffuses downwards. The region corresponding to $g_{HS} > g_{HS_0}$ is where hypertrophy is suppressed resulting in the formation of non-calcified cartilage. In this zone, chondrocytes are prevented from hypertrophying and endochondral ossification cannot take place. At 36 months the defect is mostly filled with full or near-full-density matrix, whether bone, calcified or cartilage (Fig. 6(b)). As time progresses to 48 months, the defect is now entirely filled with full-density bone and cartilage matrix, signifying the endochondral ossification process has ended and the defect has been repaired (Fig. 6(c)).

4.2. Sensitivity of parameters

The model uses a large number of dimensionless parameters. Their values were derived from literature where possible, but often had a wide range and sometimes values were assumed or guessed. The simulation results may be sensitive to some of these values, potentially indicating their biological significance. On the other hand, if the solution is not sensitive to the exact value of a parameter whose value has been approximated, then this indicates that

the exact value is not important and an approximation suffices. We therefore conducted a sensitivity analysis on parameters deemed to be important for the model, exploring specifically the sensitivity to parameters describing the endochondral ossification process, namely those relating to the signalling molecules and chondrocyte hypertrophy, including the critical cartilage density. In addition, we investigated sensitivity to the parameters whose values were assumed or guessed.

The concentration of hypertrophy-inducing signalling molecule g_{HI} is essentially a linear interpolation between its values at the two boundaries, and as a consequence its effects are very simple. If its concentration is below the threshold g_{HI_0}, hypertrophy is completely suppressed. If its concentration is however above the threshold, as in the base case, hypertrophy is governed by the critical cartilage density and the hypertrophy-suppressing molecule g_{HS} concentration.

Figures $8(a, b, c)$ show the cell and matrix densities at $t = 6$ months for varying critical cartilage matrix densities, $m_{C_{crit}} = 10\%, 50\%, 95\%$, respectively. Decreasing $m_{C_{crit}}$ from 95% to 50% activates chondrocyte hypertrophy much earlier resulting in early calcified matrix and bone formation (Fig. $8(b)$. The initial fill-up of the defect with cartilage is suppressed (Fig. 8, compare (b) and (c)). Further decreasing the critical density to 10%, however, stops

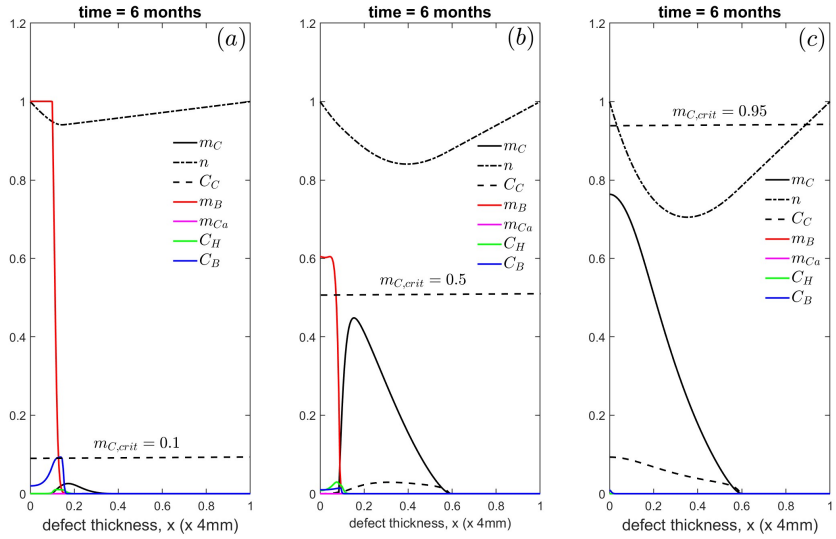

Figure 8: Cell and matrix densities at $t = 6$ months for varying the critical cartilage density, $m_{C,crit}$, at t=6 months. (a) $m_{C,crit} = 0.1$, (b) $m_{C,crit} = 0.5$ (b) and (c) $m_{C,crit} = 0.95$ (baseline value).

the initial fill of the defect with cartilage, with chondrocytes undergoing hypertrophy as soon as $m_{C,crit} > 0.1$ (Fig. $8(a)$). Bone formation begins almost immediately.

Figures $9(a, b)$ show the cell and matrix densities at $t = 48$ months for varying hypertrophy-suppressing signalling molecule threshold concentrations, $\bar{g}_{HS_0}$=20 (baseline), 80, respectively. We observe that increasing $\bar{g}_{HS_0}$, decreases the thickness of the cartilage layer remaining at the top of the defect. This can be explained using Fig. $11(a)$, where increasing the threshold concentration restricts the region where $g_{HS} > \bar{g}_{HS_0}$ to the top of the defect. Here, chondrocyte hypertrophy is suppressed and the endochondral ossification pathway is switched off.

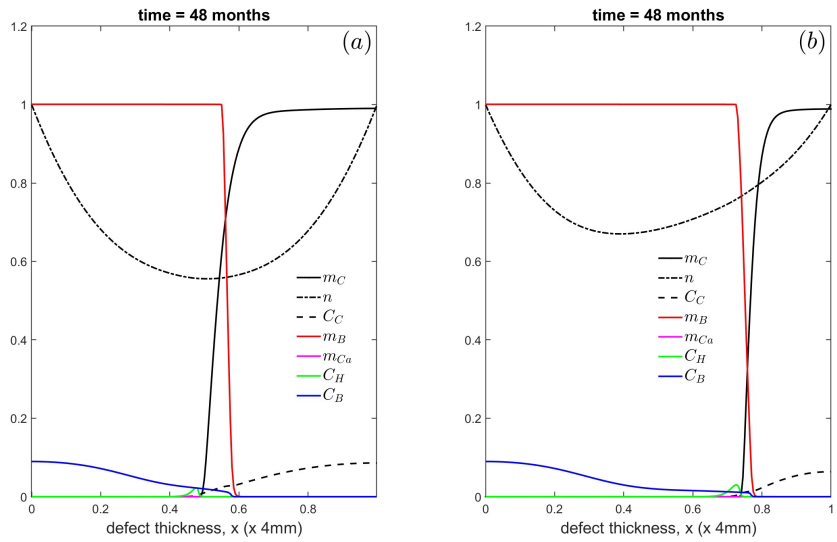

Figure 9: Cell and matrix densities for varying the hypertrophy-suppressing signalling molecule threshold concentration, $\bar{g}_{HS_0}$, at $t = 48$ months. (a) $\bar{g}_{HS_0} = 20$ (baseline value) and (b) $\bar{g}_{HS_0} = 80$.

Figures $10(a, b, c)$ show the cell and matrix densities at $t = 48$ months for varying hypertrophy-suppressing signalling molecule diffusion coefficients, $\bar{D}_{g_{HS}}$=0.5 (baseline), 1 and 5, respectively. We observe that increasing $\bar{D}_{g_{HS}}$ marginally increases the thickness of the cartilage layer remaining at the top of the defect. As $\bar{D}_{g_{HS}}$ is increased, g_{HS} produced by the chondrocytes at the top of the defect can diffuse further into the defect to suppress endochondral ossification. Figures $11(a, b, c)$ show the corresponding evolution of g_{HS} from $t = 0 - 48$ months for $\bar{D}_{g_{HS}}$=0.5 (baseline), 1 and 5, respectively. g_{HS} produced by the chondrocytes at the top of the defect diffuses rapidly through the entire defect as $\bar{D}_{g_{HS}}$ increases, suppressing endochondral ossification.

Figures $12(a, b, c)$ show the cell and matrix densities at $t = 48$ months when varying the g_{HS} flux (via $\bar{\gamma}_1$) leaking from the defect surface. Figures $13(a, b, c)$ show the corresponding g_{HS} concentration for $t = 0 - 48$ months. If the flux from the surface is not too large, then the production of g_{HS} by the surface chondrocytes offsets its removal, and the concentration of g_{HS} is observed to gradually increase (Fig. $13(b)$) albeit much slower than the baseline case (Fig. $13(a)$). This results in the endochondral ossification process continuing until it reaches the top of the defect (Fig. $12(b)$) before the g_{HS} concentration exceeds the threshold concentration to suppress hypertrophy (Fig. $13(b)$). For larger values of the flux, the leaking out of g_{HS} exceeds its production there, and as time progresses its concentration falls below the threshold value (Fig. $13(c)$). This promotes chondrocyte hypertrophy and the osteochondral ossification pathway leading to bone formation right up the top of the defect (Fig. $12(c)$); eventually the defect will fill-up entirely with bone. In this case, at $t = 48$ months there is no longer an intact layer of cartilage at the top of the defect, unlike the baseline case shown in Fig. $12(a)$.

Figures $14(a, b)$ show the cell and matrix densities at $t = 48$ months for varying hypertrophy-suppressing signalling molecule production rates by surface chondrocytes, both the default rate $\bar{p}_{21}$ and its modification via the hypertrophy-modifying molecule g_{HM}, namely $\bar{p}_{15}$. Figures $15(a, b)$ show the corresponding evolution of g_{HS} concentration for $t = 0 - 48$ months. For lower values of $\bar{p}_{15}$ and $\bar{p}_{21}$ compared to the baseline value, the production of g_{HS} by

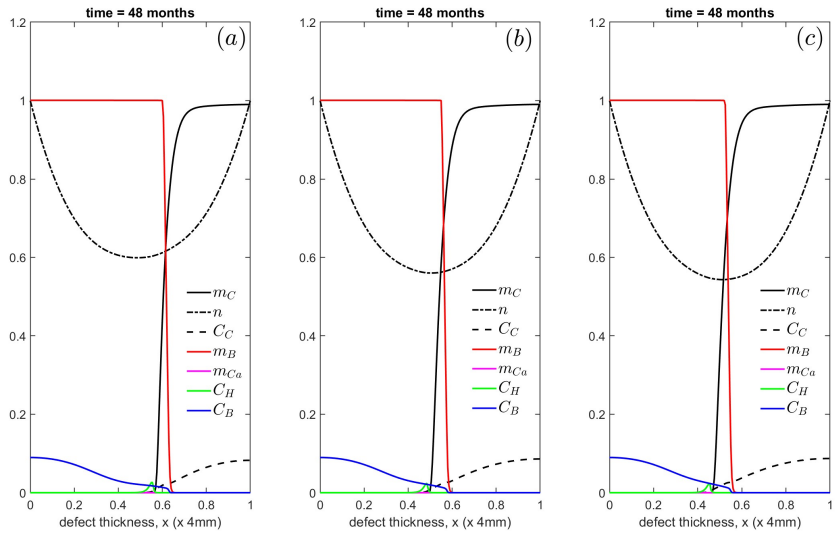

Figure 10: Cell and matrix densities for varying hypertrophy-suppressing signalling molecule diffusion coefficients, $\bar{D}_{g_{HS}}$, at $t = 48$ months. (a) $\bar{D}_{g_{HS}} = 0.5$ (baseline value), (b) $\bar{D}_{g_{HS}} = 1$ and (c) $\bar{D}_{g_{HS}} = 5$.

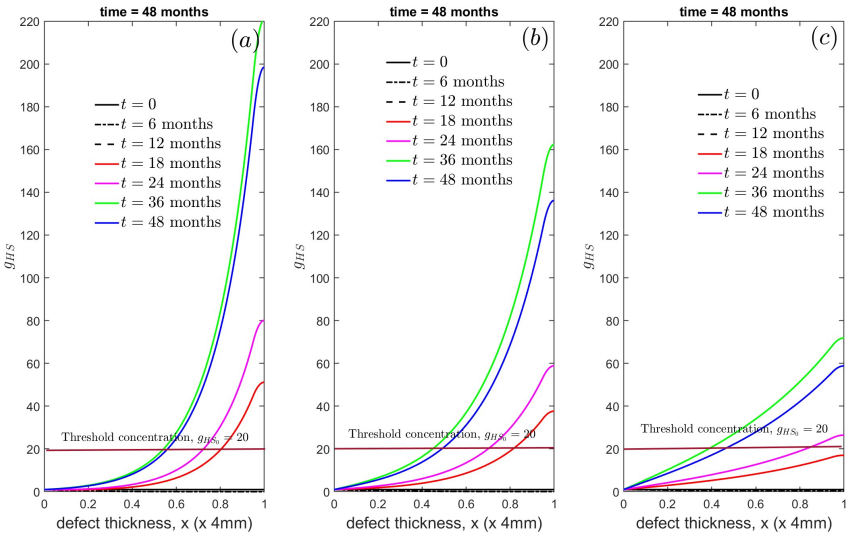

Figure 11: Evolution of g_{HS} for varying hypertrophy-suppressing signalling molecule diffusion coefficients, $\bar{D}_{g_{HS}}$, between $t = 0 - 48$ months. (a) $\bar{D}_{g_{HS}} = 0.5$ (baseline value), (b) $\bar{D}_{g_{HS}} = 1$ and (c) $\bar{D}_{g_{HS}} = 5$.

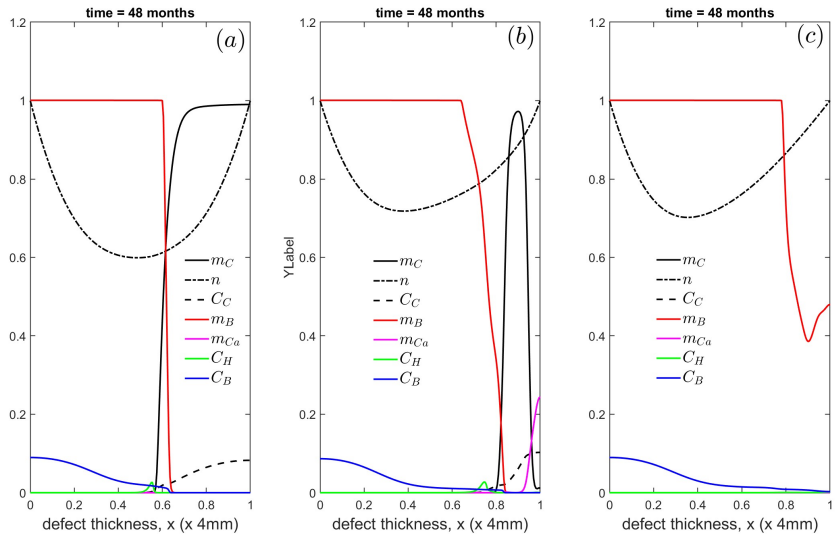

Figure 12: Cell and matrix densities at $t = 48$ months for varying g_{HS} flux via $\bar{\gamma}_1$ out of the top of the defect at $x = 1$. (a) $\bar{\gamma}_1 = 0$ (baseline value), (b) $\bar{\gamma}_1 = 10^2$ and (c) $\bar{\gamma}_1 = 10^3$.

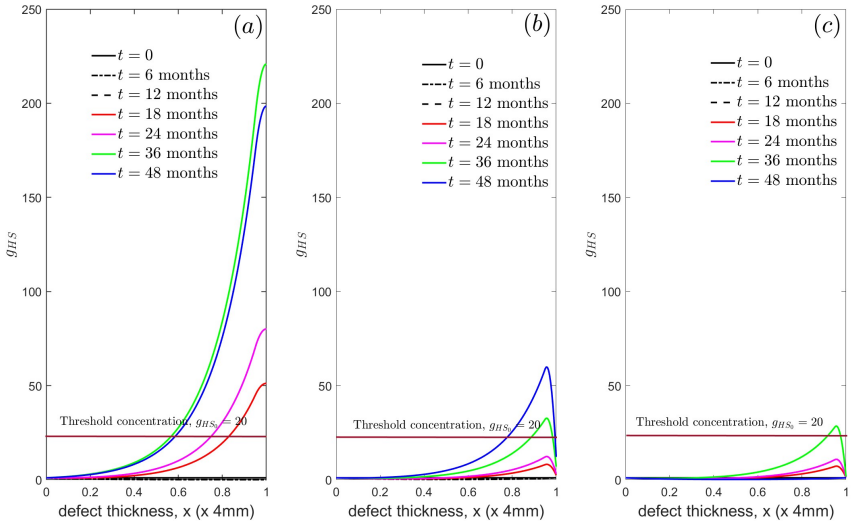

Figure 13: Evolution of g_{HS} between $t = 0 - 48$ months for varying g_{HS} flux via $\bar{\gamma}_1$ out of the top of the defect at $x = 1$. (a) $\bar{\gamma}_1 = 0$ (baseline value), (b) $\bar{\gamma}_1 = 10^2$ and (c) $\bar{\gamma}_1 = 10^3$.

the surface chondrocytes is not sufficient to overcome its degradation ($p_{22} = 15.47$), hence g_{HS} stays below the threshold value at all times (Fig. 15(a)) promoting hypertrophy and osteochondral ossification with bone filling-up the defect (Fig. 14(a)). Increasing $\bar{p}_{15}$ and $\bar{p}_{21}$ above a threshold value results in the production of g_{Hs} offsetting its degradation, allowing it to cross the threshold concentration to suppress hypertrophy and osteochondral ossification to form a cartilage layer at the top of the defect. Increasing (decreasing) the hypertrophy-suppressing signalling

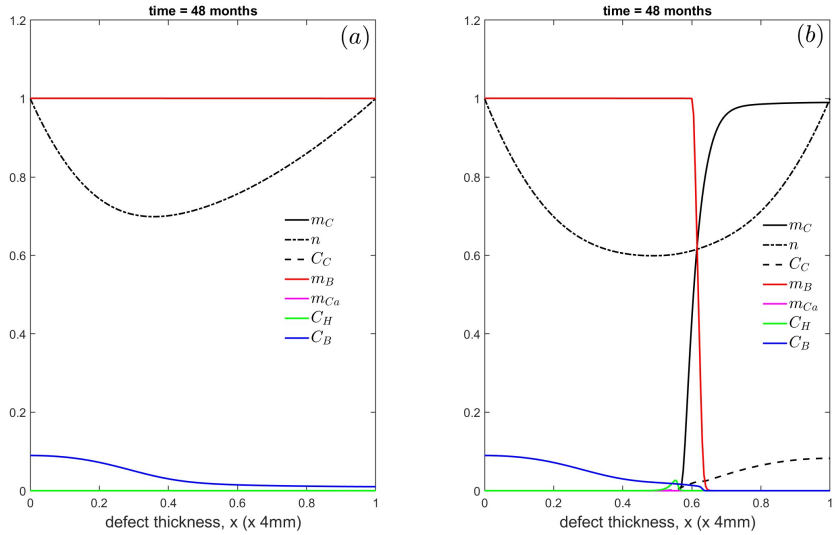

Figure 14: Cell and matrix densities for varying the hypertrophy-suppressing signalling molecule production rates by surface chondrocytes, $\bar{p}_{15}$ and $\bar{p}_{21}$, at $t = 48$ months. (a) $\bar{p}_{15} = \bar{p}_{21} = 10^2$ and (b) $\bar{p}_{15} = \bar{p}_{21} = 4 \times 10^4$ (baseline).

molecule degradation rate, $\bar{p}_{22}$, relative to p_{15} and p_{21} results in lower (higher) concentrations of $\bar{g}_{HS}$ within the defect. The results are similar to the behaviour observed in Figs. 14,15, hence we do not report them here in more detail.

Similarly, increasing (decreasing) the hypertrophy-modulating signalling molecule degradation rate, $\bar{p}_{26}$, results in lower (higher) concentrations of $\bar{g}_{HM}$ within the defect. This modulates the production of g_{HS} by surface chondrocytes. The behaviour is again similar to that shown in Figs. 14,15. Figures 16(a, b, c) show the cell and matrix densities at $t = 48$ months when varying the chondrocyte hypertrophic differentiation rate, $\bar{p}_6$. This parameter does not significantly influence the results, except a visible increase in C_H (Fig. 16(b, c)). Figures 17(a, b, c) show the cell and matrix densities at $t = 48$ months when varying the osteoblast proliferation rate, $\bar{p}_9$. Increasing $\bar{p}_9$ increases the bone cell density although the bone matrix density does not increase as much. Decreasing $\bar{p}_9$ results in less bone matrix due to lower bone cell density. Figures 18(a, b) show the cell and matrix densities at $t = 48$ months when varying the cartilage matrix degradation rate, $\bar{p}_{12_0}$. Increasing $\bar{p}_{12_0}$ results in rapid m_C degradation into m_{Ca}, although bone production remains relatively unchanged.Decreasing $\bar{p}_{12_0}$ leads to low m_{Ca} levels due to less cartilage degradation. The bone matrix levels remaining fairly unchanged since m_{Ca} conversion to m_B pathway is unaffected by varying $\bar{p}_{12_0}$.

Figures 19($a - d$) show the cell and matrix densities at $t = 48$ months when varying the calcified cartilage matrix degradation rate, $\bar{p}_{20}$. Increasing $\bar{p}_{20}$ enhances bone production, resulting in lower m_{Ca}, as bone remodelling is

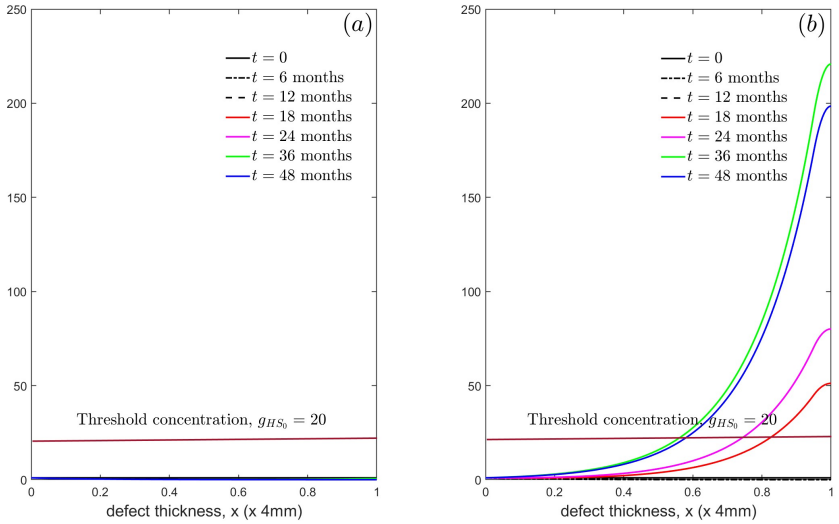

Figure 15: Evolution of g_{HS} for varying the hypertrophy-suppressing signalling molecule production rates by surface chondrocytes, $\bar{p}_{15}$ and $\bar{p}_{21}$, between $t = 0 - 48$ months. (a) $\bar{p}_{15} = \bar{p}_{21} = 10^2$ and (b) $\bar{p}_{15} = \bar{p}_{21} = 4 \times 10^4$ (baseline).

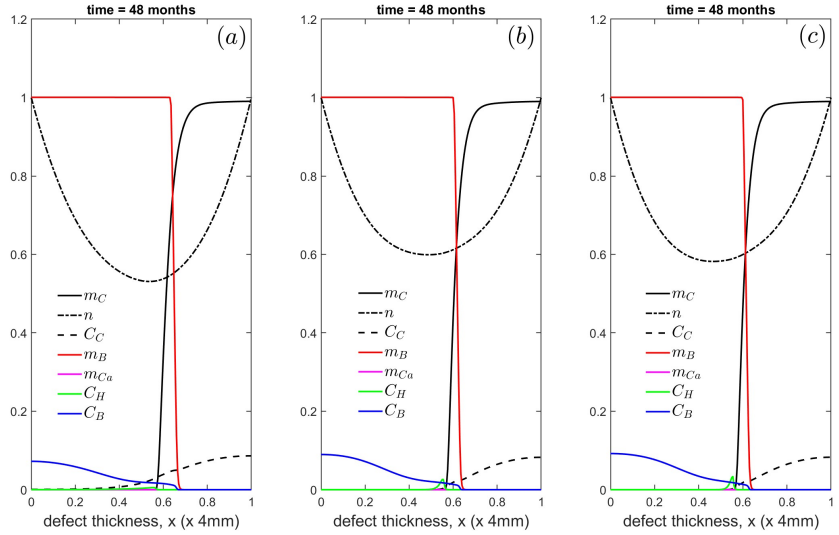

Figure 16: Cell and matrix densities for varying the chondrocyte hypertrophic differentiation rate, $\bar{p}_6$, at $t = 48$ months. (a) $\bar{p}_6 = 0.1$, (b) $\bar{p}_6 = 5$ (baseline) and (c) $\bar{p}_6 = 10$.

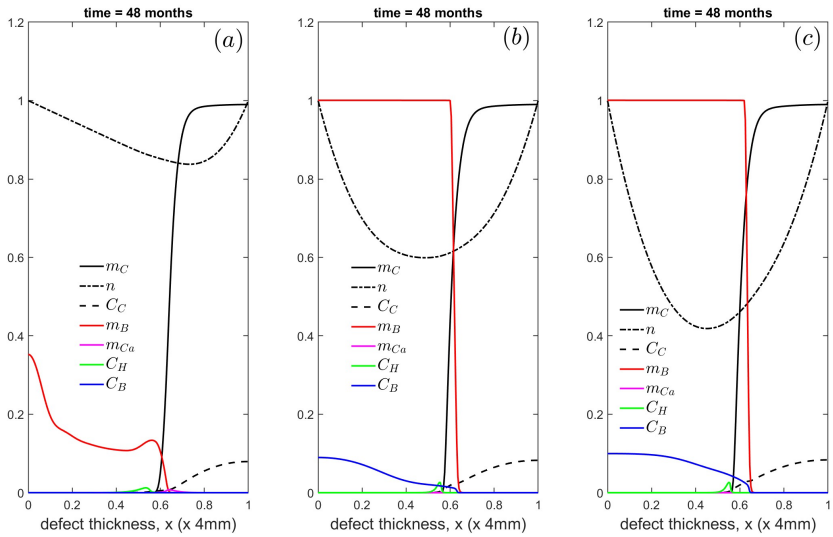

Figure 17: Cell and matrix densities for varying the osteoblast proliferation rate, $\bar{p}_9$ at $t = 48$ months. (a) $\bar{p}_9 = 10^{-3}$, (b) $\bar{p}_9 = 5.3 \times 10^{-2}$ (baseline) and (c) $\bar{p}_9 = 0.1$.

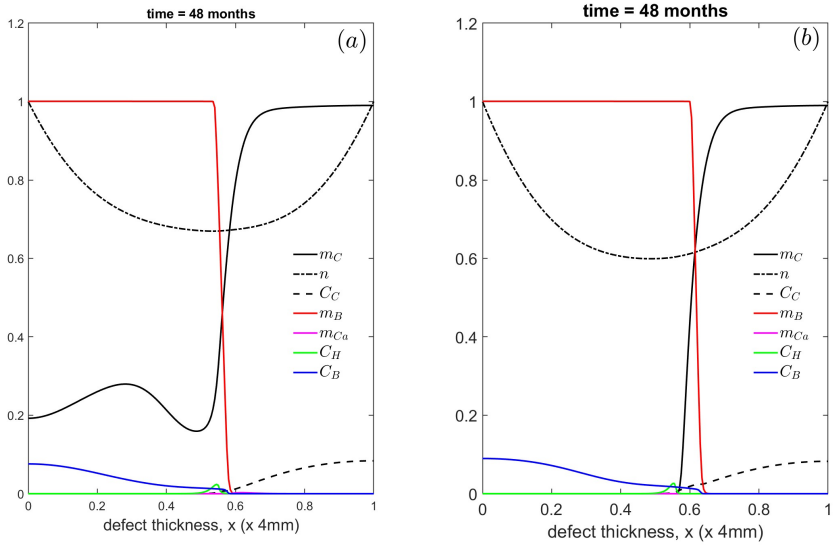

Figure 18: Cell and matrix densities for varying the cartilage matrix degradation rate, $\bar{p}_{12_0}$ at $t = 48$ months. (a) $\bar{p}_{12_0} = 10$ and (b) $\bar{p}_{12_0} = 10^4$ (baseline).

increased (Figs. $19(c,d)$). Decreasing $\bar{p}_{20}$ results in higher m_{Ca}, but bone matrix levels appear unchanged. In this case, bone is predominantly being produced by C_B. Figures $20(a,b,c)$ show the cell and matrix densities at

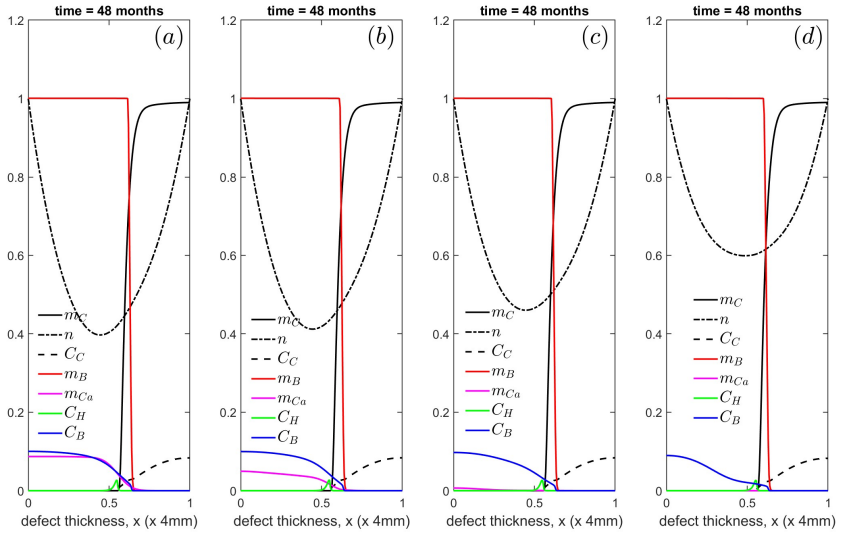

Figure 19: Cell and matrix densities for varying the calcified cartilage matrix degradation rate, $\bar{p}_{20}$ at $t = 48$ months. (a) $\bar{p}_{20} = 1$, (b) $\bar{p}_{20} = 10$, (c) $\bar{p}_{20} = 10^2$ and (d) $\bar{p}_{20} = 10^5$ (baseline).

$t = 48$ months when varying the chondrocyte proliferation rate, $\bar{p}_{5,C_0}$. For smaller values of $\bar{p}_{5,C_0}$, the proliferation of chondrocytes is not sufficient to trigger hypertrophy and osteochondral ossification, therefore the bone repair process is delayed (Fig. $20(a)$). In comparison, for larger values of $\bar{p}_{5,C_0}$, there is an adequate supply of proliferating chondrocytes to trigger the pathways for bone and cartilage production (Figs. $20(b,c)$. However, if $\bar{p}_{5,C_0}$ is very large then production of chondrocytes is also extremely high as observed in Fig. $20c$, which seems biologically unrealistic. Figures $21(a,b,c)$ show the cell and matrix densities at $t = 48$ months for varying the hypertrophic chondrocyte death rate, $\bar{p}_8$. Increasing $\bar{p}_8$ results in lower C_H levels as they degrade faster (Fig. $21(b,c)$), leading to less conversion of m_C to m_{Ca}. We observe slightly higher bone density at the base of the defect and more cartilage remaining in the defect. Decreasing $\bar{p}_8$ results in higher C_H levels and slightly higher m_{Ca}, but m_B appears unaffected.

5. Discussion

This paper aims to formulate a reaction-diffusion mathematical model describing the osteochondral defect healing process in large animals such as humans after ACI. The two specific questions to be addressed by the model are (a) Can the PTHrP-Ihh feedback loop control endochondral ossification in the healing process in large animals, and (b) Which key parameters most influence the healing process, in particular controlling the thickness of the articular cartilage in the repaired defect? Our model achieved the overall aim and simulated the key stages of natural osteochondral defect healing as observed in a large animal experiment, namely an initial fill of the defect by cartilage, followed by a process of endochondral ossification starting at the base of the defect that resulted in bone formation from the base upwards, eventually leaving a layer of articular cartilage at the top of the defect

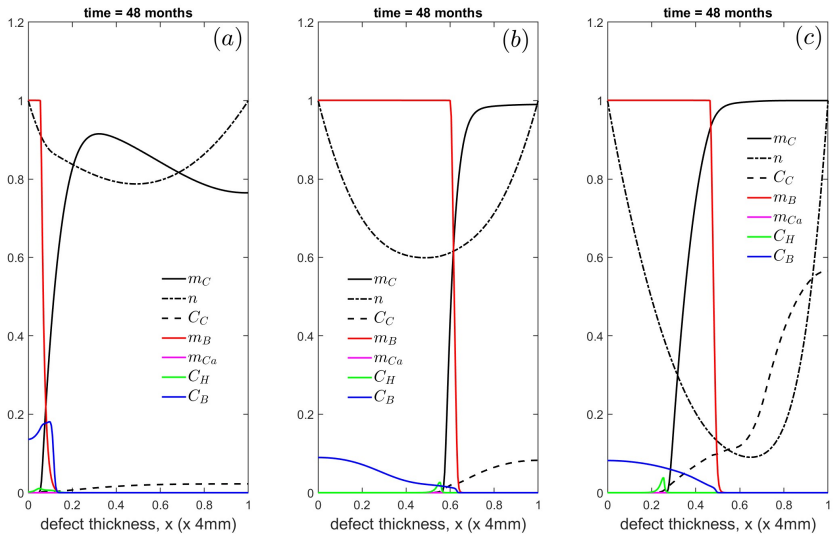

Figure 20: Cell and matrix densities for varying the chondrocyte proliferation rate, $\bar{p}_{5,C_0}$ at $t = 48$ months. (a) $\bar{p}_{5,C_0} = 10^{-3}$, (b) $\bar{p}_{5,C_0} = 0.012$ (baseline) and (c) $\bar{p}_{5,C_0} = 0.1$.

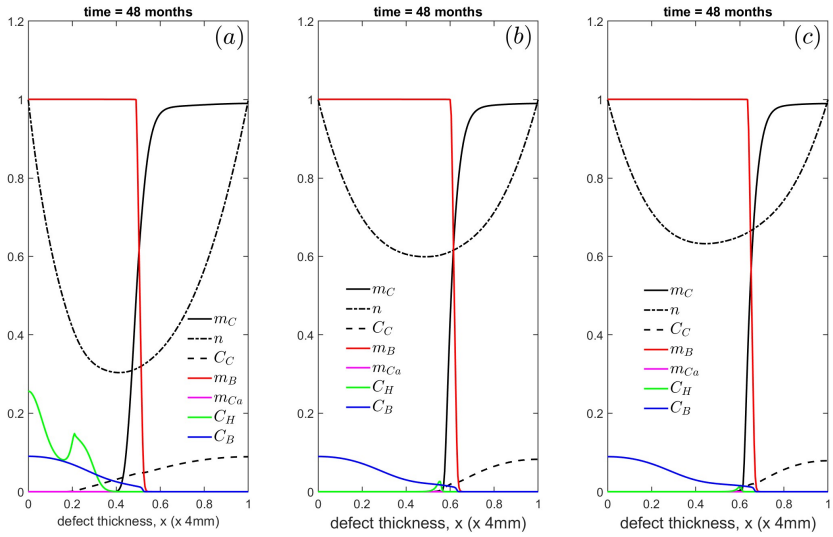

Figure 21: Cell and matrix densities for varying the hypertrophic chondrocyte death rate, $\bar{p}_8$ at $t = 48$ months. (a) $\bar{p}_8 = 0$, (b) $\bar{p}_8 = 0.5$ (baseline) and (c) $\bar{p}_8 = 1$.

separated from the bone by a thin layer of calcified cartilage (Lydon et al. (2019)). Our model thus demonstrates how an osteochondral defect, when treated by implanting chondrocytes under a patch covering the defect, heals in a way that bone and cartilage are regenerated. In doing so, the model therefore suggests that the PTHrP-Ihh feedback loop can indeed control endochondral ossification in large animals. The parameters most strongly influencing the healing process were the local factor relating to hypertrophy induction (critical cartilage density) and those related to the hypertrophy suppressing signalling molecule (PThRP), namely its baseline production rate and the modification of that production rate by the hypertrophy modifying signalling molecule (Ihh) and its surface flux.

In formulating our mathematical model, we made extensive use of the qualitative insights from a series of experiments based around an ovine model of natural osteochondral defect healing in skeletally mature animals (Lydon et al. (2019)). We did so for two main reasons. Firstly, the sheep is a relatively large animal with a knee anatomy comparable to that of humans, which makes this animal model closer to the clinical situation than for instance murine or laprine models (Ahern et al. (2009); Chu et al. (2010)). Secondly, Lydon et al. (2019) analysed 5 separate time points (1-2 weeks, 4-8 weeks, 8-12 weeks, 18 weeks and 26 weeks). Such a detailed study of the healing process over time is not uncommon when conducted using small animals (e.g. Shapiro et al. (1993); Anraku et al. (2008)), but is unique when conducted in large animals. Of course, we realise that the process by which a freshly created osteochondral defect naturally heals is not necessarily the same as that by which a clinical osteochondral defect in humans, treated using autologous chondrocytes, heals. Nevertheless, the key stages observed are also seen following chondrocyte implantation. Filling of the complete defect by cartilage or cartilage-like tissue, followed by bone forming from the base of the defect upwards, has been observed in large-animal models of ACI therapy (e.g. Munirah et al. (2007); Jurgens et al. (2013)). After one year, osteochondral defects up to 1 cm deep in humans and treated with ACI demonstrate new bone formation at the base and a layer of mature (hyaline) or immature cartilage at the top (Bentley et al. (2003)).

Our chondral defect healing models (Campbell et al. (2019a,b)) simulate the filling of a defect with cartilage, but do not simulate the conversion of cartilage into bone at the base of the defect. Lydon et al. (2019) observed that this process occurs via endochondral ossification, similar to the process observed during bone formation in the growth plate or during fracture healing. The current work therefore primarily focused on the endochondral ossification process. In this process, cartilage converts into bone via chondrocyte hypertrophy, where the hypertrophic chondrocytes form a primary spongiosa which is then invaded and remodelled by osteoblasts and osteoclasts (Lydon et al. (2019)). Crucially, not all chondrocytes hypertrophy and form primary spongiosa; a layer of hyaline cartilage is left in the top section of the defect, forming articular cartilage.

In our mathematical model we approached this by concentrating on key regulatory pathways that control chondrocyte hypertrophy during growth. Specifically, we concentrated on factors that initiate and suppress this process. Chondrocyte hypertrophy is known to be initiated by systemic factors (hormones) and locally produced signalling molecules (Mackie et al. (2011); Kozhemyakina et al. (2015)). The hypertrophy-inducing factor in our model represents the systemic factors, a prime example of which is thyroid hormone (Mackie et al. (2011)). We modelled these systemic factors as a flux coming in from the top and base of the defect. We assumed that this hypertrophy-inducing systemic factor would have to reach a threshold value before initiating hypertrophy. The local factors

were represented in our model as a critical or threshold cartilage density, below which hypertrophy is not initiated. This implementation of local factors is similar to that used in models of endochondral ossification during fracture healing (Carlier et al. (2016); Geris et al. (2008)). We chose the critical density to be around 95%, but also investigated other values in our sensitivity analysis. Both critical values would need to be reached before chondrocyte hypertrophy was initiated. In our model, the process was dominated by the local factor (critical cartilage density): once this density was reached, chondrocytes started to hypertrophy and produce calcified matrix from the cartilage model. These two processes would also halt local chondrocyte proliferation and cartilage matrix formation.

Further regulation of hypertrophy, once initiated, was implemented in our model as the Ihh-PTHrP pathway (Kronenberg (2003); Kozhemyakina et al. (2015)). The Ihh-PTHrP pathway is not only a key regulator of chondrocyte hypertrophy, but also important in relation to the question ~~why bone forms in the bottom section but not the top section of an~~ what controls the thickness of the eventual articular cartilage layer at the top of a healed osteochondral defect. PTHrP, a suppressor of hypertrophy, is produced by proliferating chondrocytes in the growth plate and restricted to chondrocytes in the superficial zone of articular cartilage (Chen et al. (2008); Jiang et al. (2008); Kronenberg (2003)). In articular cartilage, the primary regulation of PTHrP is in the form of mechanical loading (Chen et al. (2008)). Its production is also stimulated by Ihh, which is produced by pre-hypertrophic chondrocytes. In our model, we called Ihh a hypertrophy-modulating signalling molecule and assumed it would be produced by hypertrophic chondrocytes. To simulate the production of PTHrP specifically by superficial zone chondrocytes, we ~~modelled a flux of hypertrophy-suppressing signalling molecule that permeated from the upper layer of the defect. Due to its low diffusion coefficient, this growth factor only penetrated the top layer of the simulated defect~~ restricted its production to the upper 10% of the defect. The effects of PTHrP at the top of the defect were the main factor regulating the remaining cartilage layer. The hypertrophic chondrocytes produced calcified matrix, which then was converted to bone by osteoblasts and osteoclasts, simply referred to as 'osteoblasts' in our model. Finally, we assumed the underlying bone at the base of the defect and the surrounding synovial fluid at the top of the defect to provide nutrients within the model. This was unlike our previous mathematical model of a healing chondral defect treated by ACI, where we assumed the flux of nutrient from the base equals zero because subchondral bone is left intact in this treatment, preventing nutrient flow from the defect base.

In combination, this relatively simplistic approach captivates the key mechanisms driving osteochondral healing after ACI via an endochondral ossification-like process. Our model would not be valid for deep osteochondral defects where a bone-plug may be a more appropriate treatment strategy (de Windt and Saris (2014)). However, osteochondral defects with a bone defect up to 1cm in depth can be treated using cell therapy alone (Bentley et al. (2003)). Data from the German Cartilage Registry suggest that using cell therapy alone for osteochondral defects is indeed common practice: although over 60% of defects in this registry are osteochondral defects only 1 in 9 ACI cases use bone graft augmentation (Niemeyer et al. (2016)).

During the initial phase of regeneration, a purely chondral healing mechanism took place. These results corresponded to our chondral defect healing model (Campbell et al. (2019a,b)), with slightly improved matrix formation due to the nutrients available from the base of the defect. These models of chondral defect healing assumed no nutrients would flow in from the base, leading to a lack of nutrients constraining cell proliferation and matrix deposition.

By 1 year, cartilage filled the osteochondral defect, with low-density cartilage matrix at the top of the defect and a high-density matrix covering the base. By 18 months the critical cartilage density required for initiation of chondrocyte hypertrophy was reached at the defect base, initiating the conversion of cartilage to calcified matrix by hypertrophic chondrocytes followed by formation of bone. As time continued, cartilage continued to be converted into calcified matrix with bone subsequently being produced, progressing as a traveling wave upwards to the top. This pattern of conversion predicted by our model ~~followed~~ qualitatively mirrored the formation of bone and cartilage in sheep observed by Lydon et al. (2019). By 2 years the layer of cartilage that would remain at the top of the defect became more evident, with bone entirely covering the base of the defect and cartilage degradation to calcified matrix occurring in the midsection. This trend continued until 48 months, when the defect was entirely filled with new bone, aside from a section of calcified matrix and a thin layer of cartilage remaining at the top of the defect. The thickness of this layer was mainly regulated by the ~~diffusion coefficient of the hypertrophy-suppressing signalling molecule, which was produced by the chondrocytes at the top of the defect~~ parameters related the the hypertrophy-suppresing signalling molecule (PThRP), in particular its production rate (partly influenced by Ihh), its threshold level and its leakage from the top of the healing defect into the synovial fluid.. Including a population of superficial zone chondrocytes (at $\bar{x}$=0.9-1) producing hypertrophy-suppressing molecules was based on experimental observations *in vitro* by Jiang et al. (2008) and *in vivo* by Chen et al. (2008), who found that superficial zone chondrocytes in articular cartilage produce PThRP, which suppresses mineralisation of chondrocytes in deeper zones. Chen et al. (2008) also showed that mechanical loading is an important regulator of PTHrP expression in articular cartilage, but this is something we did not consider here.

The main conclusion from this work is that the Ihh-PThRP feedback loop can play a role in osteochondral healing in large animals, and that the main determinant of the resulting cartilage is related to the hypertrophy-suppressing molecule PThRP. So far, research on the role of PTHrP in post-natal osteochondral healing has been restricted to transgenic mice, needed to visualise its expression levels Chen et al. (2008). However, with the recent rapid advance in spatial transcriptomic and proteomic profiling techniques Moffitt et al. (2022), studying the expression of PThRP should now also be possible in large animals.

The assumptions we made in this model do simplify the biological process occurring during osteochondral healing, potentially limiting conclusions we can draw from this work. An important factor we do not consider directly in our model is the influence of mechanical forces on cells, in particular on cell proliferation, differentiation and matrix synthesis, which earlier mathematical models suggest to be important in chondral defect repair (Lacroix and Prendergast (2002)). Mechanical loading is also thought to influence the patterns of endochondral ossification, specifically in the formation of long bones (Wong and Carter (1990)). However, by assuming that superficial zone chondrocytes produced a hypertrophy-suppressing signaling molecule (PTHrP), we did implicitly include the effect of mechanical loading. We also excluded the effects of other local signalling molecules, in particular the influence of the fibroblast growth factor (FGF18) and C-type natriuretic peptide (CNP), which together with PTHrP and Ihh control the initiation of hypertrophy, and insulin-like growth factor (IGF1), epidermal growth factor receptor (EGFR) and reactive oxygen species (ROS), which control the later phases of chondrocyte hypertrophy (Kozhemyakina et al. (2015)). We completely ignored the latter three and simply assumed that once initiated, chondrocyte hypertrophy

would proceed autonomously. We consider this assumption justified in light of our main aim to capture the main characteristics of the repair process. Instead of FGF18/CNP signaling we used the critical cartilage density $m_{C,crit}$ as an extra local hypertrophy initiating factor, following earlier mathematical models of healing bone fractures (Carlier et al. (2016); Geris et al. (2006)). Although this simplifies the model, the effect is probably similar. FGF18 and CNP have an antagonistic effect on chondrocytes, with FGF18 produced by superficial zone chondrocytes and maintaining chondrocyte proliferation versus CNP produced by proliferating and pre-hypertrophic chondrocytes. There is no feedback control between these two molecules and hypertrophy is assumed to start once CNP levels are high enough relative to FGF18 (Kozhemyakina et al. (2015)). Effectively, our model used cartilage density as a proxy for CNP concentration. Although modelling FGF18 and CNP separately might affect the results, the change is most likely minor due to the lack of feedback. Lydon et al. (2019)describe initial cartilage formation occurring at the top edges of the defect adjacent to damaged cartilage. The reason cartilage first forms here is unknown, but could possibly be related to chondrocytes attaching preferentially to damaged cartilage rather than bone. In our 1-dimensional model we had to omit this preferential attachment to top edges of the defect because these edges were not represented. This simplification meant we also did not include the invasion of cells from the sides of the defect. In addition, when an osteochondral defect is created, damaged blood vessels nested within bone at the site of the defect are damaged. These damaged vessels produce blood which coagulates and forms a fibrous clot within the defect. This fibrous clot will act as a nutrient source at the beginning of regeneration, as well as acting as a scaffold for cells to travel along. These functions of a clot were not explicitly modelled in our work, and neither was clot formation.

We also did not consider mesenchymal stem cells to be present in this model, despite their well-documented role in osteochondral defect healing (Madry et al. (2011); Farmer et al. (2001); Getgood et al. (2012)). Lutianov et al. (2011) explore the effects of autologous chondrocyte implantation (ACI) and articular stem cell implantation (ASI) in chondral defects, which are surgical procedures where either chondrocytes or MSCs are inserted into a defect with the hope to promote healing. In that work, despite MSCs achieving higher cartilage formation at early time, overall healing time did not significantly change (Lutianov et al. (2011)). In Campbell et al. (2019a,b), we explored the effects of signalling molecules on the chondral healing process, and also how a co-implantation of MSCs and chondrocytes could promote an earlier healing time. Our work demonstrated that within the first year an enhanced rate of healing was observed when a co-implantation procedure was carried out, with an increase of up to 136% at 3 months when compared with ACI cartilage healing alone, but despite this, an earlier healing time was not achieved; the conclusion of this work was that a co-implantation procedure could have benefits by allowing a patient to become mobile sooner after surgery. The consideration of MSCs in our model could lead to MSC differentiation into chondrocytes or osteoblasts and having trophic effects, requiring extra assumptions around the control of their differentiation into osteoblasts and the mutual effect of osteoblasts and MSCs. However, based on our models of co-implanting MSCs and chondrocytes, it is doubtful whether the effects on the amount of cartilage formation would be large. MSCs may also influence the healing environment via their production of paracrine factors such as transforming growth factor /*beta* (TGF/*beta*), insulin-like growth factor 1 (IGF1), and vascular endothelial growth factor (VEGF), among others, which may influence cell function and survival and

subsequent tissue regeneration (Fontaine et al. (2016); Linero and Chaparro (2014)). It is thought MSCs may be most effective within tissue regeneration via their paracrine signalling, not their direct contribution to extracellular matrix production via differentiation to osteoblasts and chondrocytes. Based on the findings in Campbell et al. (2019a,b) on the paracrine effect of MSCs, we think it is instructive to start the modelling process by including only chondrocytes and osteoblasts.

Finally, our 1-dimensional model may capture the essential features of osteochondral healing but it is probably too simplistic for proper parameter identification. We regard this model as a first step to get these essential features in place, but a comparison to animal or human experiments will probably require a geometrically more realistic model, for instance a 2-dimensional axi-symmetric model. Given the crucial importance of the hypertrophy-suppressing signalling molecule PThRP, further work should include determining its concentration or expression levels in large animal models. Thanks to modern spatial proteomic or transcriptomic techniques this should be feasible (Moffitt et al. (2022)).

In future work, the inclusion of the modulatory effects of MSCs via their paracrine signalling would more accurately simulate the cell environment, such as the chondrocyte-MSC interaction modulated by FGF-1 and BMP-2 modeled in Campbell et al. (2019a,b).

In conclusion, our mathematical model suggests that repair of osteochondral defects following chondrocyte implantation relies on endochondral ossification processes similar to the growth plate. The reaction diffusion-type model presented here is a first step towards better understanding of osteochondral defect regeneration after cell therapy techniques.

Declaration of Competing Interest

The authors declare that there are no known competing interests that could have influenced the work reported in this paper.

Acknowledgements

This work was a part of KC's PhD research at Keele University (Campbell (2019)) supervised by SN and JH-K. Kelly gratefully acknowledges financial support from Keele University. JH-K gratefully acknowledges financial support from the Medical Research Council (MR/L010453/1 and MR/N02706X/1) and Versus Arthritis (Grants 18480 and 21156).

Author Contributions

JH-K conceptualized the work. KC, SN and JH-K contributed to developing the mathematical model. KC performed the simulations, analysed the model output, and wrote the original draft of the manuscript. SN and JH-K contributed to reviewing and editing the draft. .

References

Ahern, B., Parvizi, J., Boston, R., Shaer, T., 2009. Preclinical models in single site cartilage defect testing: A systematic review. Osteoarthritis and Cartilage 17, 705–713.

Allen, K., Thoma, L., Golightly, Y., 2022. Epidemiology of osteoarthritis. Osteoarthritis and cartilage 30, 184–195.

Anraku, Y., Mizuta, H., Sei, A., Kudo, S., Nakamura, E., Senba, K., Takagi, K., Hiraki, Y., 2008. The chondrogenic repair response of undifferentiated mesenchymal cells in rat full thickness articular cartilage defects. Osteoarthritis and Cartilage 16, 961–964.

Bailón-Plaza, A., Vander Meulen, M., 2001. A mathematical framework to study the effects of growth factor influence on fracture healing. Journal of Theoretical Biology 212, 191–209.

Bentley, G., Biant, L., Carrington, R., Akmal, M., Goldberg, A., Williams, A., Skinner, J., Pringle, J., 2003. A prospective, randomised comparison of autologous chondrocyte implantation versus mossaicplasty for osteochondral defects in the knee. Journal of Bone and Joint Surgery 85, 223–230.

Biant, L., Bentley, G., Vijayan, S., Skinner, J., Carrington, R., 2014. Chondrocyte implantation in the knee for chronic chondral and osteochondral defects. The American Journal of Sports Medicine , 2178–2183.

Brittberg, M., 2008. Autologous chondrocyte implantation - technique and long-term follow up. Injury 39, 40–49.

Campbell, K., 2019. Mathematical modelling of cartilage and bone defect healing after cell implantation. Ph.D. thesis. Keele University.

Campbell, K., Naire, S., Kuiper, J., 2019a. A mathematical model of cartilage regeneration after chondrocyte and stem cell implantation - I: The effects of growth factors. Journal of Tissue Engineering 10, 2041731419827791.

Campbell, K., Naire, S., Kuiper, J., 2019b. A mathematical model of cartilage regeneration after chondrocyte and stem cell implantation - II: The effects of co-implantation. Journal of Tissue Engineering 10, 204173141982770.

Carlier, A., Brems, H., Ashbourn, J., Nica, I., Legius, E., Geris, L., 2016. Capturing the wide variety of impaired fracture healing phenotypes in neurofibromatosis type I with eight key factors: A computational study. Sci Rep. 7, 20010.

Chen, X., Macica, C., Nasiri, A., Broadus, A., 2008. Regulation of articular chondrocyte proliferation and differentiation by indian hedgehog and parathyroid hormone-related protein in mice. Arthritis and Rheumatism 58, 3788–3797.

Chu, C., Szczodry, M., Bruno, S., 2010. Animal models for cartilage regeneration and repair. Tissue Engineering Part B: Reviews 16, 105–115.

Dahmen, J., Lambers, K., Reilingh, M., van Bergen, C., Stufkens, S., Kerkhoffs, G., 2018. No superior treatment for primary osteochondral defects of the talus. Knee Surgery, Sports Traumatology, Arthroscopy 26, 2142–2157.

De Bari, C., Roelofs, A., 2018. Stem cell-based therapeutic strategies for cartilage defects and osteoarthritis. Current Opinion in Pharmacology 40, 74–80.

Einhorn, T., 1998. The cell and molecular biology of fracture healing. Clinical Orthopaedics and Medical Research 355, S7–S21.

Falah, M., Nierenberg, G., Soudry, M., Hayden, M., Volpin, G., 2010. Treatment of articular lesions of the knee. International Orthopaedics 34, 621–630.

Farmer, J., Martin, D., Boles, C., Curl, W., 2001. Chondral and osteochondral injuries. Clinics in Sports Medicine 20, 299–320.

Fasano, A., Herrero, M., López, J., Medina, F., 2010. On the dynamics of the growth plate in primary ossification. Journal of Theoretical Biology 265, 543–553.

Fontaine, M., Shih, H., Schäfer, R., Pittenger, M., 2016. Unraveling the mesenchymal stromal cells' paracrine immunomodulatory effects. Transfusion Medicine Reviews 30, 37–43.

Francis, K., Palsson, B.O., 1997. Effective intercellular communication distances are determined by the relative time constants for cyto/chemokine secretion and diffusion. Proceedings of the National Academy of Sciences 94, 12258–12262.

Garzón-Alvarado, D., García-Aznar, J., Doblaré, M., 2009. A reaction-diffusion model for long bones growth. Biomechanics and Modelling in Mechanobiology 8, 381–395.

Geris, L., Gerisch, A., Maes, C., Carmeliet, G., Weiner, R., Sloten, J., Oosterwyck, H., 2006. Mathematical modelling of fracture healing in mice: Comparison between experimental data and numerical simulation results. Medical and Biological Engineering and Computing 44, 280–289.

Geris, L., Gerisch, A., Sloten, J., Weiner, R., Oosterwyck, H., 2008. Angiogenesis in bone fracture healing: A bioregulatory model. Journal of Theoretical Biology 251, 137–158.

Getgood, A., Kew, S., Brooks, R., Aberman, H., Simon, T., Lynn, A., Rushton, N., 2012. Evaluation of early-stage osteochondral defect repair using a biphasic scaffold based on a collagen-glycosaminoglycan biopolymer in a caprine model. Knee 19, 422–430.

Gomoll, A., Filardo, G., Almqvist, F., Bugbee, W., Jelic, M., Monllau, J., Puddu, G., Rodkey, W., Verdonk, P., Verdonk, R., Zaffagnini, S., Marcacci, M., 2012. Surgical treatment for early osteoarthritis. part II. allografts and concurrent procedures. Knee Surgery, Sports Traumatology, Arthroscopy 20, 468–486.

Gotterbarm, T., Breusch, S., Schneider, U., Jung, M., 2008. The mini pig model for experimental chondral and osteochondral defect repair in tissue engineering: retrospective analysis of 180 defects. Laboratory Animals 42, 71–82.

Guo, X., Wang, C., Duan, C., Descamps, M., Zhao, Q., Dong, L., Lü, S., Ansleme, K., Lu, J., Song, Y., 2004. Repair of osteochondral defects with autologous chondrocytes seeded onto bioceramic scaffold in sheep. Tissue Engineering 10, 1830–1840.

Jackson, D., Lalor, P., Aberman, H., Simon, T., 2001. Spontaneous repair of full-thickness defects of articular cartilage in goat model: A preliminary study. Journal of Bone & Joint Surgery 83, 53–64.

Jiang, J., Leong, N., Mung, J., Hidaka, C., Lu, H., 2008. Interactions between zonal populations of articular chondrocytes suppresses chondrocyte mineralization and this process is mediated by pthrp. Osteoarthritis and Cartilage 16, 70–82.

Jung, M., Breusch, S., Daecke, W., Gotterbarm, T., 2009. The effect of defect localization on spontaneous repair of osteochondral defects in a gottingen minipig model: A retrospective analysis of the medial patellar groove versus the medial femoral condyle. Laboratory Animals 43, 191–197.

Jurgens, W., Kroeze, R., Zandieh-Doulabi, B., van Dijk, A., Renders, G., Smit, T., van Milligen, F., Ritt, M., Helder, M., 2013. One-step surgical procedure for the treatment of osteochondral defects with adipose-derived stem cells in a caprine knee defect: A pilot study. Bioresearch Open Access 2, 315–325.

Kelly, D., Prendergast, P., 2005. Mechano-regulation of stem cell differentiation and tissue regeneration in osteochondral defects. Journal of Biomechanics 38, 1413–1422.

Kelly, D., Prendergast, P., 2006. Predicting the optimal mechanical properties for a scaffold used in osteochondral defect repair. Tissue Engineering 12, 2509–2519.

Kerkhofs, J., Roberts, S., Luyten, F., van Oosterwyck, H., Geris, L., 2012. Relating the chondrocyte gene network to growth plate morphology: From genes to phenotype. PLoS ONE 7, 1–11.

Kiaer, T., Grønlund, J., Sørensen, K., 1989. Intraosseous pressure and partial pressures of oxygen and carbondioxide in osteoarthritis, in: Seminars in Arthritis and Rheumatism. Elsevier, pp. 57–60.

Kozhemyakina, E., Lassar, A., Zelzer, E., 2015. A pathway to bone: Signalling molecules and transcription factors involved in chondrocytes development and maturation. Development 142, 817–831.

Kronenberg, H., 2003. Developmental regulation of the growth plate. Nature 423, 332–336.

Lacroix, D., Prendergast, P., 2002. A mechano-regulation model for tissue differentiation during fracture healing: Analysis of gap size and loading. Journal of Biomechanics 35, 1163–1171.

Linero, I., Chaparro, O., 2014. Paracrine effect of mesenchymal stem cells derived from human adipose tissue in bone regeneration. PLoS ONE 9.

Lutianov, M., Naire, S., Kuiper, J., 2011. A mathematical model of cartilage regeneration after cell therapy. Journal of Theoretical Biology 289, 136–150.

Lydon, H., Getgood, A., Henson, F., 2019. Healing of osteochondral defects via endochondral ossification in an ovine model. Cartilage 10, 94–101.

Mackie, E., Tatarczuch, L., Mirams, M., 2011. The skeleton: a multi-functional complex organ. the growth pate chondrocyte and endochondral ossification. Journal of Endocrinology 211, 109–121.

Madry, H., van Dijk, C.N., Mueller-Gerbl, M., 2010. The basic science of the subchondral bone. Knee surgery, sports traumatology, arthroscopy 18, 419–433.

Madry, H., Grün, U., Knutsen, G., 2011. Cartilage repair and joint preservation: medical and surgical treatment options. Deutches Ärzteblatt International 108, 669–677.

Mariani, E., Pulsatelli, L., Facchini, A., 2014. Signaling pathways in cartilage repair. International journal of molecular sciences 15, 8667–8698.

Martin, R., Burr, D., 1984. Non-invasive measurement of lobg-bone cross-sectional moment of inertia by photon absorptiometry. Journal of Biomechanics 17, 195–201.

Moffitt, J.R., Lundberg, E., Heyn, H., 2022. The emerging landscape of spatial profiling technologies. Nature Reviews Genetics 23, 741–759.

Moyad, T., 2011. Cartilage injuries in adult knee: Evaluation and management. Cartilage 2, 226–236.

Munirah, S., Samsudin, O., Chen, H., Sharifah Salmah, S., Aminuddin, B., Ruszymah, B., 2007. Articular cartilage restoration in load-bearing osteochondral defects by implantation of autologous chondrocyte-fibrin constructs: An experimental study in sheep. Journal of Bone and Joint Repair - Series B 89, 1099–1109.

Niemeyer, P., Albrecht, D., Andereya, S., Angele, P., Ateschrang, A., Aurich, M., Baumann, M.and Bosch, U., Erggelet, C., Fickert, S.and Gebhard, H., Gelse, K., G¨unther, D., Hoburg, A., Kasten, P., Kolombe, T., Madry, H., Marlovits, S., Meenen, N., M¨uller, P., Nöth, U., Petersen, J., Pietschmann, M., Richter, W., Rolauffs, B., Rhunau, K., Schewe, B., Steinert, A., Steinwachs, M., Welsch, G., Zinser, W., Fritz, J., 2016. Autologous chondrocyte implantation (aci) for cartilage defects of the knee: A guideline by the working group. Clinical Tissue Regeneration" of the German Society of Orthopaedics and Trauma (DGOU). Knee 23, 426–435.

Nizak, R., Bekkers, J., de Jong, P., Witkamp, T., Luijkx, T., Saris, D., 2017. Osteochondral lesion depth on mri can help predict the need for a sandwich procedure. European journal of radiology 90, 245–249.

Obradovic, B., Meldon, J., Freed, L., Vunjak-Novakovic, G., 2000. Glycosaminoglycandeposition in engineered cartilage: Experiments and mathematical model. AIChE Journal 46, 1860–1871.

Okano, K., Tsukazaki, T., Ohtsuru, A., Namba, H., Osaki, M., Iwasaki, K., Yamashita, S., 1995. Parathyroid hormone-related peptide in synovial fluid and disease activity of rheumatoid arthritis. Rheumatology 35, 1056–1062.

Olsen, L., Sherratt, J., Maini, P., Arnold, F., 1997. A mathematical model for the capillary endothelial cell-extracellular matrix interactions in wound-healing angiogenesis. IMA Journal of Mathematics Applied in Medicine and Biology 14, 261–281.

Rayon, T., Stamataki, D., Perez-Carrasco, R., Garcia-Perez, L., Barrington, C., Melchionda, M., Exelby, K., Lazaro, J., Tybulewicz, V.L., Fisher, E.M., et al., 2020. Species-specific pace of development is associated with differences in protein stability. Science 369, eaba7667.

Rovensky, J., Kvetnansky, R., Radikova, Z., Imrich, R., Greguska, O., Vigas, M., Macho, L., 2005. Hormone concentrations in synovial fluid of patients with rheumatoid arthritis. Clin Exp Rheumatol 23, 292–6.

Shapiro, F., Koide, S., Glimcher, M., 1993. Cell origin and differentiation in the repair of full thickness defects of articular cartilage. Journal of Bone & Joint Surgery 75.

Wakitani, S., Goto, T., Pineda, S., Young, R.G. Mansour, J., Caplan, A., Goldberg, V., 1994. Mesenchymal cell-based repair of large, full-thickness defects of articular cartilage. Journal of Bone & Joint Surgery 76, 579–592.

Williams, J., Bush-Joseph, C., Bach, J., 1998. Osteochondritis dissecans of the knee. American Journal of Knee Surgery 11, 221–232.

Williams, R., Zipfel, W., Tinsley, M., Farnum, C., 2007. Solute transport in growth plate cartilage: In vitro and in vivo. Biophysical Journal 93, 1039–1050.

Wilsman, N., Farnum, C., Green, E., Lieferman, E., Clayton, M., 1996. Cell cycle analysis of proliferative zone chondrocytes in growth plates elongating at different rates. Journal of Orthopaedic Research 14, 562–572.

de Windt, T., Saris, D., 2014. Treatment algorithms for articular cartilage repair of the knee. towards patient profiling using evidence-based tools, in: Shetty, A., Kim, S., Nakamura, N., Brittberg, M. (Eds.), Techniques in Cartilage Repair Surgery. Springer, Berlin, Heidelberg, pp. 23–31.

Wong, M., Carter, D., 1990. A theoretical model of osteochondral ossification and bone architectural construction in long bone ontogeny. Anatomy and Embroyology 181, 523–532.

Wu, L., 2013. Mesenchymal stem cells as trophic mediators in cartilage regeneration. Ph.D. thesis. University of Twente.

Zhang, C., Wei, X., Chen, C., Cao, K., Li, Y., Jiao, Q., Ding, J., Zhou, J., Fleming, B.C., Chen, Q., et al., 2014. Indian hedgehog in synovial fluid is a novel marker for early cartilage lesions in human knee joint. International journal of molecular sciences 15, 7250–7265.

Zhang, Y., Wang, F., Tan, H., Chen, G., Guo, L., Yang, L., 2012. Analysis of the mineral composition of the human calcified cartilage zone. International Journal of Medical Sciences 9, 353–360.

Zhou, S., Cui, Z., Urban, J., 2004. Factors influencing the oxygen concentration gradient from the synovial surface of articular cartilage to the cartilage bone interface: A modelling study. Arthritis & Rheumatism 50, 3915–3924.

A mathematical model of signalling molecule-mediated processes during regeneration of osteochondral defects after chondrocyte implantation

Kelly Campbell[a], Shailesh Naire[a], Jan-Herman Kuiper[b,c,*]

[a]*School of Computing and Mathematics, Keele University, Keele, ST5 5BG, U.K.*

[b]*School of Pharmacy and Bioengineering, Keele University, Keele, ST5 5BG, U.K.*

[c]*Robert Jones and Agnes Hunt Orthopaedic & District Hospital NHS Trust, Oswestry, SY10 7AG, U.K.*

Abstract

Treating bone-cartilage defects is a fundamental clinical problem. The ability of damaged cartilage to self-repair is limited due to its avascularity. Left untreated, these defects can lead to osteoarthritis. Details of osteochondral defect repair are elusive, but animal models indicate healing occurs via an endochondral ossification-like process, similar to that in the growth plate. In the growth plate, the signalling molecules parathyroid hormone-related protein (PTHrP) and Indian Hedgehog (Ihh) form a feedback loop regulating chondrocyte hypertrophy, with Ihh inducing and PTHrP suppressing hypertrophy. To better understand this repair process and to explore the regulatory role of signalling molecules on the regeneration process, we formulate a reaction-diffusion mathematical model of osteochondral defect regeneration after chondrocyte implantation. The drivers of healing are assumed to be chondrocytes and osteoblasts, and their interaction via signalling molecules. We model cell proliferation, migration and chondrocyte hypertrophy, and matrix production and conversion, spatially and temporally. We further model nutrient and signalling molecule diffusion and their interaction with the cells. We consider the PTHrP-Ihh feedback loop as the backbone mechanisms but the model is flexible to incorporate extra signalling mechanisms if needed. Our mathematical model is able to represent repair of osteochondral defects, starting with cartilage formation throughout the defect. This is followed by chondrocyte hypertrophy, matrix calcification and bone formation deep inside the defect, while cartilage at the surface is maintained and eventually separated from the deeper bone by a thin layer of calcified cartilage. The complete process requires around 48 months. A key highlight of the model demonstrates that the PTHrP-Ihh loop alone is insufficient and an extra mechanism is required to initiate chondrocyte hypertrophy, represented by a critical cartilage density. A parameter sensitivity study reveals that the timing of the repair process crucially depends on parameters, such as the critical cartilage density, and those describing the actions of PTHrP to suppress hypertrophy, such as its diffusion coefficient, threshold concentration and degradation rate.

Keywords: osteochondral defect, cartilage defect, mathematical modelling, reaction-diffusion model , endochondral ossification

*Corresponding author: School of Pharmacy and Bioengineering, Keele University, email:j.h.kuiper@keele.ac.uk

1. Introduction

Chondral and osteochondral defects are both a cause and result of osteoarthritis, a degenerative condition that causes the joints to become painful and stiff, primarily in patients over 50 years old (Falah et al. (2010); Moyad (2011); Allen et al. (2022)). Osteochondral defects of the knee can occur through acute trauma, natural wear and tear of the joint, and underlying disease of the bone (Madry et al. (2010); Williams et al. (1998)). General understanding of osteochondral defect healing has clinical significance, but little experimental data in humans is available and reliable treatment strategies are lacking. Once a joint with an osteochondral defect is osteoarthritic, repair is problematic and treatment options are limited (Gomoll et al. (2012)). Some treatment options for osteochondral defects include autologous chondrocyte implantation (ACI), osteochondral autograft transfer (OAT), osteochondral allograft transplantation surgery (OATS) and microfracture (Brittberg (2008); Dahmen et al. (2018); de Windt and Saris (2014)). Of these, ACI and the two graft procedures are able to achieve the hyaline-type cartilage needed for long-term clinical benefit and are the treatments most used in clinical practice, with ACI determined to be an effective treatment strategy (Biant et al. (2014); Brittberg (2008); De Bari and Roelofs (2018)). ACI is a two-stage surgical procedure: in stage one healthy chondrocytes (cartilage cells) are harvested from a non-weight-bearing area of the joint, to be cultured to appropriate cell numbers. Approximately two weeks later, in a second procedure, these cells are implanted into the chondral or osteochondral defect and sealed with a periosteal patch or collagen membrane, or alternatively seeded first in a biodegradable scaffold which is then placed in the defect (Brittberg (2008)). Long-term outcomes of this procedure are very good, with ACI not only the gold standard treatment for chondral defects, but also showing good outcomes in osteochondral lesions of the knee (Biant et al. (2014)).

Natural osteochondral defect healing can occur spontaneously but the underlying mechanism driving tissue regeneration is elusive. The quality of naturally regenerated tissue is unpredictable and can often be primarily fibrous, resulting in subsequent degradation. When an osteochondral defect forms, damaged blood vessels located within bone at the site of the defect produce blood which coagulates and forms a fibrous clot. Within this clot there are thought to be cartilage and bone precursors, such as mesenchymal stem cells (MSCs), along with a fibrin net that acts as a scaffold for cells to travel along (Madry et al. (2010)). The precursor cells are thought to move into the defect and differentiate into chondrocytes, fibroblasts or osteoblasts, which synthesize new tissue from the base of the defect. The tissue resulting from natural healing is generally of poor quality overall: although the defect may fill it is typically with fibro-cartilaginous tissue which is not the hyaline-type needed for long-term withstanding of the compressive forces across weight-bearing joints (Guo et al. (2004); Jackson et al. (2001)). Generally, this fibro-cartilage tissue will degrade and the original symptoms of pain and discomfort will return, putting the patient at increased risk of developing osteoarthritis (Wakitani et al. (1994)).

Lydon et al. (2019), using an ovine model, demonstrated that healing of osteochondral defects in large mammals involves endochondral ossification. They showed that healing begins with cartilage formation first occurring along the edges of the defect, filling from the sides inwards and upwards until the defect fills and forms a cartilage model. Once this process has completed, chondrocytes undergo hypertrophy and ossification takes place, with a layer of cartilage remaining along the articular surface of the defect. Other earlier studies using smaller mammals found a similar healing mechanism, such as those using the Göttingen minipig (GMP) model that show defects located in

the trochlear groove of the knee heal via endochondral ossification (Gotterbarm et al. (2008); Jung et al. (2009)). Shapiro et al. (1993) also observed an endochondral sequence starting from the base of osteochondral defects in rabbit models.

The occurrence of endochondral ossification during healing of osteochondral defects suggests that the process may be similar to processes in the growth plate (Mariani et al. (2014)). In the growth plate, the signalling molecules parathyroid hormone-related protein (PTHrP) and Indian Hedgehog (Ihh) form a negative feedback loop regulating chondrocyte hypertrophy, with Ihh produced by pre- and early-hypertrophic chondrocytes stimulating production of PTHrP, which in its turn suppresses chondrocyte hypertrophy (Figure 1; Kronenberg (2003); Mariani et al. (2014)). Indian hedgehog (Ihh) stimulates chondrocyte proliferation, along with chondrocyte and osteoblast differentiation

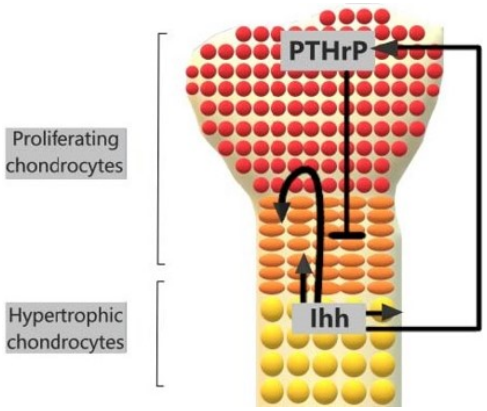

Figure 1: Schematic of the PTHrP-Ihh feedback loop that occurs during endochondral ossification. Adapted from Kronenberg (2003). Red circles represent proliferating chondrocytes, orange ovals pre-hypertrophic chondrocytes and yellow circles hypertrophic chondrocytes. Lines ending with an arrow head indicate stimulation, lines ending with a horizontal line indicate suppression.

(Kronenberg (2003)). Indian hedgehog is secreted when chondrocytes are exiting their proliferative state to undergo hypertrophy, whereas parathyroid hormone-related protein (PTHrP) is secreted by proliferating chondrocytes in the growth plate and surface zone chondrocytes in articular cartilage, the latter under the influence of mechanical loading (Jiang et al. (2008); Zhang et al. (2012)). PTHrP keeps chondrocytes in their proliferative state, inhibiting chondrocyte hypertrophy and therefore production of Ihh, thus forming a negative feedback loop (Kronenberg (2003); Zhang et al. (2012)).

Various authors have reported the need for an additional local or external signaling molecule for chondrocytes to progress from proliferative to hypertrophic state, thereby initiating the endochondral ossification process. Kerkhofs et al. (2012) explore the chondrocyte gene network controlling endochondral ossification in the growth plate, and identify a self-regulated sequential process that does however need external switching of PTHrP and Ihh levels to initiate state transitions, including that from proliferation to hypertrophy. The additional signaling molecule could be a systemic factor, such as thyroid hormone (TH, see Mackie et al. (2011) but also a local regulator, for instance a critical minimum cartilage density as implemented by Geris et al. (2008) and Carlier et al. (2016) to initiate chondrocyte hypertrophy in their bio-regulatory computer models of fracture healing. This concept of a minimum cartilage density is based on observations by Einhorn (1998) in a rat model of fracture healing that cartilage mineralisation occurs in the abundance of cartilage, similar to a critical density being achieved. Kozhemyakina

et al. (2015) describe pathways regulating the conversion of chondrocytes from a proliferative to a hypertrophic state within the growth plate, and argue that C-type natriuretic peptide (CNP) is a key regulator involved in the initiation of hypertrophy. CNP is produced by proliferative and pre-hypertrophic chondrocytes and hypertrophy is initiated when the local CNP concentration is high enough. CNP might thus underlie both Einhorn's observations and the critical cartilage density hypothesis used in fracture healing models: a regulator outside the PTHrP-Ihh loop initiating the conversion from proliferation to hypertrophy in chondrocytes.

As indicated above, the direct evidence for the role of the PTHrP-Ihh feedback loop in endochondral bone formation comes from small animal (mouse and rat) models. This is related to the fact that the gene expression levels for the two proteins are low, requiring the use of transgenic mice and reporter genes (Chen et al. (2008)). However, in these animals cartilage thickness is small. A widely cited paper argues that intercellular communication distances are restricted to around 250 µm (Francis and Palsson (1997)), which would be reasonable for mice. However, an osteochondral defect can be over 10 mm deep in adult humans (Nizak et al. (2017)) and it is therefore not clear if this feedback loop can work in humans. Mathematical models can help to address such a question. Moreover, these models can also explain and explore the complex interactions between the cell types and signalling molecules that contribute to osteochondral defect repair and mediate the endochondral ossification process. The aim of this study is to formulate a mathematical model to describe the osteochondral defect healing process as occurs in large animals after ACI. The model aims to incorporate the main characteristics of healing as described above, focusing on healing via the endochondral ossification pathway.

Current mathematical models of osteochondral defect repair are primarily concerned with mechanical stimuli, exploring the properties of relevant scaffolds used in defect repair (Kelly and Prendergast (2006)) and mechanical influence on mesenchymal stem cell differentiation within a defect (Kelly and Prendergast (2005)). Though these models explore some aspects of the healing process, our study will develop a mathematical model to depict the key mechanisms of osteochondral defect healing via endochondral ossification.

In previous work, we formulated a series of reaction-diffusion type mathematical models exploring the processes involved in chondral defect healing after cell therapy. Lutianov et al. (2011) simulated cartilage regeneration following ACI or autologous stem cell implantation (ASCI), an ACI-like therapy where mesenchymal stem cells are implanted instead of chondrocytes. The simulations compared healing patterns between the two cell therapies, concluding there was no difference in overall healing time while highlighting differences in cell behaviour and healing evolution. Following on from this work, the effects of two signalling molecules were incorporated into this model to simulate the interactions between chondrocytes and mesenchymal stem cells in a co-implantation cell therapy procedure (Campbell et al. (2019a,b)). This work highlighted the importance to chondral healing of cell-to-cell interactions between mesenchymal stem cells and chondrocytes. Specifically, it built on an in vitro model by Wu (2013) and demonstrated how the co-implantation of these two cell types led to a growth-factor mediated trophic effect on healing at early times, though there was no difference in overall healing time.

Mathematical models relevant to our approach study bone fracture healing and include Bailón-Plaza and Van-der Meulen (2001), who proposed a modelling framework for fracture healing, primarily focused on the role of

signalling molecules on the healing process. Their model includes the process of endochondral ossification regulated by extracellular matrix density (ECM). Geris et al. (2006) formulated a mathematical model of fracture healing in mice to validate experimental data; their model utilised modelling principles similar to Bailón-Plaza and Van-der Meulen (2001), and achieved results similar to those of the experimental data in murine models, along with a bio-regulatory model for bone fracture healing that utilised an endochondral ossification process including a critical density to regulate chondrocyte hypertrophy (Geris et al. (2008)).

We follow the modelling approaches undertaken in our work so far, combined with those in Bailón-Plaza and Vander Meulen (2001), Geris et al. (2006) and Geris et al. (2008), and apply them to our aim of formulating a reaction-diffusion mathematical model to describe the osteochondral defect healing process after ACI. The model will address two key questions: (a) Can the PTHrP-Ihh feedback loop control endochondral ossification in the healing process in large animals, and (b) Which key parameters most influence the healing process, in particular controlling the thickness of the articular cartilage in the repaired defect? The plan of the paper is as follows. In §2 we describe the basic model and the assumptions made, the boundary and initial conditions used, estimates of the parameter values and the scalings used to non-dimensionalise the equations. The results of our simulations are discussed in §4, where a sensitivity analysis is undertaken in §4.2 to validate our parameters and highlight those most sensitive to change within the model. Finally, in §5 we explore the implications of the model and suggest future work.

2. Mathematical model

2.1. Model formulation

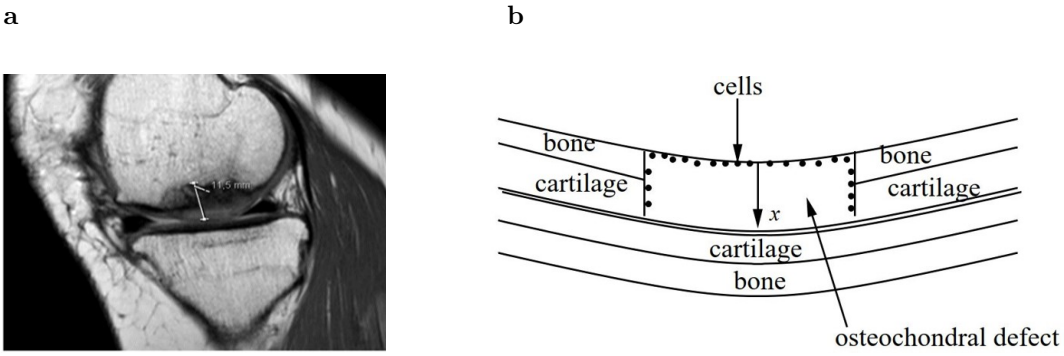

Figure 2: (a) Magnetic Resonance (MR) image of an 11.5mm deep osteochondral defect in the knee (Nizak et al. (2017)); (b) Schematic cross-section of the defect shown in (a). The axis denoted by x in (b) is along the depth of the defect. After debridement of the defect, chondrocytes are seeded along the defect boundaries.

A typical osteochondral defect has small aspect ratio, i.e., its length and width are much larger than its depth, see Fig. 2a. Hence, cell growth along the width of the defect can be assumed negligible compared to that along its depth. This is valid in the middle section of the defect, away from the walls. This assumption enables us to simplify to a one-dimensional problem where we model cell growth along the defect depth only, shown as the x direction in Fig. 2b.

Our model assumes a regenerating osteochondral defect can be populated by three cell types, namely chondrocytes, hypertrophic chondrocytes and osteoblasts, which each produce their specific matrix: cartilage, calcified cartilage or

bone, respectively. Depending on cell type, the cells are able to migrate non-directed (random diffusion), proliferate via the uptake of nutrients, differentiate, undergo hypertrophy and deposit matrix via nutrient uptake. In order to explore our central hypothesis that the PTHrP-Ihh feedback loop, important in endochondral ossification, also controls the healing of osteochondral defects, we include a particular mechanism representing the signaling molecules in this feedback loop and their stimulative and suppressive influence on chondrocyte hypertrophy. We do not include mechanobiological signals, known to influence bone resorption and remodelling as well as patterns of endochondral ossification, even though they may play a role in the repair process. We also do not explicitly include chemotaxis (directed motility). As with the model formulated in Campbell et al. (2019a,b), cell motility (assumed to occur through diffusion) is modelled proportional to nutrient concentration, with cell proliferation and differentiation ceasing when nutrient levels are low. At these levels, cell motility is the driving force of changing cell densities, with cells migrating towards locations of higher nutrient concentration. We now develop a mathematical model for the evolution of each species in time, t, and space, x, where x is measured along the depth of the defect (see Fig. 2b). Much of the model formulation follows from our previous models of chondral defect regeneration (Campbell et al. (2019a,b); Lutianov et al. (2011)).

The variables in our model are three cell densities (chondrocyte density C_C, mature (or hypertrophied) chondrocyte density C_H and osteoblast density C_B, all expressed as cells/mm^3), four matrix densities (total matrix density m, which is made up of cartilage matrix density m_C, bone matrix density m_B and calcified cartilage density m_{Ca}, all expressed in g/mm^3), the nutrient concentration n (moles/mm^3) and three signaling molecules (hypertrophy-inducing molecule concentration g_{HI}, hypertrophy-suppressing molecule concentration g_{HS} and hypertrophy modulating molecule concentration g_{HM}, all expressed in moles/mm^3).

Osteochondral defect repair follows a sequential healing process, with the defect first filling entirely with cartilage, before chondrocyte hypertrophy and eventual conversion into bone occurs (Lydon et al. (2019)). We focus here on formulating the cartilage-to-calcified cartilage and calcified cartilage-to-bone transitions in the endochondral ossification pathway and the role of signaling molecules, in particular PTHrP and Ihh, and other factors such as cartilage matrix density mediating these. We assume three signaling molecules regulate these stages, represented in the model by g_{HI} , g_{HM}, g_{HS}. Here, we use g_{HI} to represent a locally produced molecule that induces hypertrophy. Once hypertrophic chondrocytes are being produced, a modulating molecule g_{HM} is released that acts as an intermediate step within the signalling pathway. This factor g_{HM} represents Ihh which stimulates chondrocytes to produce a hypertrophy-suppressing signalling molecule g_{HS}, representing effects similar to PTHrP, and suppressing hypertrophy by keeping chondrocytes proliferating (Kerkhofs et al. (2012)). Figure 3 shows a schematic of the signalling feedback loop.

We also include a local regulator that allows chondrocytes to switch from a proliferative to a hypertrophic state, namely the critical cartilage density $m_{C,crit}$. Once $m_{C,crit}$ is reached, cartilage can begin conversion into calcified matrix which is subsequently remodelled to bone as seen in bone fracture healing (Carlier et al. (2016); Geris et al. (2008)). This conversion of cartilage to calcified matrix can only occur at locations where m_C reaches $m_{C,crit}$ by allowing chondrocytes to convert from a proliferative to a hypertrophic state. Below we describe in detail how the above mechanisms are incorporated in our model.

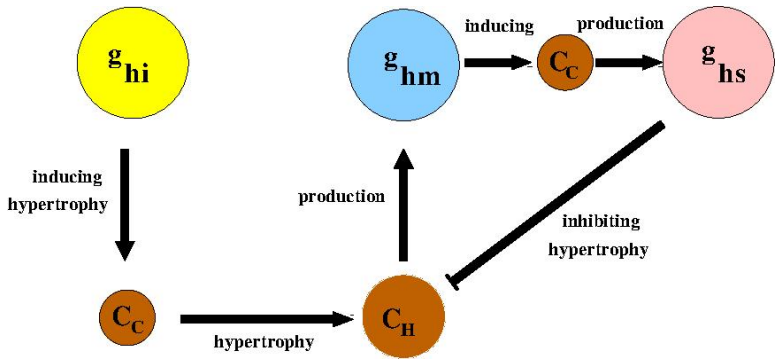

Figure 3: Schematic of signaling molecule feedback loop of endochondral ossification with inducing (g_{HI}), modulating (g_{HM}) and suppressing signalling molecules (g_{HS}). PTHrP and Ihh are the prototype suppressing and modulating signalling molecules, respectively, whereas several candidates exist for the inducing molecule. Solid black lines with arrows indicate inducing and without arrows represent inhibiting. C_C and C_H represent chondrocytes and hypertrophic chondrocytes, respectively.

Chondrocytes proliferate by uptake of nutrients, they can migrate and can undergo hypertrophy. Based on these processes, the rate of change of chondrocyte density is modelled as:

$$\begin{aligned}\frac{\partial C_C}{\partial t} = \frac{\partial}{\partial x}\left(D_{C_C}(m)\frac{\partial C_C}{\partial x}\right) + p_5\left(m, \frac{C_C}{C_{C,max}(m)}\right) C_C \frac{n}{n+n_0} H\left(n-n_1\right) \\ - p_6 C_C H\left(g_{HI} - g_{HI_0}\right) H\left(g_{HS_0} - g_{HS}\right) H\left(m_C - m_{C,crit}\right) - p_7 C_c H\left(n_1 - n\right).\end{aligned} \tag{1}$$

The first term on the right of Eq. (1) represents random chondrocyte migration, modelled as a diffusion process, with an effective chondrocyte diffusion coefficient, D_{C_C}. This coefficient is assumed to depend on the total matrix density, m, where $m = m_C + m_B + m_{Ca}$. This is based on the argument that cells can only migrate by attaching to a substrate (in this case, matrix). We use a density-weighted formula for the effective chondrocyte diffusion coefficient, D_{C_C}, based on the diffusivity through cartilage, $D_{C_{C,C}}$, calcified cartilage, $D_{C_{C,Ca}}$, and bone matrix, $D_{C_{C,B}}$, using a mixtures rule (analogous to the total circuit resistance of parallel resistors in an electrical circuit). We follow Olsen et al. (1997) and Bailón-Plaza and Vander Meulen (2001) in choosing expressions for $D_{C_{C,C}}$, $D_{C_{C,Ca}}$ and $D_{C_{C,B}}$.

$$\begin{aligned}&\frac{1}{D_{C_C}(m)} = \left(\frac{m_C}{m}\right)^{\alpha}\frac{1}{D_{C_{C,C}}(m_C)} + \left(\frac{m_B}{m}\right)^{\alpha}\frac{1}{D_{C_{C,B}}(m_B)} + \left(\frac{m_{Ca}}{m}\right)^{\alpha}\frac{1}{D_{C_{C,Ca}}(m_{Ca})}, \quad \alpha \geq 2 \\ &D_{C_{C,C}}(m_C) = D_{C_{C,C_0}}\frac{m_C}{m_C^2 + m_{C,1}^2} \qquad D_{C_{C,B}}(m_B) = D_{C_{C,B_0}}\frac{m_B}{m_B^2 + m_{B,1}^2} \\ &D_{C_{C,Ca}}(m_{Ca}) = D_{C_{C,Ca_0}}\frac{m_{Ca}}{m_{Ca}^2 + m_{Ca,1}^2}\end{aligned} \tag{2}$$

where $(D_{C_{C,C_0}}, D_{C_{C,B_0}}, D_{C_{C,Ca_0}})$ are reference diffusion ratios of chondrocytes, cartilage, bone and calcified cartilage, respectively, and $(m_{C,1}, m_{B,1}, m_{Ca,1})$ are reference matrix densities. The exponent $\alpha \geq 2$ is chosen so that we mimic the low motility of cells for the limiting cases when there is no cartilage (or bone) present and for large cartilage (or bone) matrix densities.

The second term on the right of Eq. (1) represents chondrocyte proliferation. Cell proliferation is assumed to be proportional to the chondrocyte density and the nutrient concentration. This process is assumed to start only when the nutrient concentration exceeds a critical value, n_1 (or, alternatively, cell proliferation is switched-off when

the nutrient concentration falls below this critical value). This is modelled by the Heaviside function, $H(n-n_1)$, which takes the unit value when $n > n_1$ and zero otherwise. The chondrocyte proliferation rate is given by p_5. The proliferation rate is assumed to depend on both the chondrocyte and total matrix densities. We choose

$$
\begin{aligned}
& p_5\left(m, \frac{C_C}{C_{C,max}(m)}\right) = p_{5,m}\left(1 - \frac{C_C}{C_{C,max}(m)}\right) \\
& \frac{1}{p_{5,m}(m)} = \left(\frac{m_{C_{tot}}}{m}\right)^{\alpha} \frac{1}{p_{5,C}(m_{C_{tot}})} + \left(\frac{m_B}{m}\right)^{\alpha} \frac{1}{p_{5,B}(m_B)}, \quad \alpha \geq 2 \\
& p_{5,C}(m_{C_{tot}}) = p_{5,C_0} \frac{m_{C_{tot}}}{m_{C_{tot}}^2 + m_{C,2}^2} \qquad p_{5,B}(m_B) = p_{5,B_0} \frac{m_B}{m_B^2 + m_{B,2}^2} \\
& C_{C,max}(m) = C_{C,max0}\left(1 - \frac{m}{m_{max}}\right).
\end{aligned}
\tag{3}
$$

The dependence of p_5 on the total matrix density is represented by $p_{5,m}(m)$. A density-weighted formula (similar to the effective cell migration/diffusion coefficient) is used to model the effective proliferation rate based on the cell proliferation rate in the presence of cartilage (represented by $p_{5,C}$) and bone (represented by $p_{5,B}$). The dependence of $(p_{5,C}, p_{5,B})$ on the matrix density $(m_{C_{tot}}, m_B)$ are chosen so that $(p_{5,C}, p_{5,B}) = 0$ when $(m_{C_{tot}}, m_B) = 0$, $(p_{5,C}, p_{5,B}) \to 0$ for large $(m_{C_{tot}}, m_B)$ and $(p_{5,C}, p_{5,B})$ attain a maximum at some intermediate matrix density, $(m_{C_{tot}}, m_B) = (m_{C,2}, m_{B,2})$. The coefficients, (p_{5,C_0}, p_{5,B_0}), represent chondrocyte proliferation rates in the presence of cartilage and bone, respectively. We assume that $p_{5,C}$ depends on the total cartilage matrix density, $m_{C_{tot}} = m_C + m_{Ca}$ and not on the cartilage type, i.e., whether regular or calcified cartilage. The dependence of p_5 on the chondrocyte density is assumed to follow a logistic growth model with the proliferation rate decreasing as the chondrocyte density approaches its maximum value, $C_{C,max}$. This maximum chondrocyte density is assumed to decrease linearly with total matrix density, m, because the presence of matrix will limit the space for cells. C_{C,max_0} is a reference maximum chondrocyte density.

The third term on the right of Eq. (1) models chondrocyte maturation (hypertrophic state). This is assumed to be proportional to the chondrocyte density and is regulated by the hypertrophy-inducing and suppressing signaling molecules g_{HI} and g_{HS}, respectively, and the critical cartilage density $m_{C,crit}$. The maturation rate is p_6 and assumed constant. The dependence on these signaling molecule concentrations is modelled using the Heaviside function, $H(g_{HI} - g_{HI_0})$ and $H(g_{HS_0} - g_{HS})$, where g_{HI_0} and g_{HS_0} are a threshold hypertrophy-inducing and suppressing molecule concentration, respectively. The first Heaviside function promotes hypertrophy once the hypertrophy-inducing signaling molecule concentration exceeds its threshold value, g_{HI_0}, and the second suppresses hypertrophy once the hypertrophy-suppressing signaling molecule concentration exceeds its threshold value, g_{HS_0}. The Heaviside function, $H(m_C - m_{C,crit})$, initiates chondrocyte hypertrophy only if $m_C > m_{C,crit}$ at any location in the defect.

The last term in Eq. (1) represents cell death due to lack of adequate nutrients. This process starts when the nutrient concentration falls below the critical value, n_1, and is modelled using the Heaviside function, $H(n_1 - n)$, which takes the unit value when $n < n_1$ and zero otherwise. The cell death rate is p_7, and is assumed constant.

The rate of change of mature hypertrophic chondrocyte density is modelled as:

$$\frac{\partial C_H}{\partial t} = \frac{\partial}{\partial x}\left(D_{C_H}(m)\frac{\partial C_H}{\partial x}\right) - p_8 C_H + p_6 C_C H\left(g_{HI} - g_{HI_0}\right) H\left(g_{HS_0} - g_{HS}\right) H\left(m_C - m_{C,crit}\right), \tag{4}$$

where D_{C_H} is the migration (diffusion) coefficient and p_8 is the death rate. We use similar expressions as in Eq. (2) for

$$\begin{aligned}
&\frac{1}{D_{C_H}(m)} = \left(\frac{m_C}{m}\right)^{\alpha}\frac{1}{D_{C_{H,C}}(m_C)} + \left(\frac{m_B}{m}\right)^{\alpha}\frac{1}{D_{C_{H,B}}(m_B)} + \left(\frac{m_{Ca}}{m}\right)^{\alpha}\frac{1}{D_{C_{H,Ca}}(m_{Ca})}, \quad \alpha \geq 2 \\
&D_{C_{H,C}}(m_C) = D_{C_{H,C_0}}\frac{m_C}{m_C^2 + m_{C,1}^2} \qquad D_{C_{H,B}}(m_B) = D_{C_{H,B_0}}\frac{m_B}{m_B^2 + m_{B,1}^2} \\
&D_{C_{H,Ca}}(m_{Ca}) = D_{C_{H,Ca_0}}\frac{m_{Ca}}{m_{Ca}^2 + m_{Ca,1}^2},
\end{aligned} \tag{5}$$

where $(D_{C_{H,C_0}}, D_{C_{H,B_0}}, D_{C_{H,Ca_0}})$ are reference diffusion rates of hypertrophic chondrocytes through cartilage, bone and calcified cartilage, respectively. The last term in Eq. (4) models formation of hypertrophic chondrocytes modulated by the hypertrophy-inducing and suppressing signaling molecule concentrations, and the critical cartilage densiyt, $m_{C,crit}$.

The rate of change of osteoblast density is modelled as:

$$\begin{aligned}
\frac{\partial C_B}{\partial t} = &\frac{\partial}{\partial x}\left(D_{C_B}(m)\frac{\partial C_B}{\partial x}\right) + p_9\left(m, \frac{C_B}{C_{B,max}(m)}\right) C_B \frac{n}{n + n_0} H\left(n - n_1\right) \\
&- p_{10} C_B H\left(n_1 - n\right),
\end{aligned} \tag{6}$$

where D_{C_B} is the osteoblast migration (diffusion) coefficient, p_9 is the osteoblast proliferation rate and p_{10} is the osteoblast death rate. We use similar expressions as in Eqs. (2,3,5) for the matrix-dependent osteoblast diffusion and proliferation coefficients, given by

$$\begin{aligned}
&\frac{1}{D_{C_B}(m)} = \left(\frac{m_C}{m}\right)^{\alpha}\frac{1}{D_{C_{B,C}}(m_C)} + \left(\frac{m_B}{m}\right)^{\alpha}\frac{1}{D_{C_{B,B}}(m_B)} + \left(\frac{m_{Ca}}{m}\right)^{\alpha}\frac{1}{D_{C_{B,Ca}}(m_{Ca})}, \quad \alpha \geq 2 \\
&D_{C_{B,C}}(m_C) = D_{C_{B,C_0}}\frac{m_C}{m_C^2 + m_{C,1}^2} \qquad D_{C_{B,B}}(m_B) = D_{C_{B,B_0}}\frac{m_B}{m_B^2 + m_{B,1}^2} \\
&D_{C_{B,Ca}}(m_{Ca}) = D_{C_{B,Ca_0}}\frac{m_{Ca}}{m_{Ca}^2 + m_{Ca,1}^2} \qquad p_9\left(m, \frac{C_B}{C_{B,max}(m)}\right) = p_{9,m}\left(1 - \frac{C_B}{C_{B,max}(m)}\right) \\
&\frac{1}{p_{9,m}(m)} = \left(\frac{m_{C_{tot}}}{m}\right)^{\alpha}\frac{1}{p_{9,C}(m_{C_{tot}})} + \left(\frac{m_B}{m}\right)^{\alpha}\frac{1}{p_{9,B}(m_B)}, \quad \alpha \geq 2 \\
&p_{9,C}(m_{C_{tot}}) = p_{9,C_0}\frac{m_{C_{tot}}}{m_{C_{tot}}^2 + m_{C,2}^2} \qquad p_{9,B}(m_B) = p_{9,B_0}\frac{m_B}{m_B^2 + m_{B,2}^2} \\
&C_{B,max}(m) = C_{B,max0}\left(1 - \frac{m}{m_{max}}\right),
\end{aligned} \tag{7}$$

where $(D_{C_{B,C_0}}, D_{C_{B,B_0}}, D_{C_{B,Ca_0}})$ are reference osteoblast migration rates through cartilage, bone and calcified cartilage, respectively, and (p_{9,C_0}, p_{9,B_0}) are reference osteoblast proliferation rates in the presence of cartilage and bone, respectively. The maximum osteoblast density, $C_{B,max}$, is assumed to decrease linearly with total matrix density, m. C_{B,max_0} is a reference maximum osteoblast density. We choose the reference maximum stem cell, normal

and mature chondrocyte and osteoblast densities, C_{S,max_0}, C_{C,max_0}, C_{H,max_0}, C_{B,max_0}, respectively, such that $C_{S,max_0} + C_{C,max_0} + C_{H,max_0} + C_{B,max_0} = C_{total,max_0}$, where C_{total,max_0} is a reference maximum total cell density. Hence, using the expressions for $C_{S,max}$, $C_{C,max}$ and $C_{B,max}$ in Eqs. (2,7) gives, $(C_{S,max} + C_{C,max} + C_{B,max})(m) = (C_{total,max_0} - C_{H,max_0})(1 - m/m_{max})$.

The rate of change of cartilage matrix density is modelled as:

$$\frac{\partial m_C}{\partial t} = D_{m_C}\frac{\partial^2 m_C}{\partial x^2} + p_{11}(m_C)\frac{n}{n+n_0}C_C - p_{12}(m_C)C_H, \tag{8}$$

where D_{m_C} is the cartilage matrix diffusion coefficient (assumed constant), p_{11} is the cartilage matrix synthesis rate and p_{12} is the rate of localized cartilage matrix degradation. We choose

$$p_{11}(m_C) = p_{11_0} - p_{11_1}m_C, \tag{9}$$

where p_{11_0} is a cartilage matrix production rate and p_{11_1} is its degradation rate. This assumes that the cartilage matrix synthesis rate decreases linearly with increasing cartilage matrix density (Olsen et al. (1997), Bailón-Plaza and Vander Meulen (2001)). The last term in Eq. (8) models localized degradation of cartilage matrix and is assumed to be proportional to the hypertrophic chondrocyte density. We choose

$$p_{12}(m_C) = p_{12_0}m_C, \tag{10}$$

where p_{12_0} is a cartilage matrix degradation rate. This assumes that the degradation is proportional to the cartilage matrix density. We allow cartilage degradation to occur once $\bar{m}_C$ has reached the critical density $m_{C_{crit}}$ and to cease when m_{Ca} and m_B have reached the maximum matrix density.

The rate of change of calcified cartilage matrix density is modelled as:

$$\frac{\partial m_{Ca}}{\partial t} = p_{12}(m_C)C_H - p_{20}m_{Ca}C_B. \tag{11}$$

The first term on the right of Eq. (11) describes the formation of calcified cartilage as the cartilage matrix degrades in the presence of hypertrophic chondrocytes. This term is switched on only when m_C has reached the critical density $m_{C_{crit}}$. The second term describes degradation of calcified cartilage matrix and is assumed to be proportional to its density and the osteoblast density, and p_{20} the degradation rate. Here, we do not distinguish between osteoblasts and osteoclasts which are responsible for converting calcified cartilage into bone.

The rate of change of bone matrix density is modelled as:

$$\frac{\partial m_B}{\partial t} = D_{m_B}\frac{\partial^2 m_B}{\partial x^2} + p_{13}(m_B)\frac{n}{n+n_0}C_B + p_{20}m_{Ca}C_B, \tag{12}$$

where D_{m_B} is the bone matrix diffusion coefficient (assumed constant) and p_{13} is the bone matrix synthesis rate. We choose

$$p_{13}(m_B) = p_{13_0} - p_{13_1}m_B, \tag{13}$$

where p_{13_0} is a bone matrix production rate and p_{13_1} is its degradation rate. The last term in Eq. (12) models bone matrix formation from calcified cartilage matrix.

The rate of change of hypertrophy-inducing signaling molecule concentration is modelled as:

$$\frac{\partial g_{HI}}{\partial t} = D_{g_{HI}} \frac{\partial^2 g_{HI}}{\partial x^2} - p_{25} g_{HI}, \tag{14}$$

where $D_{g_{HI}}$ is the hypertrophy-inducing signaling molecule diffusion coefficient (assumed constant) and p_{25} is the rate of degradation (assumed constant).

The rate of change of hypertrophy-suppressing signaling molecule concentration is modelled as:

$$\frac{\partial g_{HS}}{\partial t} = D_{g_{HS}} \frac{\partial^2 g_{HS}}{\partial x^2} + \ p_{21} C_C H\left(x - 90\%d\right) + p_{15} g_{HM} C_C H\left(x - 90\%d\right) \ - p_{22} g_{HS}, \tag{15}$$

where $D_{g_{HS}}$ is the hypertrophy-suppressing signaling molecule diffusion coefficient (assumed constant), p_{21} is the production rate by surface chondrocytes, p_{15} represents its production rate, and p_{22} is the degradation rate (assumed constant). The second term in Eq. (15) models the production of a hypertrophy-suppressing signalling molecule from chondrocytes and is assumed to be proportional to the chondrocyte density. We assume here that this signalling molecule is produced only by the chondrocytes at the upper 10% of the defect (denoted by $x = 90\%d$). The third term models the production of hypertrophy-suppressing signalling molecule via the stimulation of chondrocytes by the hypertrophy-modulating signalling molecule, and is assumed to be proportional to hypertrophy-modulating signalling molecule concentration and the chondrocyte density (only chondrocytes in the upper 10% of the defect). The fourth term represents the degradation of this signalling molecule (assumed to be proportional to the hypertrophy-suppressing signalling molecule concentration).

The rate of change of hypertrophy-modulating signalling molecule concentration is modelled as:

$$\frac{\partial g_{HM}}{\partial t} = D_{g_{HM}} \frac{\partial^2 g_{HM}}{\partial x^2} + p_{23} C_H - p_{26} g_{HM}, \tag{16}$$

where $D_{g_{HM}}$ is the hypertrophy-modulating signalling molecule diffusion coefficient (assumed constant), p_{23} is the production rate by hypertrophic chondrocytes, and p_{26} represents its degradation rate (assumed constant). The production of the hypertrophy-modulating molecule is assumed to be proportional to the hypertrophic chondrocyte density (second term in Eq. (16)).

Finally, the rate of change of nutrient concentration is modelled as

$$\frac{\partial n}{\partial t} = D_n \frac{\partial^2 n}{\partial x^2} - \frac{n}{n + n_0} \left(p_{17} C_C + p_{18} C_B + p_{19} C_H\right), \tag{17}$$

where D_n is the nutrient diffusion coefficient (assumed constant), p_{17}, p_{18} and p_{19} represent the nutrient uptake rate by chondrocytes, osteoblasts and mature chondrocytes, respectively (assumed constant).

2.2. Boundary conditions

We need to specify two boundary conditions for each species (except m_{Ca}, which does not require spatial boundary conditions). These are specified at either end of the defect domain. We assume $x = 0$ at the subchondral bone interface ("base" of the defect) and $x = d$ at the interface with the opposing normal cartilage ("top" of the defect, see Fig. 2b). The boundary conditions chosen at $x = 0$ are:

$$\begin{gathered} -D_{C_C}(m)\frac{\partial C_C}{\partial x} = -D_{C_H}(m)\frac{\partial C_H}{\partial x} = -D_{m_C}\frac{\partial m_C}{\partial x} = -D_{m_B}\frac{\partial m_B}{\partial x} = 0 \\ C_B = C_{B_0} \qquad n = N_0 \qquad g_{HI} = g_{HI_1} \qquad g_{HS} = g_{HS_1} \qquad g_{HM} = g_{HM_1} \end{gathered} \tag{18}$$

The first four boundary conditions represent no flux of chondrocytes, hypertrophic chondrocytes, cartilage matrix and osteoblasts from the subchondral bone. We assume that a reservoir of osteoblasts from the underlying intact bone, with uniform cell density, C_{B_0}, and nutrients from the underlying vascular network, with uniform concentration, N_0, are always available at this end. This is represented by the sixth and seventh boundary conditions, respectively. The last three boundary conditions represent a constant supply of hypertrophy-inducing, suppressing and modulating signalling molecules from the underlying vascular network, with uniform concentration, g_{HI_1}, g_{HS_1} and g_{HM_1}, respectively.

At $x = d$, we impose:

$$\begin{aligned} &- D_{C_C}(m)\frac{\partial C_C}{\partial x} = -D_{C_B}(m)\frac{\partial C_B}{\partial x} = -D_{C_H}(m)\frac{\partial C_H}{\partial x} = -D_{m_C}\frac{\partial m_C}{\partial x} = -D_{m_B}\frac{\partial m_B}{\partial x} = 0 \\ &n = N_1 \qquad g_{HI} = g_{HI_2} \qquad - D_{g_{HS}}\frac{\partial g_{HS}}{\partial x} = \gamma_1(g_{HS} - g_{HS_2}) \qquad - D_{g_{HM}}\frac{\partial g_{HM}}{\partial x} = \gamma_2(g_{HM} - g_{HM_2}) \end{aligned} \tag{19}$$

The first four boundary conditions represent no flux of chondrocytes, osteoblasts, hypertrophic chondrocytes and matrix, respectively, from the normal cartilage interface. We assume that a reservoir of nutrients with uniform concentration, N_1, is always available at this end. A constant supply of hypertrophy-inducing signalling molecule, with uniform concentration, g_{HI_2} is available at this boundary. We allow the hypertrophy-suppressing and modulating molecules to permeate (diffuse) through this boundary, represented by the eight and ninth boundary conditions, respectively, with the diffusive flux proportional to the signalling molecule concentration, and constant of proportionality $\gamma_{1,2}$, respectively (assumed constant). Here, g_{HS_2,HM_2} represent the concentrations of the hypertrophy-suppressing and modulating signalling molecules in the overlying articular cartilage (assumed constant)

2.3. Initial conditions

We need to prescribe profiles for each species at time $t = 0$. We are interested in one implantation scenario, related to Autologous Chondrocyte Implantation (ACI). Initially, chondrocytes are implanted into a nutrient-filled defect with a small amount of matrix present. The initial conditions chosen for this case are:

$$\begin{aligned} &C_C = C_C^{(0)}h(x) \qquad C_B = C_{B_0}h_1(x) \qquad C_H = 0 \qquad n = N_0 - (N_0 - N_1)\frac{x}{d} \qquad m_C = m_{C,3} \\ &m_B = m_{B,3} \qquad m_{Ca} = 0 \qquad g_{HI} = g_{HI_1} - (g_{HI_1} - g_{HI_2})\frac{x}{d} \qquad g_{HS} = g_{HS_1} \qquad g_{HM} = g_{HM_1} \end{aligned} \tag{20}$$

Here, $C_C^{(0)}$, $h(x)$ and $h_1(x)$ are an initial chondrocyte density, and specified initial spatial profiles for chondrocytes and osteoblasts, respectively.

There are several parameters appearing in the model. Their estimated values and the references from which they are obtained are provided in Table 1. All approximated parameters are disclosed in this table and references are provided where available.

dimensional parameters	estimated value
defect depth d	3-5 mm - 1-2 mm cartilage, 2-3 mm bone (Ahern et al. (2009) for

maximum chondrocyte migration (or diffusion) coefficient in cartilage, $D_{C_{C,C}}$	3.6×10^{-4} mm^2/hr Obradovic et al. (2000), in silico
maximum chondrocyte migration (or diffusion) coefficient in bone, $D_{C_{C,B}}$	3.6×10^{-4} mm^2/hr (assumed same as $D_{C_{C,C}}$)
maximum chondrocyte migration (or diffusion) coefficient in calcified cartilage, $D_{C_{C,Ca}}$	3.6×10^{-4} mm^2/hr (assumed same as $D_{C_{C,C}}$)
maximum mature chondrocyte migration (or diffusion) coefficient in cartilage, $D_{C_{H,C}}$	10^{-5} mm^2/hr (guess)
maximum mature chondrocyte migration (or diffusion) coefficient in bone, $D_{C_{H,B}}$	10^{-5} mm^2/hr (assumed same as $D_{C_{H,C}}$)
maximum mature chondrocyte migration (or diffusion) coefficient in calcified cartilage, $D_{C_{H,Ca}}$	10^{-5} mm^2/hr (assumed same as $D_{C_{H,C}}$)
maximum osteoblast migration (or diffusion) coefficient in cartilage, $D_{C_{B,C}}$	10^{-6} - 10^{-5} mm^2/hr (guess)
maximum osteoblast migration (or diffusion) coefficient in bone, $D_{C_{B,B}}$	10^{-4} - 10^{-3} mm^2/hr (guess)
maximum osteoblast migration (or diffusion) coefficient in calcified cartilage, $D_{C_{B,Ca}}$	10^{-4} - 10^{-3} mm^2/hr (guess)
chondrocyte migration (or diffusion) coefficient, $D_{C_{C,C_0}} = 2m_{C,1}D_{C_{C,C}}$	7.2×10^{-9} (mm^2/hr) (g/mm^3) (assuming $m_{C,1} = 10^{-5}$ g/mm^3)
chondrocyte migration (or diffusion) coefficient, $D_{C_{C,B_0}} = 2m_{B,1}D_{C_{C,B}}$	7.2×10^{-9} (mm^2/hr) (g/mm^3) (assuming $m_{B,1} = 10^{-5}$ g/mm^3)
chondrocyte migration (or diffusion) coefficient, $D_{C_{C,Ca_0}} = 2m_{Ca,1}D_{C_{C,Ca}}$	7.2×10^{-9} (mm^2/hr) (g/mm^3) (assuming $m_{Ca,1} = 10^{-5}$ g/mm^3)
mature chondrocyte migration (or diffusion) coefficient, $D_{C_{H,C_0}} = 2m_{C,1}D_{C_{H,C}}$	10^{-10} (mm^2/hr) (g/mm^3) (assuming $m_{C,1} = 10^{-5}$ g/mm^3)
mature chondrocyte migration (or diffusion) coefficient, $D_{C_{H,B_0}} = 2m_{B,1}D_{C_{H,B}}$	10^{-10} (mm^2/hr) (g/mm^3) (assuming $m_{B,1} = 10^{-5}$ g/mm^3)
mature chondrocyte migration (or diffusion) coefficient, $D_{C_{H,Ca_0}} = 2m_{Ca,1}D_{C_{H,Ca}}$	10^{-10} (mm^2/hr) (g/mm^3) (assuming $m_{Ca,1} = 10^{-5}$ g/mm^3)
osteoblast migration (or diffusion) coefficient, $D_{C_{B,C_0}} = 2m_{C,1}D_{C_{B,C}}$	10^{-11} - 10^{-10} (mm^2/hr) (g/mm^3) (assuming $m_{C,1} = 10^{-5}$ g/mm^3)
osteoblast migration (or diffusion) coefficient, $D_{C_{B,B_0}} = 2m_{B,1}D_{C_{B,B}}$	10^{-9} (mm^2/hr) (g/mm^3) (assuming $m_{B,1} = 10^{-5}$ g/mm^3)
osteoblast migration (or diffusion) coefficient, $D_{C_{B,Ca_0}} = 2m_{Ca,1}D_{C_{B,Ca}}$	10^{-9} (mm^2/hr) (g/mm^3) (assuming $m_{Ca,1} = 10^{-5}$ g/mm^3)

nutrient diffusion coefficient, D_n	4.6 mm^2/hr Zhou et al. (2004), mathematical model
cartilage matrix diffusion coefficient, D_{m_C}	0-2.5 $\times 10^{-5}$ mm^2/hr Obradovic et al. (2000), in silico
bone matrix diffusion coefficient, D_{m_B}	0-10^{-6} mm^2/hr (guess)
hypertrophy-inducing signalling molecule diffusion coefficient, $D_{g_{HI}}$	0.8 mm^2/hr Williams et al. (2007), in vitro, in vivo
hypertrophy-suppressing signalling molecule diffusion coefficient, $D_{g_{HS}}$	0.18 mm^2/hr Fasano et al. (2010), mathematical model, in vivo
hypertrophy-modulating signalling molecule diffusion coefficient, $D_{g_{HM}}$	0.18 mm^2/hr Fasano et al. (2010), mathematical model, in vivo
maximum chondrocyte proliferation rate in cartilage, $p_{5,C}$	2×10^{-4}/hr (guess)
maximum chondrocyte proliferation rate in bone, $p_{5,B}$	2×10^{-4}/hr (assumed same as $p_{5,C}$)
chondrocyte proliferation rate, $p_{5_{C,0}} = 2m_{C,2}p_{5,C}$	4×10^{-9} g/mm^3/hr (assuming $m_{C,2} = 10^{-5}$ g/mm^3)
chondrocyte proliferation rate, $p_{5_{B,0}} = 2m_{B,2}p_{5,B}$	4×10^{-9} g/mm^3/hr (assuming $m_{B,2} = 10^{-5}$ g/mm^3)
chondrocyte hypertrophic differentiation rate, p_6	2×10^{-2}/hr Wilsman et al. (1996), in vivo
chondrocyte death rate, p_7	3.75×10^{-3}/hr (guess)
mature chondrocyte death rate, p_8	6×10^{-3}/hr Wilsman et al. (1996), in vivo
maximum osteoblast proliferation rate in cartilage, $p_{9,C}$	(10^{-3}-10^{-2})/hr (guess)
maximum osteoblast proliferation rate in bone, $p_{9,B}$	(10^{-3}-10^{-2})/hr (assumed same as $p_{9,C}$)
osteoblast proliferation rate, $p_{9,C_0} = 2m_{C,2}p_{9,C}$	$2 \times$ (10^{-8}-10^{-7}) g/mm^3/hr (assuming $m_{C,2} = 10^{-5}$ g/mm^3)
osteoblast proliferation rate, $p_{9,B_0} = 2m_{B,2}p_{9,B}$	$2 \times$ (10^{-8}-10^{-7}) g/mm^3/hr (assuming $m_{B,2} = 10^{-5}$ g/mm^3)
osteoblast death rate, p_{10}	10^{-3}/hr (guess)
cartilage matrix production rate, p_{11_0}	3.75×10^{-13}(g/mm^3)/((N_C/mm^3) hr) Obradovic et al. (2000), in silico
cartilage matrix degradation rate, p_{11_1}	3.75×10^{-9}/((N_C/mm^3) hr) Obradovic et al. (2000), in silico
cartilage matrix degradation rate by hypertrophic chondrocytes, p_{12_0}	4×10^{-5} /((N_C/mm^3) hr) Wilsman et al. (1996), in vivo
bone matrix production rate, p_{13_0}	5×10^{-12} (g/mm^3)/((N_C/mm^3) hr)
bone matrix degradation rate, p_{13_1}	10^{-12}/((N_C/mm^3) hr) (guess)
nutrient uptake rate by chondrocytes, p_{17}	1.5×10^{-14} mol/(N_C hr) Zhou et al. (2004), mathematical model
nutrient uptake rate by osteoblasts, p_{18}	1.5×10^{-14} mol/(N_C hr) (assumed same as p_{17})
nutrient uptake rate by mature chondrocytes, p_{19}	1.5×10^{-14} mol/(N_C hr) (assumed same as p_{17})
calcified cartilage matrix degradation rate, p_{20}	$8 \times$ (10^{-3}-10^{-2})/((N_C/mm^3) hr)

	Bailón-Plaza and Vander Meulen (2001), mathematical model
hypertrophy-inducing signalling molecule degradation rate, p_{25}	5.78×10^{-2} /hr (assuming half-life 12 hours, Rayon et al. (2020))
hypertrophy-suppressing signalling molecule production rate by surface chondrocytes, p_{21}	3.3×10^{-22} mol/(N_C hr) Garzón-Alvarado et al. (2009), mathematical model
hypertrophy-suppressing signalling molecule production rate by proliferating chondrocytes, p_{15}	10^{-6}/((N_C/mm^3) hr) (guess)
hypertrophy-suppressing signalling molecule degradation rate, p_{22}	5.78×10^{-2} /hr (assuming half-life 12 hours, Rayon et al. (2020))
hypertrophy-modulating signalling molecule production rate, p_{23}	2.6×10^{-21} mol/(N_C hr) Garzón-Alvarado et al. (2009) mathematical model
hypertrophy-modulating signalling molecule degradation rate, p_{26}	5.78×10^{-2} /hr (assuming half-life 12 hours, Rayon et al. (2020))
maximum total cell density, C_{total,max_0}	10^6 N_C/mm^3 (assuming $10\mu m$ cell diameter)
maximum chondrocyte density, C_{C,max_0}	$0 - 10^6$ N_C/mm^3
maximum mature chondrocyte density, C_{H,max_0}	$0 - 10^6$ N_C/mm^3
maximum osteoblast density, C_{B,max_0}	$0 - 10^6$ N_C/mm^3
maximum cartilage matrix density, $m_{C,max}$	10^{-4} g/mm^3 Bailón-Plaza and Vander Meulen (2001), mathematical model
maximum bone matrix density, $m_{B,max}$	1×10^{-3} g/mm^3 (based on density of cortical bone)
maximum calcified cartilage matrix density, $m_{Ca,max}$	$(1 - 2) \times 10^{-3}$ g/mm^3 (assumed same as $m_{B,max}$)
maximum matrix density, $m_{max} = m_{C,max} + m_{B,max} + m_{Ca,max}$	$(2.1 - 4.1) \times 10^{-3}$ g/mm^3
maximum total cartilage matrix density, $m_{C_{tot,max}} = m_{C,max} + m_{Ca,max}$	$(1.1 - 2.1) \times 10^{-3}$ g/mm^3
initial chondrocyte cell density, $C_C^{(0)}$	2.5×10^5 N_C/mm^3 (based on 10^6 cells in 20mm x 20mm x 10μm volume)
reference cartilage matrix density, $m_{C,1}$	10^{-5} g/mm^3 (assumed m_{max}/100)
intermediate cartilage matrix density, $m_{C,2}$	10^{-5} g/mm^3 (assumed m_{max}/100)
reference calcified cartilage density, $m_{Ca,1}$	10^{-5} g/mm^3 (assumed m_{max}/100)
reference bone matrix density, $m_{B,1}$	10^{-5} g/mm^3 (assumed m_{max}/100)
intermediate bone matrix density, $m_{B,2}$	10^{-5} g/mm^3 (assumed m_{max}/100)
initial cartilage/bone matrix density, $m_{C,3}$,$m_{B,3}$	10^{-8} g/mm^3 (assumed $m_{max}/10^5$)
initial nutrient concentration, N_1	(2.85 - 9.5) $\times$ 10^{-11} mol/mm^3 (3-10% oxygen tension) Zhou et al. (2004), mathematical model
initial nutrient concentration, N_0	9.5×10^{-11} mol/mm^3 (Kiaer et al. (1989), human

threshold nutrient concentration, n_0	2.3×10^{-11} mol/mm^3 Zhou et al. (2004), mathematical model
critical nutrient concentration, n_1	9.5×10^{-12} mol/mm^3 (assumed $N_0/10$)
threshold hypertrophy-inducing signalling molecule concentration, g_{HI_0}	$(0.5 - 1) \times 10^{-15}$ mol/mm^3
threshold hypertrophy-suppressing signalling molecule concentration, g_{HS_0}	40×10^{-18} mol/mm^3 (guess)
initial hypertrophy-inducing signalling molecule concentration, g_{HI_1}	2×10^{-15} mol/mm^3 Rovensky et al. (2005)
initial hypertrophy-inducing signalling molecule concentration, g_{HI_2}	2×10^{-15} mol/mm^3 Rovensky et al. (2005)
hypertrophy-suppressing signalling molecule concentration, g_{HS_1}	2×10^{-18} mol/mm^3 Okano et al. (1995)
hypertrophy-suppressing signalling molecule concentration, g_{HS_2}	2×10^{-18} mol/mm^3 Okano et al. (1995)
hypertrophy-modulating signalling molecule concentration, g_{HM_1}	3×10^{-16} mol/mm^3 Zhang et al. (2014)
hypertrophy-modulating signalling molecule concentration, g_{HM_2}	3×10^{-16} mol/mm^3 Zhang et al. (2014)
initial osteoblast cell density, C_{B_0}	9×10^3 N$_C$/mm^3 Martin and Burr (1984), human
hypertrophy-suppressing signalling molecule flux parameter, γ_1	0 mm/hr (no flux - guess)
hypertrophy-modulating signalling molecule flux parameter, γ_2	0 mm/hr (no flux - guess)
critical cartilage density, $m_{C,crit}$	95% $m_{C,max}$

Table 1: Estimated values of dimensional parameters. In the above, N_C represents number of cells.

3. Non-dimensionalisation of model equations, boundary and initial conditions

It is instructive to non-dimensionalise (make dimensionless) the above equations, boundary and initial conditions. One can then compare (or measure) the variables against their corresponding characteristic quantities. We introduce

the following dimensionless variables based on characteristic quantities for each variable:

$$\bar{x} = x/d \qquad \bar{t} = t(p_{11_0} C_{total,max_0}/m_{C,max}) \qquad (\bar{C}_C, \bar{C}_H, \bar{C}_B) = (C_C, C_H, C_B)/C_{total,max_0}$$

$$(\bar{m}, \bar{m}_C, \bar{m}_{Ca}, \bar{m}_B, \bar{m}_{C_{tot}}) = (m/m_{max}, m_C/m_{C,max}, m_{Ca}/m_{Ca,max}, m_B/m_{B,max}, m_{C_{tot}}/m_{C_{tot,max}}) \tag{21}$$

$$\bar{n} = n/N_1 \qquad \bar{g}_{HI} = g_{HI}/g_{HI_1} \qquad \bar{g}_{HM} = g_{HM}/g_{HM_1} \qquad \bar{g}_{HS} = g_{HS}/g_{HS_1},$$

where the overbars represent dimensionless quantities. The characteristic quantities used to measure the spatial variable, x, cell densities, matrix densities, nutrient concentration and the hypertrophy-inducing, suppressing and modulating signalling molecule concentrations are the defect depth, d, the reference maximum total cell density, C_{total,max_0}, the maximum cartilage and bone matrix densities, $m_{C,max}$, $m_{Ca,max}$, $m_{B,max}$, respectively, the total matrix density, $m_{max} = m_{C,max} + m_{Ca,max} + m_{B,max}$, the total cartilage matrix density, $m_{C_{total},max} = m_{C,max} + m_{Ca,max}$, the initial nutrient concentration at $x = d$, N_1, and the initial hypertrophy-inducing, suppressing and modulating signalling molecule concentrations at $x = 0$, g_{HI_1}, g_{HS_1} and g_{HM_1}, respectively. We choose to measure time, t, based on the cartilage matrix production time scale, $m_{C,max}/(p_{11_0} C_{total,max_0})$. Using the parameter values in Table 1, we estimate this time scale to be approximately 11 days (a unit of time corresponds to approximately 11 days).

Using the above dimensionless variables, the non-dimensional equations can be written as:

$$\frac{\partial \bar{C}_C}{\partial \bar{t}} = \frac{\partial}{\partial \bar{x}}\left(\bar{D}_{C_C}(\bar{m})\frac{\partial \bar{C}_C}{\partial \bar{x}}\right) + \bar{p}_5\left(\bar{m}, \frac{\bar{C}_C}{\bar{C}_{C,max}(\bar{m})}\right)\frac{\bar{n}}{\bar{n}+\bar{n}_0}\bar{C}_C H(\bar{n}-\bar{n}_1)$$

$$- \bar{p}_6 \bar{C}_C H(\bar{g}_{HI} - \bar{g}_{HI_0}) H(\bar{g}_{HS_0} - \bar{g}_{HS}) H(\bar{m}_C - \bar{m}_{C,crit}) - \bar{p}_7 \bar{C}_C H(\bar{n}_1 - \bar{n}) \tag{22a}$$

$$\frac{\partial \bar{C}_H}{\partial \bar{t}} = \frac{\partial}{\partial \bar{x}}\left(\bar{D}_{C_H}(\bar{m})\frac{\partial \bar{C}_H}{\partial \bar{x}}\right) + \bar{p}_6 \bar{C}_C H(\bar{g}_{HI} - \bar{g}_{HI_0}) H(\bar{g}_{HS_0} - \bar{g}_{HS}) H(\bar{m}_C - \bar{m}_{C,crit}) - \bar{p}_8 \bar{C}_H \tag{22b}$$

$$\frac{\partial \bar{C}_B}{\partial \bar{t}} = \frac{\partial}{\partial \bar{x}}\left(\bar{D}_{C_B}(\bar{m})\frac{\partial \bar{C}_B}{\partial \bar{x}}\right) + \bar{p}_9\left(\bar{m}, \frac{\bar{C}_B}{\bar{C}_{B,max}(\bar{m})}\right)\frac{\bar{n}}{\bar{n}+\bar{n}_0}\bar{C}_B H(\bar{n}-\bar{n}_1) - \bar{p}_{10}\bar{C}_B H(\bar{n}_1 - \bar{n}) \tag{22c}$$

$$\frac{\partial \bar{m}_C}{\partial \bar{t}} = \bar{D}_{m_C}\frac{\partial^2 \bar{m}_C}{\partial \bar{x}^2} + \bar{p}_{11}(\bar{m})\frac{\bar{n}}{\bar{n}+\bar{n}_0}\bar{C}_C - \bar{p}_{12}(\bar{m}_C)\bar{C}_H \tag{22d}$$

$$\frac{\partial \bar{m}_{Ca}}{\partial \bar{t}} = \frac{\bar{p}_{12}}{\Gamma_1}(\bar{m}_C)\bar{C}_H - \bar{p}_{20}\bar{m}_{Ca}\bar{C}_B \tag{22e}$$

$$\frac{\partial \bar{m}_B}{\partial \bar{t}} = \bar{D}_{m_B}\frac{\partial^2 \bar{m}_B}{\partial \bar{x}^2} + \bar{p}_{13}(\bar{m})\frac{\bar{n}}{\bar{n}+\bar{n}_0}\bar{C}_B + \bar{p}_{20}\frac{\Gamma_1}{\Gamma}\bar{m}_{Ca}\bar{C}_B \tag{22f}$$

$$\frac{\partial \bar{g}_{HI}}{\partial \bar{t}} = \bar{D}_{g_{HI}}\frac{\partial^2 \bar{g}_{HI}}{\partial \bar{x}^2} - \bar{p}_{25}\bar{g}_{HI} \tag{22g}$$

$$\frac{\partial \bar{g}_{HS}}{\partial \bar{t}} = \bar{D}_{g_{HS}}\frac{\partial^2 \bar{g}_{HS}}{\partial \bar{x}^2} + \left(\bar{p}_{21}\bar{C}_C + \bar{p}_{15}\bar{g}_{HM}\bar{C}_C\right) H\left(\bar{x} - 0.9\right) - \bar{p}_{22}\bar{g}_{HS} \tag{22h}$$

$$\frac{\partial \bar{g}_{HM}}{\partial \bar{t}} = \bar{D}_{g_{HM}}\frac{\partial^2 \bar{g}_{HM}}{\partial \bar{x}^2} + \bar{p}_{23}\bar{C}_H - \bar{p}_{26}\bar{g}_{HM} \tag{22i}$$

$$\frac{\partial \bar{n}}{\partial \bar{t}} = \bar{D}_n\frac{\partial^2 \bar{n}}{\partial \bar{x}^2} - \frac{\bar{n}}{\bar{n}+\bar{n}_0}\left(\bar{p}_{17}\bar{C}_C + \bar{p}_{18}\bar{C}_B + \bar{p}_{19}\bar{C}_H\right), \tag{22j}$$

where

$$\bar{p_5}\left(\bar{m}, \frac{\bar{C}_C}{\bar{C}_{C,max}(\bar{m})}\right) = \bar{p}_{5,m}(\bar{m})\left(1 - \frac{\bar{C}_C}{\bar{C}_{C,max}(\bar{m})}\right) \qquad \bar{C}_{C,max}(\bar{m}) = \bar{C}_{C,max_0}(1-\bar{m})$$

$$\frac{1}{\bar{p}_{5,m}(\bar{m})} = (\beta+\epsilon)^\alpha \left(\frac{\bar{m}_{C_{total}}}{\bar{m}}\right)^\alpha \frac{1}{\bar{p}_{5,C}(\bar{m}_{C_{total}})} + \eta^\alpha \left(\frac{\bar{m}_B}{\bar{m}}\right)^\alpha \frac{1}{\bar{p}_{5,B}(\bar{m}_B)}, \;\; \alpha \geq 2$$

$$\bar{p}_{5,C}(\bar{m}_{C_{total}}) = \bar{p}_{5,C_0}\frac{\bar{m}_{C_{total}}}{\bar{m}^2_{C_{total}} + \bar{m}^2_{C,2}} \qquad \bar{p}_{5,B}(\bar{m}_B) = \bar{p}_{5,B_0}\frac{\bar{m}_B}{\bar{m}^2_B + \bar{m}^2_{B,2}}$$

$$\bar{p_9}\left(\bar{m}, \frac{\bar{C}_B}{\bar{C}_{B,max}(\bar{m})}\right) = \bar{p}_{9,m}(\bar{m})\left(1 - \frac{\bar{C}_B}{\bar{C}_{B,max}(\bar{m})}\right) \qquad \bar{C}_{B,max}(\bar{m}) = \bar{C}_{B,max_0}(1-\bar{m})$$

$$\frac{1}{\bar{p}_{9,m}(\bar{m})} = (\beta+\epsilon)^\alpha \left(\frac{\bar{m}_{C_{total}}}{\bar{m}}\right)^\alpha \frac{1}{\bar{p}_{9,C}(\bar{m}_{C_{total}})} + \eta^\alpha \left(\frac{\bar{m}_B}{\bar{m}}\right)^\alpha \frac{1}{\bar{p}_{9,B}(\bar{m}_B)}, \;\; \alpha \geq 2$$

$$\bar{p}_{9,C}(\bar{m}_{C_{total}}) = \bar{p}_{9,C_0}\frac{\bar{m}_{C_{total}}}{\bar{m}^2_{C_{total}} + \bar{m}^2_{C,2}} \qquad \bar{p}_{9,B}(\bar{m}_B) = \bar{p}_{9,B_0}\frac{\bar{m}_B}{\bar{m}^2_B + \bar{m}^2_{B,2}}$$

$$\bar{p}_{11}(\bar{m}_C) = 1 - \bar{p}_{11_1}\bar{m}_C \qquad \bar{p}_{12}(\bar{m}_C) = \bar{p}_{12_0}\bar{m}_C \qquad \bar{p}_{13}(\bar{m}_B) = \bar{p}_{13_0} - \bar{p}_{13_1}\bar{m}_B$$

$$\bar{D}_{C_{C,C}}(\bar{m}_C) = \bar{D}_{C_{C,C_0}}\frac{\bar{m}_C}{\bar{m}^2_C + \bar{m}^2_{C,1}} \qquad \bar{D}_{C_{C,B}}(\bar{m}_B) = \bar{D}_{C_{C,B_0}}\frac{\bar{m}_B}{\bar{m}^2_B + \bar{m}^2_{B,1}} \tag{23}$$

$$\bar{D}_{C_{C,Ca}}(\bar{m}_{Ca}) = \bar{D}_{C_{C,Ca_0}}\frac{\bar{m}_{Ca}}{\bar{m}^2_{Ca} + \bar{m}^2_{Ca,1}}$$

$$\frac{1}{\bar{D}_{C_H}(\bar{m})} = \beta^\alpha \left(\frac{\bar{m}_C}{\bar{m}}\right)^\alpha \frac{1}{\bar{D}_{C_{H,C}}(\bar{m}_C)} + \eta^\alpha \left(\frac{\bar{m}_B}{\bar{m}}\right)^\alpha \frac{1}{\bar{D}_{C_{H,B}}(\bar{m}_B)} + \epsilon^\alpha \left(\frac{\bar{m}_{Ca}}{\bar{m}}\right)^\alpha \frac{1}{\bar{D}_{C_{H,Ca}}(\bar{m}_{Ca})}$$

$$\bar{D}_{C_{H,C}}(\bar{m}_C) = \bar{D}_{C_{H,C_0}}\frac{\bar{m}_C}{\bar{m}^2_C + \bar{m}^2_{C,1}} \qquad \bar{D}_{C_{H,B}}(\bar{m}_B) = \bar{D}_{C_{H,B_0}}\frac{\bar{m}_B}{\bar{m}^2_B + \bar{m}^2_{B,1}}$$

$$\bar{D}_{C_{H,Ca}}(\bar{m}_{Ca}) = \bar{D}_{C_{H,Ca_0}}\frac{\bar{m}_{Ca}}{\bar{m}^2_{Ca} + \bar{m}^2_{Ca,1}}$$

$$\frac{1}{\bar{D}_{C_B}(\bar{m})} = \beta^\alpha \left(\frac{\bar{m}_C}{\bar{m}}\right)^\alpha \frac{1}{\bar{D}_{C_{B,C}}(\bar{m}_C)} + \eta^\alpha \left(\frac{\bar{m}_B}{\bar{m}}\right)^\alpha \frac{1}{\bar{D}_{C_{B,B}}(\bar{m}_B)} + \epsilon^\alpha \left(\frac{\bar{m}_{Ca}}{\bar{m}}\right)^\alpha \frac{1}{\bar{D}_{C_{B,Ca}}(\bar{m}_{Ca})}$$

$$\bar{D}_{C_{B,C}}(\bar{m}_C) = \bar{D}_{C_{B,C_0}}\frac{\bar{m}_C}{\bar{m}^2_C + \bar{m}^2_{C,1}} \qquad \bar{D}_{C_{B,B}}(\bar{m}_B) = \bar{D}_{C_{B,B_0}}\frac{\bar{m}_B}{\bar{m}^2_B + \bar{m}^2_{B,1}}$$

$$\bar{D}_{C_{B,Ca}}(\bar{m}_{Ca}) = \bar{D}_{C_{B,Ca_0}}\frac{\bar{m}_{Ca}}{\bar{m}^2_{Ca} + \bar{m}^2_{Ca,1}} \qquad \bar{C}_{C,max_0} + \bar{C}_{B,max_0} = 1 - \bar{C}_{H,max_0}$$

The non-dimensional boundary and initial conditions are:

$$-\bar{D}_{C_C}(\bar{m})\frac{\partial \bar{C}_C}{\partial \bar{x}} = -\bar{D}_{C_H}(\bar{m})\frac{\partial \bar{C}_H}{\partial \bar{x}} = -\bar{D}_{m_C}\frac{\partial \bar{m}_C}{\partial \bar{x}} = -\bar{D}_{m_B}\frac{\partial \bar{m}_B}{\partial \bar{x}} = 0 \tag{24a}$$

$$\bar{C}_B = \bar{C}_{B_0} \qquad \bar{n} = \bar{N}_0 \qquad \bar{g}_{HI} = 1 \qquad \bar{g}_{HS} = \bar{g}_{HM} = 1 \qquad \text{at } \bar{x} = 0$$

$$-\bar{D}_{C_C}(\bar{m})\frac{\partial \bar{C}_C}{\partial \bar{x}} = -\bar{D}_{C_H}(\bar{m})\frac{\partial \bar{C}_H}{\partial \bar{x}} = -\bar{D}_{C_B}(\bar{m})\frac{\partial \bar{C}_C}{\partial \bar{x}} = -\bar{D}_{m_C}\frac{\partial \bar{m}_C}{\partial \bar{x}} = -\bar{D}_{m_B}\frac{\partial \bar{m}_B}{\partial \bar{x}} = 0 \tag{24b}$$

$$\bar{n} = 1 \qquad \bar{g}_{HI} = \bar{g}_{HI_2} \qquad -\bar{D}_{g_{HS}}\frac{\partial \bar{g}_{HS}}{\partial \bar{x}} = \bar{\gamma}_1(\bar{g}_{HS} - \bar{g}_{HS_2})$$

$$-\bar{D}_{g_{HM}}\frac{\partial \bar{g}_{HM}}{\partial \bar{x}} = \bar{\gamma}_2(\bar{g}_{HM} - \bar{g}_{HM_2}) \qquad \text{at } \bar{x} = 1$$

$$\bar{C}_C = \bar{C}_C^{(0)}\bar{h}(\bar{x}) \qquad \bar{C}_B = \bar{C}_{B_0}\bar{h}_1(\bar{x}) \qquad \bar{C}_H = 0 \tag{24c}$$

$$\bar{n} = \bar{N}_0 - (\bar{N}_0 - 1)\bar{x} \qquad \bar{m}_C = \bar{m}_{C,3} \qquad \bar{m}_B = \bar{m}_{B,3} \qquad \bar{m}_{Ca} = 0$$

$$\bar{g}_{HI} = 1 - (1 - \bar{g}_{HI_2})\bar{x} \qquad \bar{g}_{HS} = \bar{g}_{HM} = 1 \qquad \text{at } \bar{t} = 0.$$

The dimensionless parameters and their estimated values are provided in Table 2.

dimensionless parameters		estimated value
chondrocyte migration (or diffusion) coefficient (cartilage)	$\bar{D}_{C_{C,C_0}} = D_{C_{C,C_0}}/(p_{11_0}C_{total,max_0}d^2)$	10^{-3}
chondrocyte migration (or diffusion) coefficient (bone)	$\bar{D}_{C_{C,B_0}} = D_{C_{C,B_0}}/(p_{11_0}C_{total,max_0}d^2\Gamma)$	10^{-3}
chondrocyte migration (or diffusion) coefficient (calcified cartilage)	$\bar{D}_{C_{C,Ca_0}} = D_{C_{C,Ca_0}}/(p_{11_0}C_{total,max_0}d^2\Gamma_1)$	10^{-3}
hypertrophic chondrocyte migration (or diffusion) coefficient (cartilage)	$\bar{D}_{C_{H,C_0}} = D_{C_{H,C_0}}/(p_{11_0}C_{total,max_0}d^2)$	10^{-5}
hypertrophic chondrocyte migration (or diffusion) coefficient (bone)	$\bar{D}_{C_{H,B_0}} = D_{C_{H,B_0}}/(p_{11_0}C_{total,max_0}d^2\Gamma)$	10^{-5}
hypertrophic chondrocyte migration (or diffusion) coefficient (calcified cartilage)	$\bar{D}_{C_{H,Ca_0}} = D_{C_{H,Ca_0}}/(p_{11_0}C_{total,max_0}d^2\Gamma_1)$	10^{-5}
osteoblast migration (or diffusion) coefficient (cartilage)	$\bar{D}_{C_{B,C_0}} = D_{C_{B,C_0}}/(p_{11_0}C_{total,max_0}d^2)$	10^{-6}
osteoblast migration (or diffusion) coefficient (bone)	$\bar{D}_{C_{B,B_0}} = D_{C_{B,B_0}}/(p_{11_0}C_{total,max_0}d^2\Gamma)$	10^{-4}
osteoblast migration (or diffusion) coefficient (calcified cartilage)	$\bar{D}_{C_{B,Ca_0}} = D_{C_{B,Ca_0}}/(p_{11_0}C_{total,max_0}d^2\Gamma_1)$	10^{-4}
cartilage matrix diffusion	$\bar{D}_{m_C} = D_{m_C}m_{C,max}/(p_{11_0}C_{total,max_0}d^2)$	10^{-3}

coefficient		
bone matrix diffusion coefficient	$\bar{D}_{m_B} = D_{m_B} m_{C,max}/(p_{11_0} C_{total,max_0} d^2)$	10^{-5}
nutrient diffusion coefficient	$\bar{D}_n = D_n m_{C,max}/(p_{11_0} C_{total,max_0} d^2)$	100
hypertrophy-inducing signalling molecule diffusion coefficient	$\bar{D}_{g_{HI}} = D_{g_{HI}} m_{C,max}/(p_{11_0} C_{total,max_0} d^2)$	2
hypertrophy-suppressing signalling molecule diffusion coefficient	$\bar{D}_{g_{HS}} = D_{g_{HS}} m_{C,max}/(p_{11_0} C_{total,max_0} d^2)$	0.5
hypertrophy-modulating signalling molecule diffusion coefficient	$\bar{D}_{g_{HM}} = D_{g_{HM}} m_{C,max}/(p_{11_0} C_{total,max_0} d^2)$	0.5
chondrocyte proliferation rate (cartilage)	$\bar{p}_{5,C_0} = p_{5,C_0}/(p_{11_0} C_{total,max_0}/\tau)$	10^{-3}
chondrocyte proliferation rate (bone)	$\bar{p}_{5,B_0} = p_{5,B_0}/(p_{11_0} C_{total,max_0} \Gamma)$	10^{-3}
chondrocyte hypertrophic differentiation rate	$\bar{p}_6 = p_6 m_{C,max}/(p_{11_0} C_{total,max_0})$	5
chondrocyte death rate	$\bar{p}_7 = p_7 m_{C,max}/(p_{11_0} C_{total,max_0})$	1
hypertrophic chondrocyte death rate	$\bar{p}_8 = p_8 m_{C,max}/(p_{11_0} C_{total,max_0})$	1.6
osteoblast proliferation rate (cartilage)	$\bar{p}_{9,C_0} = p_{9,C_0}/(p_{11_0} C_{total,max_0}/\tau)$	5.3×10^{-2}
osteoblast proliferation rate (bone)	$\bar{p}_{9,B_0} = p_{9,B_0}/(p_{11_0} C_{total,max_0} \Gamma)$	5.3×10^{-2}
osteoblast death rate	$\bar{p}_{10} = p_{10} m_{C,max}/(p_{11_0} C_{total,max_0})$	0.2
cartilage matrix degradation rate	$\bar{p}_{11_1} = p_{11_1} m_{C,max}/p_{11_0}$	1
cartilage matrix degradation rate	$\bar{p}_{12_0} = p_{12_0} m_{C,max}/p_{11_0}$	10^4
bone matrix production rate	$\bar{p}_{13_0} = p_{13_0}/(p_{11_0} \eta)$	13
bone matrix degradation rate	$\bar{p}_{13_1} = p_{13_1} m_{C,max}/p_{11_0}$	3×10^{-4}
nutrient uptake rate by chondrocytes	$\bar{p}_{17} = p_{17} m_{C,max}/(p_{11_0} N_1)$	10^4
nutrient uptake rate by osteoblasts	$\bar{p}_{18} = p_{18} m_{C,max}/(p_{11_0} N_1)$	10^4
nutrient uptake rate by hypertrophic chondrocytes	$\bar{p}_{19} = p_{19} m_{C,max}/(p_{11_0} N_1)$	10^4
calcified cartilage matrix degradation rate	$\bar{p}_{20} = p_{20} m_{C,max}/p_{11_0}$	10^5
hypertrophy-suppressing signalling molecule production rate by surface chondrocytes	$\bar{p}_{21} = p_{21} m_{C,max}/(p_{11_0} g_{HS_1})$	4×10^4
hypertrophy-suppressing signalling molecule production rate by hypertrophy-modulating signalling molecule	$\bar{p}_{15} = p_{15} m_{C,max} g_{HM_1}/(p_{11_0} g_{HS_1})$	4×10^4
hypertrophy-suppressing signalling molecule	$\bar{p}_{22} = p_{22} m_{C,max}/(p_{11_0} C_{total,max_0})$	15.47

degradation rate		
hypertrophy-modulating signalling molecule production rate by hypertrophic chondrocytes	$\bar{p}_{23} = p_{23} m_{C,max}/(p_{11_0} g_{HM_1})$	2.3×10^3
hypertrophy-modulating signalling molecule degradation rate	$\bar{p}_{26} = p_{26} m_{C,max}/(p_{11_0} C_{total,max_0})$	15.47
hypertrophy-inducing signalling molecule degradation rate	$\bar{p}_{25} = p_{25} m_{C,max}/(p_{11_0} C_{total,max_0})$	15.47
maximum mature chondrocyte density	$\bar{C}_{H,max_0} = C_{H,max_0}/C_{total,max_0}$	0-1
maximum osteoblast density	$\bar{C}_{B,max_0} = C_{B,max_0}/C_{total,max_0}$	0-1
initial chondrocyte density	$\bar{C}_C^{(0)} = C_C^{(0)}/C_{total,max_0}$	0.25
initial nutrient concentration	$\bar{N}_0 = N_0/N_1$	1-3
threshold nutrient concentration	$\bar{n}_0 = n_0/N_1$	0.24-0.81
critical nutrient concentration	$\bar{n}_1 = n_1/N_1$	0.1
reference cartilage matrix density	$\bar{m}_{C,1} = m_{C,1}/m_{C,max}$	0.1
intermediate cartilage matrix density	$\bar{m}_{C,2} = m_{C,2}/m_{C_{tot},max}$	0.1
reference calcified cartilage density	$\bar{m}_{Ca,1} = m_{Ca,1}/m_{Ca,max}$	0.1
reference bone matrix density	$\bar{m}_{B,1} = m_{B,1}/m_{B,max}$	10^{-2}
intermediate bone matrix density	$\bar{m}_{B,2} = m_{B,2}/m_{B,max}$	10^{-2}
initial cartilage matrix density	$\bar{m}_{C,3} = m_{C,3}/m_{C,max}$	10^{-5}
initial bone matrix density	$\bar{m}_{B,3} = m_{B,3}/m_{B,max}$	10^{-5}
threshold hypertrophy-inducing signalling molecule concentration	$\bar{g}_{HI_0} = g_{HI_0}/g_{HI_1}$	0.5
threshold hypertrophy-suppressing signalling molecule concentration	$\bar{g}_{HS_0} = g_{HS_0}/g_{HS_1}$	20
initial hypertrophy-inducing signalling molecule concentration	$\bar{g}_{HI_2} = g_{HI_2}/g_{HI_1}$	1
hypertrophy-suppressing signalling molecule concentration	$\bar{g}_{HS_2} = g_{HS_2}/g_{HS_1}$	1
hypertrophy-modulating signalling molecule concentration	$\bar{g}_{HM_2} = g_{HM_2}/g_{HM_1}$	1
initial osteoblast density	$\bar{C}_{B_0} = C_{B_0}/C_{total,max_0}$	10^{-2}
maximum cartilage matrix density	$\beta = m_{C,max}/m_{max}$	0.1
maximum bone matrix density	$\eta = m_{B,max}/m_{max}$	1
maximum calcified matrix density	$\epsilon = m_{Ca,max}/m_{max}$	1
ratio maximum bone to cartilage density	$\Gamma = m_{B,max}/m_{C,max}$	10
ratio maximum calcified cartilage to cartilage density	$\Gamma_1 = m_{Ca,max}/m_{C,max}$	10
ratio maximum calcified cartilage	$\tau = m_{Ca,max}/m_{C_{tot,max}}$	1

to total cartilage density		
exponent	α	2
hypertrophy-suppressing signalling molecule flux parameter	$\bar{\gamma}_1 = \gamma_1 d/D_{g_{HS}}$	0
hypertrophy-modulating signalling molecule flux parameter	$\bar{\gamma}_2 = \gamma_2 d/D_{g_{HM}}$	0
critical cartilage matrix density	$\bar{m}_{C,crit}/m_{C,max}$	0.95

Table 2: Estimated values of dimensionless parameters.

3.1. Implementation and simulated case

We use a second order accurate finite-difference discretisation scheme to discretise the spatial variable x in Eqs. 22-24, keeping the time derivative t continuous. The resulting ordinary differential equations are solved in MATLAB (Release 2013a, The MathWorks, Inc., Natick, Massachusetts, United States) using the stiff ODE solver ode15s. The time step was controlled within the solver to maintain the stability of the numerical solutions. The accuracy and convergence of the numerical scheme are formally checked by systematically reducing the mesh size Δx and measuring the error in the solution. Based on this, we choose the mesh size $\Delta x = 5 \times 10^{-3}$ (200 mesh points) to present the numerical solutions below. We confirm that for this choice of Δx the solutions are an accurate reflection of the evolution process and also practical with respect to the computational time taken to run simulations to time equivalent to 48 months.

The dimensionless parameters and their estimated baseline values are provided in Table 2. Initially we have a population of chondrocytes, $\bar{C}_C^{(0)}$, implanted at the base of the defect at the subchondral bone interface ($\bar{x} = 0$), corresponding to an ACI procedure (Lutianov et al. (2011); Campbell et al. (2019a,b)). The initial chondrocyte cell density spatial profile is $\bar{C}_C(x,0) = \bar{C}_C^{(0)}[1 - \tanh(A(\bar{x} - \bar{x}_0))]/2$, with $A = 10^4$ and $\bar{x}_0 = 0.1$. We also include an initial population of bone cells, $\bar{C}_{B_0}$, assumed to be constant at the subchondral bone interface. The bone cell density spatial profile is $\bar{C}_B(x,0) = \bar{C}_{B_0}[1 - \tanh(A(\bar{x} - \bar{x}_1))]/2$, with $A = 10^4$ and $\bar{x}_1 = 10^{-3}$. Dimensionally, this corresponds to a chondrocyte density, 2.5×10^5 cells/mm^3, seeded within a region of thickness 500μm near $x = 0$, and zero everywhere else. The initial bone cell density corresponds to 9×10^3 cells/mm^3 present within a region of thickness 5nm near $x = 0$, and zero everywhere else.

We simulate the evolution of chondrocytes, C_C, hypertrophic chondrocytes, C_H, bone cells, C_B, cartilage matrix, m_C, calcified matrix, m_{Ca}, bone matrix, m_B, and nutrients, n, along with signalling molecules, $g_{HS,HM}$.

4. Results and parameter sensitivity analysis

4.1. Numerical results

Figures 4-6 show the evolution of osteochondral defect healing following an ACI procedure, for time ranging from 1 month to 48 months post implantation. As early as 1 month chondrocytes produce cartilage matrix, m_C, and

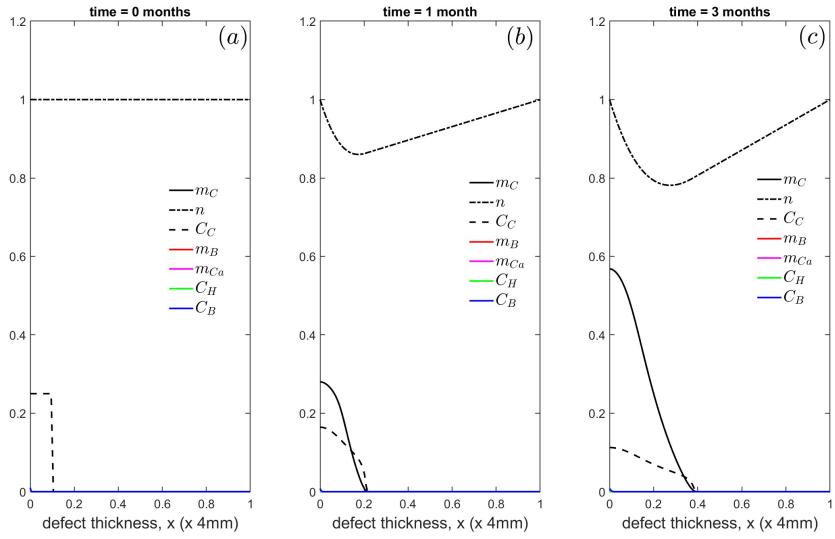

Figure 4: Evolution of cell and matrix densities, and nutrient concentration at (a) t =0 days, (b) $t = 1$ month and (c) $t = 3$ months, following implantation of chondrocytes.

migrate through the matrix towards the top of the defect (Lutianov et al. (2011)). Due to the low proliferation rate of chondrocytes ($\bar{p}_{5,C_0} = 10^{-3}$), migration is their main means of evolution and by 3 months they have extended and deposited cartilage matrix in the bottom half of the defect. These results replicate those of our previous chondral regeneration model, with evolution of cartilage deposition occurring at a fast pace due to high availability of nutrients (Lutianov et al. (2011)). During this initial stage of the regeneration process, a purely chondral regeneration mechanism takes place. At 6 months, m_C is steadily increasing from the base of the defect, with chondrocyte hypertrophy and matrix calcification not yet initiated. As time progresses to 12 months, we observe the defect continuing to fill, with chondrocytes and new cartilage matrix having reached the top of the defect and with a cartilage density over 90% at the defect base (Fig. 5(b)). At the defect base, the critical cartilage matrix density, assumed 95%, is reached at 18 months (Fig. 5(c)). The chondrocytes here start to convert from a proliferative to a hypertrophic state, converting cartilage matrix into calcified matrix, ready to initiate bone production via endochondral ossification (Fig. 5(c)). The hypertrophic chondrocytes convert cartilage matrix at the defect base entirely into calcified matrix, m_{Ca}. Osteoblasts at the defect base further convert this matrix to bone matrix, m_B. The conversion rate of m_C to m_{Ca} and m_{Ca} to m_B is very rapid owing to the large values of $\bar{p}_{12_0} = 10^4$ and $\bar{p}_{20} = 10^5$, therefore m_{Ca} levels observed are very low. This signifies the end of cartilage formation at this location and the beginning of the endochondral ossification process. The modulating and suppressing signalling molecules regulate chondrocyte hypertrophy and cartilage calcification from this time on. At 24 months, our simulations show an upward moving narrow zone where chondrocytes are undergoing hypertrophy and converting cartilage matrix into calcified matrix (Fig. 6(a)). The base of the defect is filled with bone matrix, m_B, with a narrow middle zone of calcified cartilage and a top layer of cartilage that has not yet reached its full density across the top of the defect. As bone matrix was deposited from the defect base, bone cells such as osteoblasts and osteoclasts are able to migrate within this matrix towards the top of the defect. At 36 months, more of the defect has been filled with m_B (Fig.

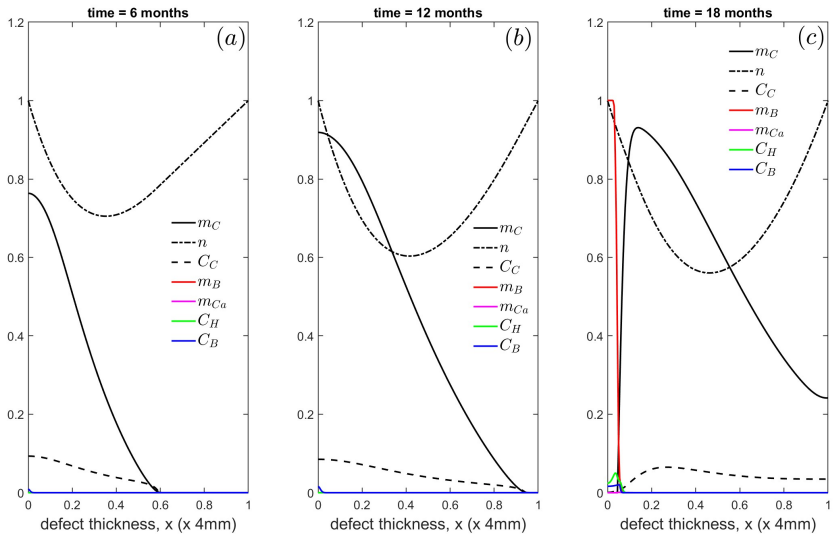

Figure 5: Evolution of cell and matrix densities, and nutrient concentration at (a) $t = 6$ months, (b) $t = 12$ months and (c) $t = 18$ months.

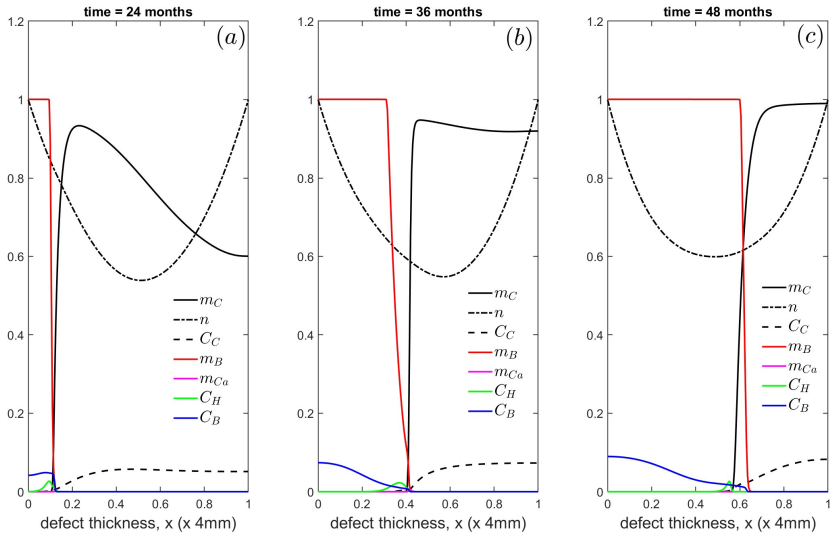

Figure 6: Evolution of cell and matrix densities, and nutrient concentration at (a) $t = 24$ months, (b) $t = 36$ months and (c) $t = 48$ months.

6(b)). The middle zone of active endochondral ossification has moved towards the top, with m_C being remodelled into m_{Ca}, ready for conversion into m_B where bone cells are present (Fig. 6(b)). At the top of the defect, there is a section of cartilage that has not calcified (Fig. 6(b)). This is due to a flux of hypertrophy-suppressing signalling molecule, g_{HS}, diffusing downwards from the top of the defect where it is produced by the surface chondrocytes, both directly and through g_{HM} stimulation of these cells.

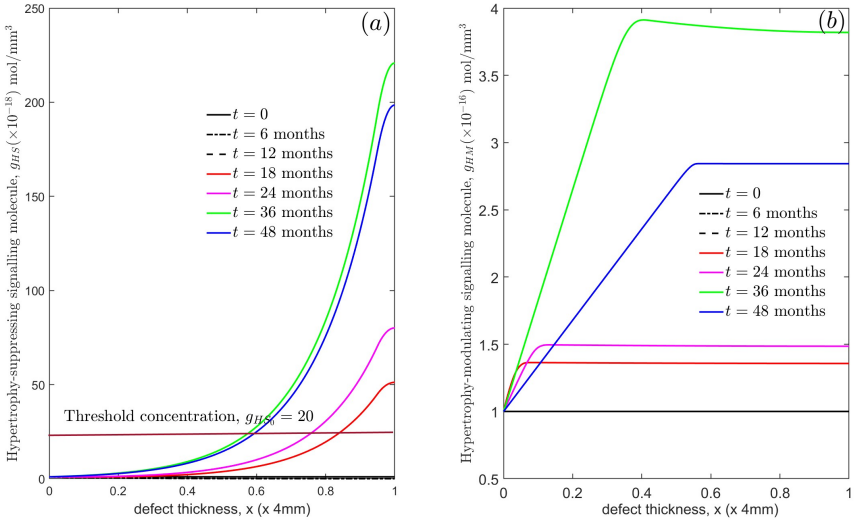

Figure 7: Evolution of the concentration of (a) hypertrophy-suppressing, g_{HS} and (b) hypertrophy-modulating, g_{HM}, signalling molecules from $t = 0 - 48$ months.

Throughout the simulation ($t = 0 - 48$ months), the hypertrophy-inducing molecule g_{HI} concentration remains constant ($g_{HI} = 1$) along the defect height, above its threshold value $\bar{g}_{HI_0} = 0.5$. Hypertrophy is nevertheless suppressed until $t = 18$ months because the cartilage matrix density is below its critical level $m_{Ccrit} = 0.95$, combined with the activity of hypertrophy modifying and suppressing signalling molecules $g_{HS,HM}$ at later times. Figure 7(a, b) show the evolution of $g_{HS,HM}$. The threshold g_{HS} concentration above which hypertrophy is suppressed is $\bar{g}_{HS_0} = 20$, and we assume no-flux of signalling molecules out of the top of the defect ($\bar{\gamma}_1 = \bar{\gamma}_2 = 0$). We observe a progressive build-up of g_{HS} at the top of the defect which diffuses downwards. The region corresponding to $g_{HS} > g_{HS_0}$ is where hypertrophy is suppressed resulting in the formation of non-calcified cartilage. In this zone, chondrocytes are prevented from hypertrophying and endochondral ossification cannot take place. At 36 months the defect is mostly filled with full or near-full-density matrix, whether bone, calcified or cartilage (Fig. 6(b)). As time progresses to 48 months, the defect is now entirely filled with full-density bone and cartilage matrix, signifying the endochondral ossification process has ended and the defect has been repaired (Fig. 6(c)).

4.2. Sensitivity of parameters

The model uses a large number of dimensionless parameters. Their values were derived from literature where possible, but often had a wide range and sometimes values were assumed or guessed. The simulation results may be sensitive to some of these values, potentially indicating their biological significance. On the other hand, if the solution is not sensitive to the exact value of a parameter whose value has been approximated, then this indicates that

the exact value is not important and an approximation suffices. We therefore conducted a sensitivity analysis on parameters deemed to be important for the model, exploring specifically the sensitivity to parameters describing the endochondral ossification process, namely those relating to the signalling molecules and chondrocyte hypertrophy, including the critical cartilage density. In addition, we investigated sensitivity to the parameters whose values were assumed or guessed.

The concentration of hypertrophy-inducing signalling molecule g_{HI} is essentially a linear interpolation between its values at the two boundaries, and as a consequence its effects are very simple. If its concentration is below the threshold g_{HI_0}, hypertrophy is completely suppressed. If its concentration is however above the threshold, as in the base case, hypertrophy is governed by the critical cartilage density and the hypertrophy-suppressing molecule g_{HS} concentration.

Figures $8(a, b, c)$ show the cell and matrix densities at $t = 6$ months for varying critical cartilage matrix densities, $m_{C_{crit}} = 10\%, 50\%, 95\%$, respectively. Decreasing $m_{C_{crit}}$ from 95% to 50% activates chondrocyte hypertrophy much earlier resulting in early calcified matrix and bone formation (Fig. $8(b)$. The initial fill-up of the defect with cartilage is suppressed (Fig. 8, compare (b) and (c)). Further decreasing the critical density to 10%, however, stops

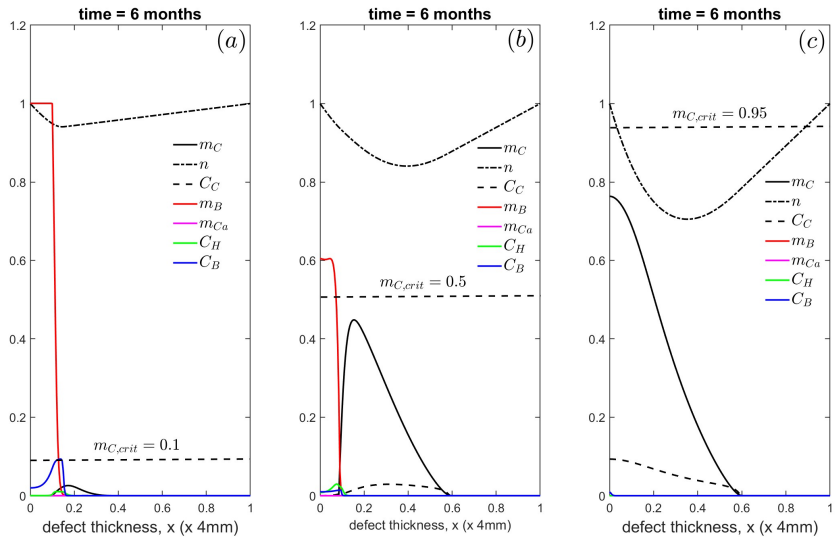

Figure 8: Cell and matrix densities at $t = 6$ months for varying the critical cartilage density, $m_{C,crit}$, at t=6 months. (a) $m_{C,crit} = 0.1$, (b) $m_{C,crit} = 0.5$ (b) and (c) $m_{C,crit} = 0.95$ (baseline value).

the initial fill of the defect with cartilage, with chondrocytes undergoing hypertrophy as soon as $m_{C,crit} > 0.1$ (Fig. $8(a)$). Bone formation begins almost immediately.

Figures $9(a, b)$ show the cell and matrix densities at $t = 48$ months for varying hypertrophy-suppressing signalling molecule threshold concentrations, $\bar{g}_{HS_0}$=20 (baseline), 80, respectively. We observe that increasing $\bar{g}_{HS_0}$, decreases the thickness of the cartilage layer remaining at the top of the defect. This can be explained using Fig. $11(a)$, where increasing the threshold concentration restricts the region where $g_{HS} > \bar{g}_{HS_0}$ to the top of the defect. Here, chondrocyte hypertrophy is suppressed and the endochondral ossification pathway is switched off.

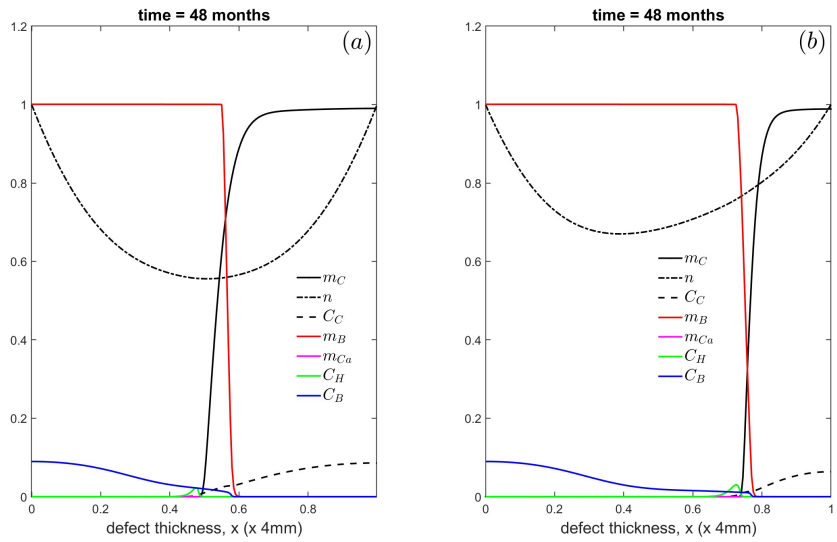

Figure 9: Cell and matrix densities for varying the hypertrophy-suppressing signalling molecule threshold concentration, $\bar{g}_{HS_0}$, at $t = 48$ months. (a) $\bar{g}_{HS_0} = 20$ (baseline value) and (b) $\bar{g}_{HS_0} = 80$.

Figures $10(a, b, c)$ show the cell and matrix densities at $t = 48$ months for varying hypertrophy-suppressing signalling molecule diffusion coefficients, $\bar{D}_{g_{HS}}$=0.5 (baseline), 1 and 5, respectively. We observe that increasing $\bar{D}_{g_{HS}}$ marginally increases the thickness of the cartilage layer remaining at the top of the defect. As $\bar{D}_{g_{HS}}$ is increased, g_{HS} produced by the chondrocytes at the top of the defect can diffuse further into the defect to suppress endochondral ossification. Figures $11(a, b, c)$ show the corresponding evolution of g_{HS} from $t = 0 - 48$ months for $\bar{D}_{g_{HS}}$=0.5 (baseline), 1 and 5, respectively. g_{HS} produced by the chondrocytes at the top of the defect diffuses rapidly through the entire defect as $\bar{D}_{g_{HS}}$ increases, suppressing endochondral ossification.

Figures $12(a, b, c)$ show the cell and matrix densities at $t = 48$ months when varying the g_{HS} flux (via $\bar{\gamma}_1$) leaking from the defect surface. Figures $13(a, b, c)$ show the corresponding g_{HS} concentration for $t = 0 - 48$ months. If the flux from the surface is not too large, then the production of g_{HS} by the surface chondrocytes offsets its removal, and the concentration of g_{HS} is observed to gradually increase (Fig. $13(b)$) albeit much slower than the baseline case (Fig. $13(a)$). This results in the endochondral ossification process continuing until it reaches the top of the defect (Fig. $12(b)$) before the g_{HS} concentration exceeds the threshold concentration to suppress hypertrophy (Fig. $13(b)$). For larger values of the flux, the leaking out of g_{HS} exceeds its production there, and as time progresses its concentration falls below the threshold value (Fig. $13(c)$). This promotes chondrocyte hypertrophy and the osteochondral ossification pathway leading to bone formation right up the top of the defect (Fig. $12(c)$); eventually the defect will fill-up entirely with bone. In this case, at $t = 48$ months there is no longer an intact layer of cartilage at the top of the defect, unlike the baseline case shown in Fig. $12(a)$.

Figures $14(a, b)$ show the cell and matrix densities at $t = 48$ months for varying hypertrophy-suppressing signalling molecule production rates by surface chondrocytes, both the default rate $\bar{p}_{21}$ and its modification via the hypertrophy-modifying molecule g_{HM}, namely $\bar{p}_{15}$. Figures $15(a, b)$ show the corresponding evolution of g_{HS} concentration for $t = 0 - 48$ months. For lower values of $\bar{p}_{15}$ and $\bar{p}_{21}$ compared to the baseline value, the production of g_{HS} by

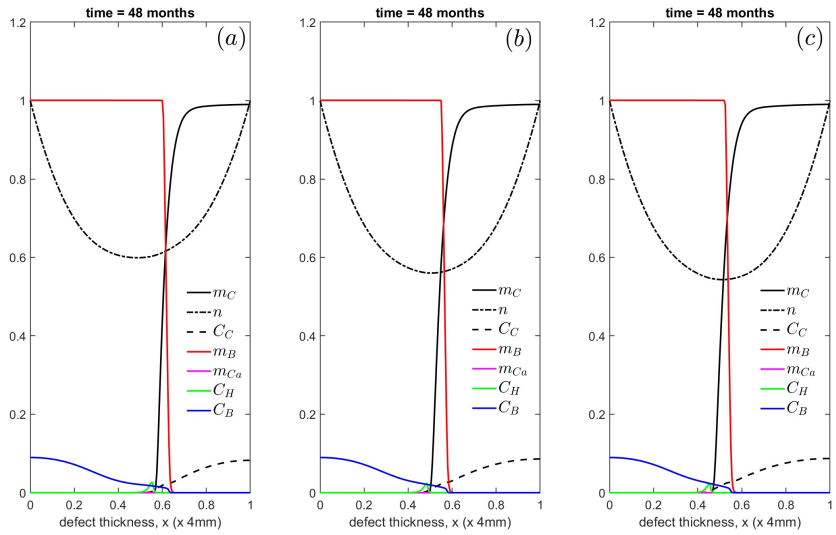

Figure 10: Cell and matrix densities for varying hypertrophy-suppressing signalling molecule diffusion coefficients, $\bar{D}_{g_{HS}}$, at $t = 48$ months. (a) $\bar{D}_{g_{HS}} = 0.5$ (baseline value), (b) $\bar{D}_{g_{HS}} = 1$ and (c) $\bar{D}_{g_{HS}} = 5$.

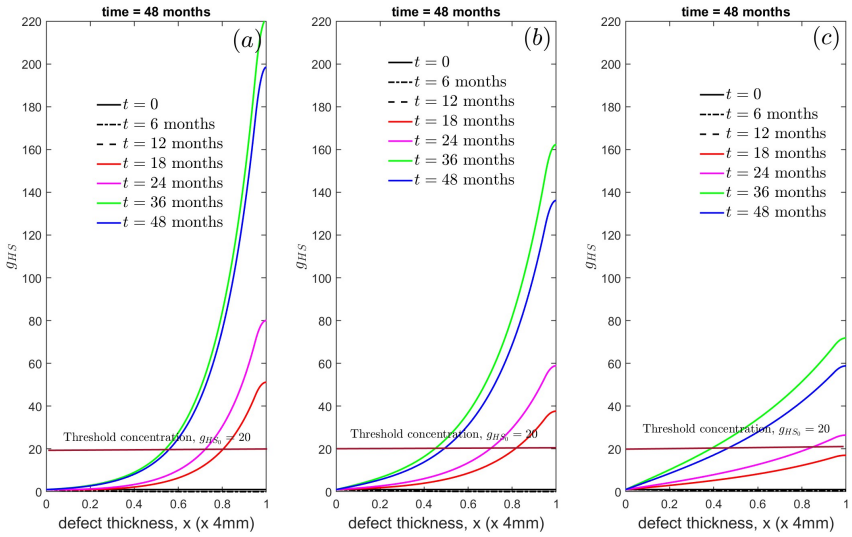

Figure 11: Evolution of g_{HS} for varying hypertrophy-suppressing signalling molecule diffusion coefficients, $\bar{D}_{g_{HS}}$, between $t = 0 - 48$ months. (a) $\bar{D}_{g_{HS}} = 0.5$ (baseline value), (b) $\bar{D}_{g_{HS}} = 1$ and (c) $\bar{D}_{g_{HS}} = 5$.

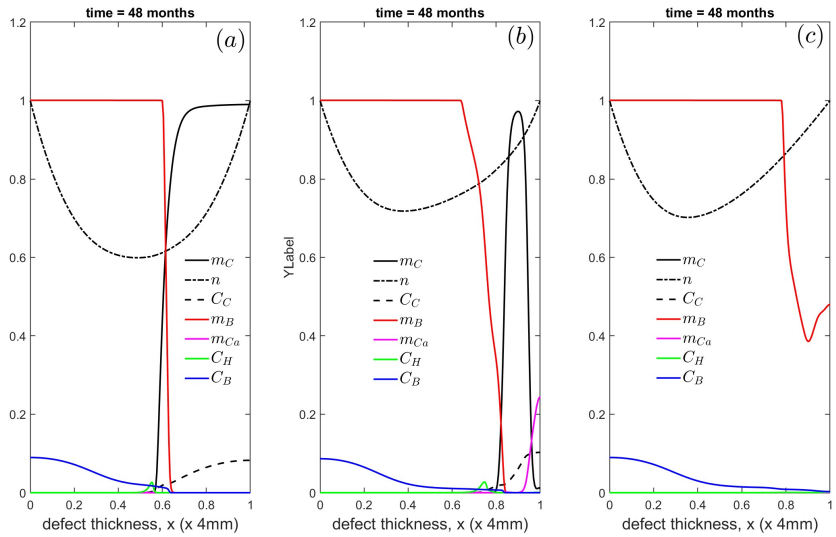

Figure 12: Cell and matrix densities at $t = 48$ months for varying g_{HS} flux via $\bar{\gamma}_1$ out of the top of the defect at $x = 1$. (a) $\bar{\gamma}_1 = 0$ (baseline value), (b) $\bar{\gamma}_1 = 10^2$ and (c) $\bar{\gamma}_1 = 10^3$.

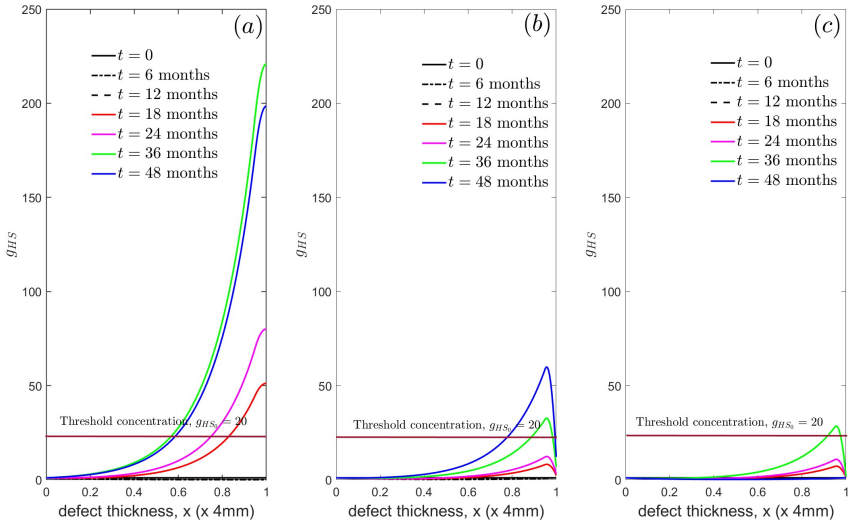

Figure 13: Evolution of g_{HS} between $t = 0 - 48$ months for varying g_{HS} flux via $\bar{\gamma}_1$ out of the top of the defect at $x = 1$. (a) $\bar{\gamma}_1 = 0$ (baseline value), (b) $\bar{\gamma}_1 = 10^2$ and (c) $\bar{\gamma}_1 = 10^3$.

the surface chondrocytes is not sufficient to overcome its degradation ($p_{22} = 15.47$), hence g_{HS} stays below the threshold value at all times (Fig. 15(a)) promoting hypertrophy and osteochondral ossification with bone filling-up the defect (Fig. 14(a)). Increasing $\bar{p}_{15}$ and $\bar{p}_{21}$ above a threshold value results in the production of g_{Hs} offsetting its degradation, allowing it to cross the threshold concentration to suppress hypertrophy and osteochondral ossification to form a cartilage layer at the top of the defect. Increasing (decreasing) the hypertrophy-suppressing signalling

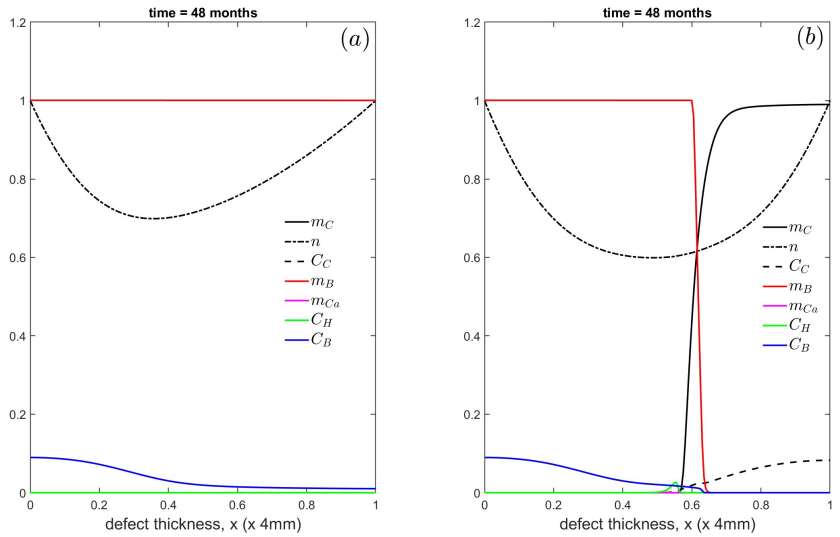

Figure 14: Cell and matrix densities for varying the hypertrophy-suppressing signalling molecule production rates by surface chondrocytes, $\bar{p}_{15}$ and $\bar{p}_{21}$, at $t = 48$ months. (a) $\bar{p}_{15} = \bar{p}_{21} = 10^2$ and (b) $\bar{p}_{15} = \bar{p}_{21} = 4 \times 10^4$ (baseline).

molecule degradation rate, $\bar{p}_{22}$, relative to p_{15} and p_{21} results in lower (higher) concentrations of $\bar{g}_{HS}$ within the defect. The results are similar to the behaviour observed in Figs. 14,15, hence we do not report them here in more detail.

Similarly, increasing (decreasing) the hypertrophy-modulating signalling molecule degradation rate, $\bar{p}_{26}$, results in lower (higher) concentrations of $\bar{g}_{HM}$ within the defect. This modulates the production of g_{HS} by surface chondrocytes. The behaviour is again similar to that shown in Figs. 14,15. Figures 16(a, b, c) show the cell and matrix densities at $t = 48$ months when varying the chondrocyte hypertrophic differentiation rate, $\bar{p}_6$. This parameter does not significantly influence the results, except a visible increase in C_H (Fig. 16(b, c)). Figures 17(a, b, c) show the cell and matrix densities at $t = 48$ months when varying the osteoblast proliferation rate, $\bar{p}_9$. Increasing $\bar{p}_9$ increases the bone cell density although the bone matrix density does not increase as much. Decreasing $\bar{p}_9$ results in less bone matrix due to lower bone cell density. Figures 18(a, b) show the cell and matrix densities at $t = 48$ months when varying the cartilage matrix degradation rate, $\bar{p}_{12_0}$. Increasing $\bar{p}_{12_0}$ results in rapid m_C degradation into m_{Ca}, although bone production remains relatively unchanged.Decreasing $\bar{p}_{12_0}$ leads to low m_{Ca} levels due to less cartilage degradation. The bone matrix levels remaining fairly unchanged since m_{Ca} conversion to m_B pathway is unaffected by varying $\bar{p}_{12_0}$.

Figures 19($a - d$) show the cell and matrix densities at $t = 48$ months when varying the calcified cartilage matrix degradation rate, $\bar{p}_{20}$. Increasing $\bar{p}_{20}$ enhances bone production, resulting in lower m_{Ca}, as bone remodelling is

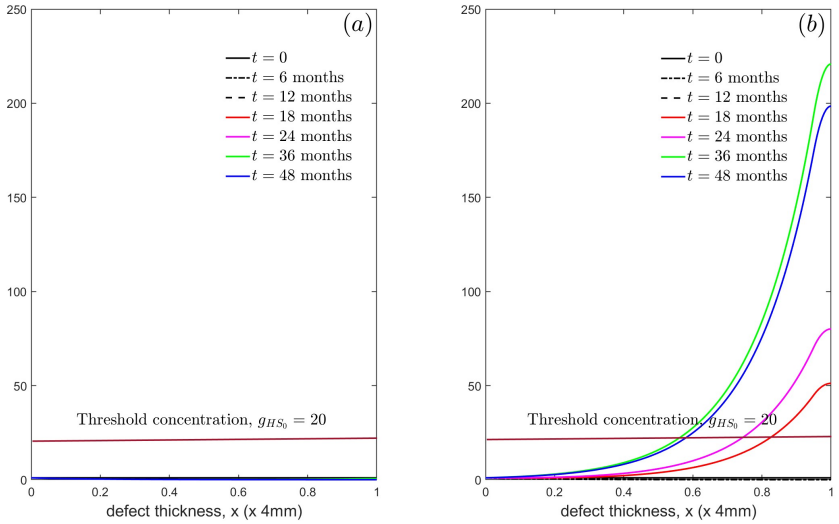

Figure 15: Evolution of g_{HS} for varying the hypertrophy-suppressing signalling molecule production rates by surface chondrocytes, $\bar{p}_{15}$ and $\bar{p}_{21}$, between $t = 0 - 48$ months. (a) $\bar{p}_{15} = \bar{p}_{21} = 10^2$ and (b) $\bar{p}_{15} = \bar{p}_{21} = 4 \times 10^4$ (baseline).

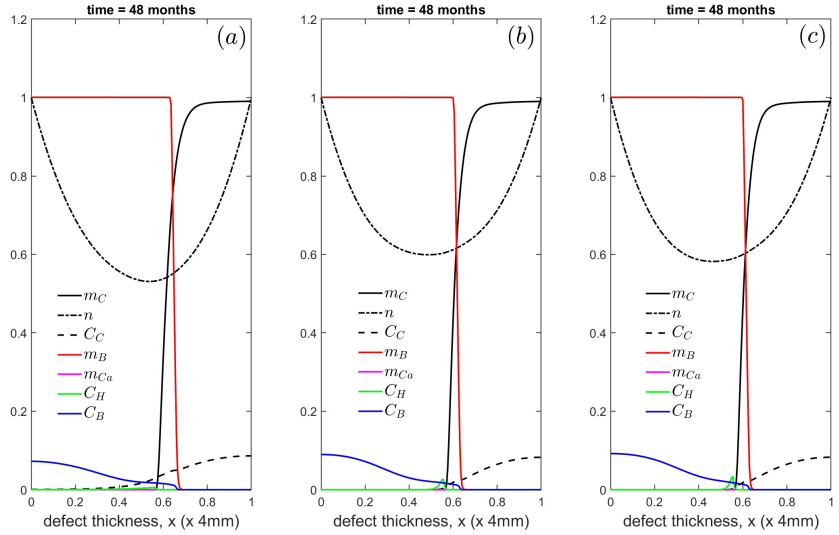

Figure 16: Cell and matrix densities for varying the chondrocyte hypertrophic differentiation rate, $\bar{p}_6$, at $t = 48$ months. (a) $\bar{p}_6 = 0.1$, (b) $\bar{p}_6 = 5$ (baseline) and (c) $\bar{p}_6 = 10$.

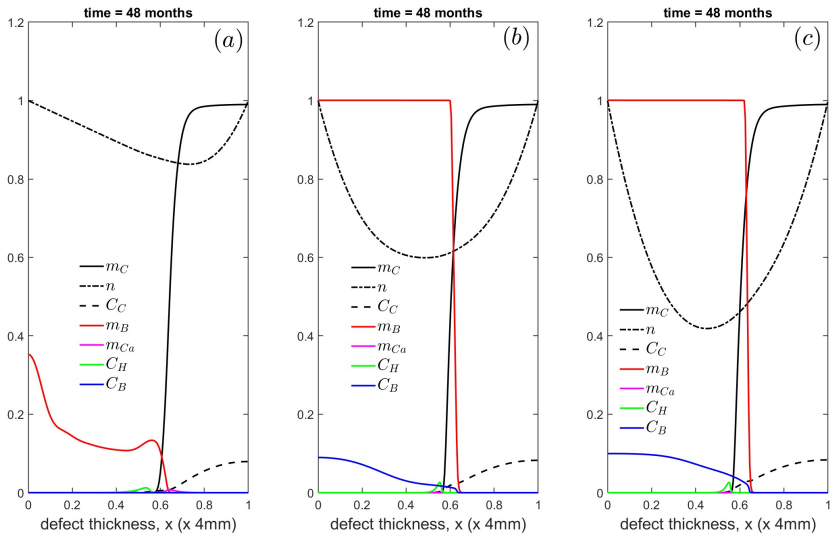

Figure 17: Cell and matrix densities for varying the osteoblast proliferation rate, $\bar{p}_9$ at $t = 48$ months. (a) $\bar{p}_9 = 10^{-3}$, (b) $\bar{p}_9 = 5.3 \times 10^{-2}$ (baseline) and (c) $\bar{p}_9 = 0.1$.

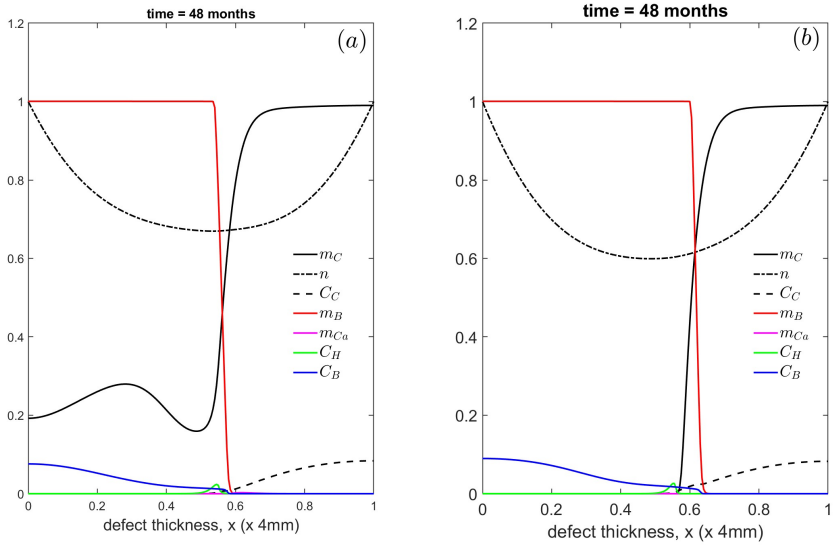

Figure 18: Cell and matrix densities for varying the cartilage matrix degradation rate, $\bar{p}_{12_0}$ at $t = 48$ months. (a) $\bar{p}_{12_0} = 10$ and (b) $\bar{p}_{12_0} = 10^4$ (baseline).

increased (Figs. $19(c,d)$). Decreasing $\bar{p}_{20}$ results in higher m_{Ca}, but bone matrix levels appear unchanged. In this case, bone is predominantly being produced by C_B. Figures $20(a,b,c)$ show the cell and matrix densities at

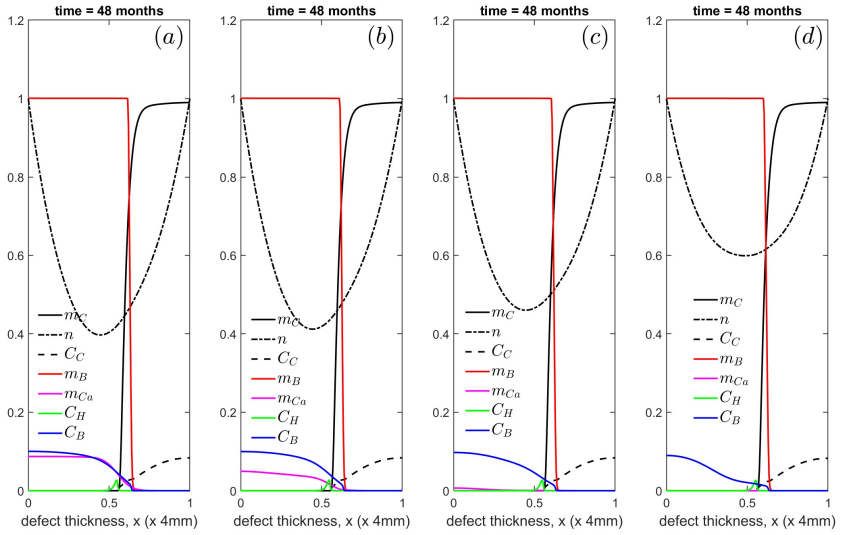

Figure 19: Cell and matrix densities for varying the calcified cartilage matrix degradation rate, $\bar{p}_{20}$ at $t = 48$ months. (a) $\bar{p}_{20} = 1$, (b) $\bar{p}_{20} = 10$, (c) $\bar{p}_{20} = 10^2$ and (d) $\bar{p}_{20} = 10^5$ (baseline).

$t = 48$ months when varying the chondrocyte proliferation rate, $\bar{p}_{5,C_0}$. For smaller values of $\bar{p}_{5,C_0}$, the proliferation of chondrocytes is not sufficient to trigger hypertrophy and osteochondral ossification, therefore the bone repair process is delayed (Fig. $20(a)$. In comparison, for larger values of $\bar{p}_{5,C_0}$, there is an adequate supply of proliferating chondrocytes to trigger the pathways for bone and cartilage production (Figs. $20(b,c)$. However, if $\bar{p}_{5,C_0}$ is very large then production of chondrocytes is also extremely high as observed in Fig. $20c$, which seems biologically unrealistic. Figures $21(a,b,c)$ show the cell and matrix densities at $t = 48$ months for varying the hypertrophic chondrocyte death rate, $\bar{p}_8$. Increasing $\bar{p}_8$ results in lower C_H levels as they degrade faster (Fig. $21(b,c)$), leading to less conversion of m_C to m_{Ca}. We observe slightly higher bone density at the base of the defect and more cartilage remaining in the defect. Decreasing $\bar{p}_8$ results in higher C_H levels and slightly higher m_{Ca}, but m_B appears unaffected.

5. Discussion

This paper aims to formulate a reaction-diffusion mathematical model describing the osteochondral defect healing process in large animals such as humans after ACI. The two specific questions to be addressed by the model are (a) Can the PTHrP-Ihh feedback loop control endochondral ossification in the healing process in large animals, and (b) Which key parameters most influence the healing process, in particular controlling the thickness of the articular cartilage in the repaired defect? Our model achieved the overall aim and simulated the key stages of natural osteochondral defect healing as observed in a large animal experiment, namely an initial fill of the defect by cartilage, followed by a process of endochondral ossification starting at the base of the defect that resulted in bone formation from the base upwards, eventually leaving a layer of articular cartilage at the top of the defect

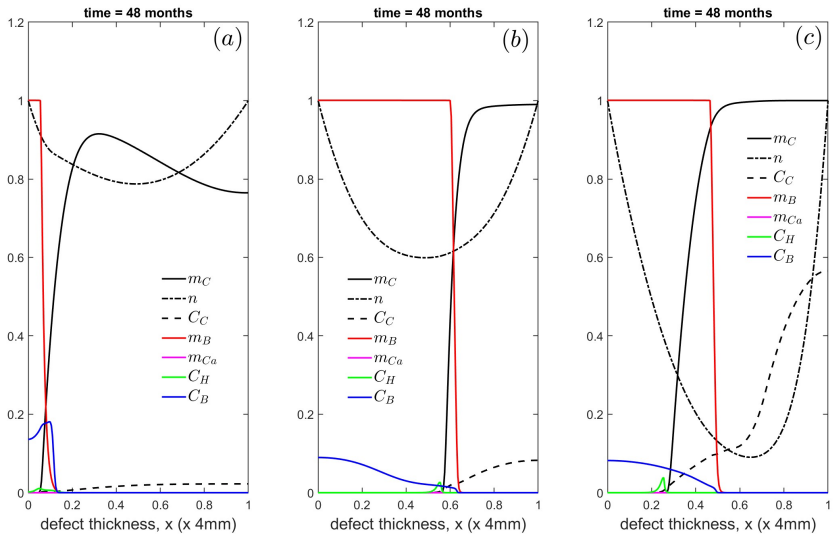

Figure 20: Cell and matrix densities for varying the chondrocyte proliferation rate, $\bar{p}_{5,C_0}$ at $t = 48$ months. (a) $\bar{p}_{5,C_0} = 10^{-3}$, (b) $\bar{p}_{5,C_0} = 0.012$ (baseline) and (c) $\bar{p}_{5,C_0} = 0.1$.

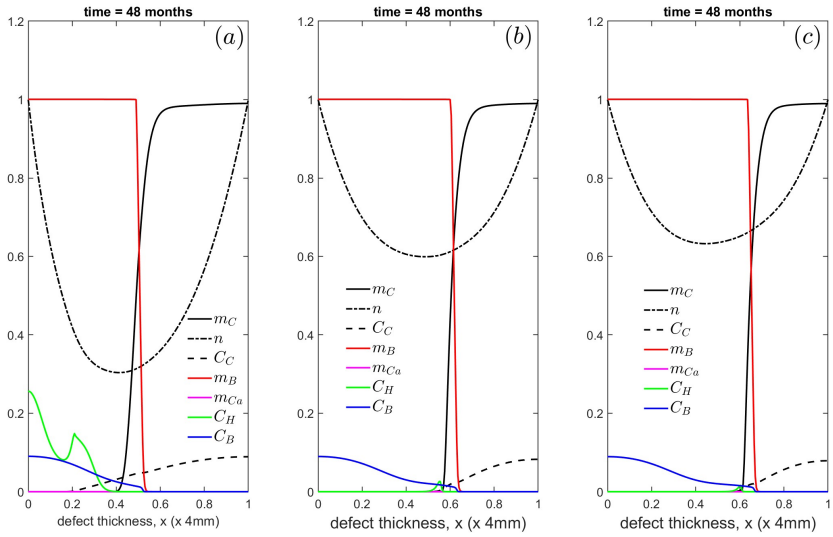

Figure 21: Cell and matrix densities for varying the hypertrophic chondrocyte death rate, $\bar{p}_8$ at $t = 48$ months. (a) $\bar{p}_8 = 0$, (b) $\bar{p}_8 = 0.5$ (baseline) and (c) $\bar{p}_8 = 1$.

separated from the bone by a thin layer of calcified cartilage (Lydon et al. (2019)). Our model thus demonstrates how an osteochondral defect, when treated by implanting chondrocytes under a patch covering the defect, heals in a way that bone and cartilage are regenerated. In doing so, the model therefore suggests that the PTHrP-Ihh feedback loop can indeed control endochondral ossification in large animals. The parameters most strongly influencing the healing process were the local factor relating to hypertrophy induction (critical cartilage density) and those related to the hypertrophy suppressing signalling molecule (PThRP), namely its baseline production rate and the modification of that production rate by the hypertrophy modifying signalling molecule (Ihh) and its surface flux.

In formulating our mathematical model, we made extensive use of the qualitative insights from a series of experiments based around an ovine model of natural osteochondral defect healing in skeletally mature animals (Lydon et al. (2019)). We did so for two main reasons. Firstly, the sheep is a relatively large animal with a knee anatomy comparable to that of humans, which makes this animal model closer to the clinical situation than for instance murine or laprine models (Ahern et al. (2009); Chu et al. (2010)). Secondly, Lydon et al. (2019) analysed 5 separate time points (1-2 weeks, 4-8 weeks, 8-12 weeks, 18 weeks and 26 weeks). Such a detailed study of the healing process over time is not uncommon when conducted using small animals (e.g. Shapiro et al. (1993); Anraku et al. (2008)), but is unique when conducted in large animals. Of course, we realise that the process by which a freshly created osteochondral defect naturally heals is not necessarily the same as that by which a clinical osteochondral defect in humans, treated using autologous chondrocytes, heals. Nevertheless, the key stages observed are also seen following chondrocyte implantation. Filling of the complete defect by cartilage or cartilage-like tissue, followed by bone forming from the base of the defect upwards, has been observed in large-animal models of ACI therapy (e.g. Munirah et al. (2007); Jurgens et al. (2013)). After one year, osteochondral defects up to 1 cm deep in humans and treated with ACI demonstrate new bone formation at the base and a layer of mature (hyaline) or immature cartilage at the top (Bentley et al. (2003)).

Our chondral defect healing models (Campbell et al. (2019a,b)) simulate the filling of a defect with cartilage, but do not simulate the conversion of cartilage into bone at the base of the defect. Lydon et al. (2019) observed that this process occurs via endochondral ossification, similar to the process observed during bone formation in the growth plate or during fracture healing. The current work therefore primarily focused on the endochondral ossification process. In this process, cartilage converts into bone via chondrocyte hypertrophy, where the hypertrophic chondrocytes form a primary spongiosa which is then invaded and remodelled by osteoblasts and osteoclasts (Lydon et al. (2019)). Crucially, not all chondrocytes hypertrophy and form primary spongiosa; a layer of hyaline cartilage is left in the top section of the defect, forming articular cartilage.

In our mathematical model we approached this by concentrating on key regulatory pathways that control chondrocyte hypertrophy during growth. Specifically, we concentrated on factors that initiate and suppress this process. Chondrocyte hypertrophy is known to be initiated by systemic factors (hormones) and locally produced signalling molecules (Mackie et al. (2011); Kozhemyakina et al. (2015)). The hypertrophy-inducing factor in our model represents the systemic factors, a prime example of which is thyroid hormone (Mackie et al. (2011)). We modelled these systemic factors as a flux coming in from the top and base of the defect. We assumed that this hypertrophy-inducing systemic factor would have to reach a threshold value before initiating hypertrophy. The local factors

were represented in our model as a critical or threshold cartilage density, below which hypertrophy is not initiated. This implementation of local factors is similar to that used in models of endochondral ossification during fracture healing (Carlier et al. (2016); Geris et al. (2008)). We chose the critical density to be around 95%, but also investigated other values in our sensitivity analysis. Both critical values would need to be reached before chondrocyte hypertrophy was initiated. In our model, the process was dominated by the local factor (critical cartilage density): once this density was reached, chondrocytes started to hypertrophy and produce calcified matrix from the cartilage model. These two processes would also halt local chondrocyte proliferation and cartilage matrix formation.

Further regulation of hypertrophy, once initiated, was implemented in our model as the Ihh-PTHrP pathway (Kronenberg (2003); Kozhemyakina et al. (2015)). The Ihh-PTHrP pathway is not only a key regulator of chondrocyte hypertrophy, but also important in relation to the question what controls the thickness of the eventual articular cartilage layer at the top of a healed osteochondral defect. PTHrP, a suppressor of hypertrophy, is produced by proliferating chondrocytes in the growth plate and restricted to chondrocytes in the superficial zone of articular cartilage (Chen et al. (2008); Jiang et al. (2008); Kronenberg (2003)). In articular cartilage, the primary regulation of PTHrP is in the form of mechanical loading (Chen et al. (2008)). Its production is also stimulated by Ihh, which is produced by pre-hypertrophic chondrocytes. In our model, we called Ihh a hypertrophy-modulating signalling molecule and assumed it would be produced by hypertrophic chondrocytes. To simulate the production of PTHrP specifically by superficial zone chondrocytes, we restricted its production to the upper 10% of the defect. The effects of PTHrP at the top of the defect were the main factor regulating the remaining cartilage layer. The hypertrophic chondrocytes produced calcified matrix, which then was converted to bone by osteoblasts and osteoclasts, simply referred to as 'osteoblasts' in our model. Finally, we assumed the underlying bone at the base of the defect and the surrounding synovial fluid at the top of the defect to provide nutrients within the model. This was unlike our previous mathematical model of a healing chondral defect treated by ACI, where we assumed the flux of nutrient from the base equals zero because subchondral bone is left intact in this treatment, preventing nutrient flow from the defect base.

In combination, this relatively simplistic approach captivates the key mechanisms driving osteochondral healing after ACI via an endochondral ossification-like process. Our model would not be valid for deep osteochondral defects where a bone-plug may be a more appropriate treatment strategy (de Windt and Saris (2014)). However, osteochondral defects with a bone defect up to 1cm in depth can be treated using cell therapy alone (Bentley et al. (2003)). Data from the German Cartilage Registry suggest that using cell therapy alone for osteochondral defects is indeed common practice: although over 60% of defects in this registry are osteochondral defects only 1 in 9 ACI cases use bone graft augmentation (Niemeyer et al. (2016)).

During the initial phase of regeneration, a purely chondral healing mechanism took place. These results corresponded to our chondral defect healing model (Campbell et al. (2019a,b)), with slightly improved matrix formation due to the nutrients available from the base of the defect. These models of chondral defect healing assumed no nutrients would flow in from the base, leading to a lack of nutrients constraining cell proliferation and matrix deposition. By 1 year, cartilage filled the osteochondral defect, with low-density cartilage matrix at the top of the defect and a high-density matrix covering the base. By 18 months the critical cartilage density required for initiation of chondrocyte

hypertrophy was reached at the defect base, initiating the conversion of cartilage to calcified matrix by hypertrophic chondrocytes followed by formation of bone. As time continued, cartilage continued to be converted into calcified matrix with bone subsequently being produced, progressing as a traveling wave upwards to the top. This pattern of conversion predicted by our model qualitatively mirrored the formation of bone and cartilage in sheep observed by Lydon et al. (2019). By 2 years the layer of cartilage that would remain at the top of the defect became more evident, with bone entirely covering the base of the defect and cartilage degradation to calcified matrix occurring in the midsection. This trend continued until 48 months, when the defect was entirely filled with new bone, aside from a section of calcified matrix and a thin layer of cartilage remaining at the top of the defect. The thickness of this layer was mainly regulated by the parameters related the the hypertrophy-suppresing signalling molecule (PThRP), in particular its production rate (partly influenced by Ihh), its threshold level and its leakage from the top of the healing defect into the synovial fluid.. Including a population of superficial zone chondrocytes (at $\bar{x}$=0.9-1) producing hypertrophy-suppressing molecules was based on experimental observations *in vitro* by Jiang et al. (2008) and *in vivo* by Chen et al. (2008), who found that superficial zone chondrocytes in articular cartilage produce PThRP, which suppresses mineralisation of chondrocytes in deeper zones. Chen et al. (2008) also showed that mechanical loading is an important regulator of PTHrP expression in articular cartilage, but this is something we did not consider here.

The main conclusion from this work is that the Ihh-PThRP feedback loop can play a role in osteochondral healing in large animals, and that the main determinant of the resulting cartilage is related to the hypertrophy-suppressing molecule PThRP. So far, research on the role of PTHrP in post-natal osteochondral healing has been restricted to transgenic mice, needed to visualise its expression levels Chen et al. (2008). However, with the recent rapid advance in spatial transcriptomic and proteomic profiling techniques Moffitt et al. (2022), studying the expression of PThRP should now also be possible in large animals.

The assumptions we made in this model do simplify the biological process occurring during osteochondral healing, potentially limiting conclusions we can draw from this work. An important factor we do not consider directly in our model is the influence of mechanical forces on cells, in particular on cell proliferation, differentiation and matrix synthesis, which earlier mathematical models suggest to be important in chondral defect repair (Lacroix and Prendergast (2002)). Mechanical loading is also thought to influence the patterns of endochondral ossification, specifically in the formation of long bones (Wong and Carter (1990)). However, by assuming that superficial zone chondrocytes produced a hypertrophy-suppressing signaling molecule (PTHrP), we did implicitly include the effect of mechanical loading. We also excluded the effects of other local signalling molecules, in particular the influence of the fibroblast growth factor (FGF18) and C-type natriuretic peptide (CNP), which together with PTHrP and Ihh control the initiation of hypertrophy, and insulin-like growth factor (IGF1), epidermal growth factor receptor (EGFR) and reactive oxygen species (ROS), which control the later phases of chondrocyte hypertrophy (Kozhemyakina et al. (2015)). We completely ignored the latter three and simply assumed that once initiated, chondrocyte hypertrophy would proceed autonomously. We consider this assumption justified in light of our main aim to capture the main characteristics of the repair process. Instead of FGF18/CNP signaling we used the critical cartilage density $m_{C,crit}$ as an extra local hypertrophy initiating factor, following earlier mathematical models of healing bone fractures

(Carlier et al. (2016); Geris et al. (2006)). Although this simplifies the model, the effect is probably similar. FGF18 and CNP have an antagonistic effect on chondrocytes, with FGF18 produced by superficial zone chondrocytes and maintaining chondrocyte proliferation versus CNP produced by proliferating and pre-hypertrophic chondrocytes. There is no feedback control between these two molecules and hypertrophy is assumed to start once CNP levels are high enough relative to FGF18 (Kozhemyakina et al. (2015)). Effectively, our model used cartilage density as a proxy for CNP concentration. Although modelling FGF18 and CNP separately might affect the results, the change is most likely minor due to the lack of feedback. Lydon et al. (2019)describe initial cartilage formation occurring at the top edges of the defect adjacent to damaged cartilage. The reason cartilage first forms here is unknown, but could possibly be related to chondrocytes attaching preferentially to damaged cartilage rather than bone. In our 1-dimensional model we had to omit this preferential attachment to top edges of the defect because these edges were not represented. This simplification meant we also did not include the invasion of cells from the sides of the defect. In addition, when an osteochondral defect is created, damaged blood vessels nested within bone at the site of the defect are damaged. These damaged vessels produce blood which coagulates and forms a fibrous clot within the defect. This fibrous clot will act as a nutrient source at the beginning of regeneration, as well as acting as a scaffold for cells to travel along. These functions of a clot were not explicitly modelled in our work, and neither was clot formation.

We also did not consider mesenchymal stem cells to be present in this model, despite their well-documented role in osteochondral defect healing (Madry et al. (2011); Farmer et al. (2001); Getgood et al. (2012)). Lutianov et al. (2011) explore the effects of autologous chondrocyte implantation (ACI) and articular stem cell implantation (ASI) in chondral defects, which are surgical procedures where either chondrocytes or MSCs are inserted into a defect with the hope to promote healing. In that work, despite MSCs achieving higher cartilage formation at early time, overall healing time did not significantly change (Lutianov et al. (2011)). In Campbell et al. (2019a,b), we explored the effects of signalling molecules on the chondral healing process, and also how a co-implantation of MSCs and chondrocytes could promote an earlier healing time. Our work demonstrated that within the first year an enhanced rate of healing was observed when a co-implantation procedure was carried out, with an increase of up to 136% at 3 months when compared with ACI cartilage healing alone, but despite this, an earlier healing time was not achieved; the conclusion of this work was that a co-implantation procedure could have benefits by allowing a patient to become mobile sooner after surgery. The consideration of MSCs in our model could lead to MSC differentiation into chondrocytes or osteoblasts and having trophic effects, requiring extra assumptions around the control of their differentiation into osteoblasts and the mutual effect of osteoblasts and MSCs. However, based on our models of co-implanting MSCs and chondrocytes, it is doubtful whether the effects on the amount of cartilage formation would be large. MSCs may also influence the healing environment via their production of paracrine factors such as transforming growth factor /*beta* (TGF/*beta*), insulin-like growth factor 1 (IGF1), and vascular endothelial growth factor (VEGF), among others, which may influence cell function and survival and subsequent tissue regeneration (Fontaine et al. (2016); Linero and Chaparro (2014)). It is thought MSCs may be most effective within tissue regeneration via their paracrine signalling, not their direct contribution to extracellular matrix production via differentiation to osteoblasts and chondrocytes. Based on the findings in Campbell et al.

(2019a,b) on the paracrine effect of MSCs, we think it is instructive to start the modelling process by including only chondrocytes and osteoblasts.

Finally, our 1-dimensional model may capture the essential features of osteochondral healing but it is probably too simplistic for proper parameter identification. We regard this model as a first step to get these essential features in place, but a comparison to animal or human experiments will probably require a geometrically more realistic model, for instance a 2-dimensional axi-symmetric model. Given the crucial importance of the hypertrophy-suppressing signalling molecule PThRP, further work should include determining its concentration or expression levels in large animal models. Thanks to modern spatial proteomic or transcriptomic techniques this should be feasible (Moffitt et al. (2022)).

In future work, the inclusion of the modulatory effects of MSCs via their paracrine signalling would more accurately simulate the cell environment, such as the chondrocyte-MSC interaction modulated by FGF-1 and BMP-2 modeled in Campbell et al. (2019a,b).

In conclusion, our mathematical model suggests that repair of osteochondral defects following chondrocyte implantation relies on endochondral ossification processes similar to the growth plate. The reaction diffusion-type model presented here is a first step towards better understanding of osteochondral defect regeneration after cell therapy techniques.

Declaration of Competing Interest

The authors declare that there are no known competing interests that could have influenced the work reported in this paper.

Acknowledgements

This work was a part of KC's PhD research at Keele University (Campbell (2019)) supervised by SN and JH-K. Kelly gratefully acknowledges financial support from Keele University. JH-K gratefully acknowledges financial support from the Medical Research Council (MR/L010453/1 and MR/N02706X/1) and Versus Arthritis (Grants 18480 and 21156).

Author Contributions

JH-K conceptualized the work. KC, SN and JH-K contributed to developing the mathematical model. KC performed the simulations, analysed the model output, and wrote the original draft of the manuscript. SN and JH-K contributed to reviewing and editing the draft. .

References

Ahern, B., Parvizi, J., Boston, R., Shaer, T., 2009. Preclinical models in single site cartilage defect testing: A systematic review. Osteoarthritis and Cartilage 17, 705–713.

Allen, K., Thoma, L., Golightly, Y., 2022. Epidemiology of osteoarthritis. Osteoarthritis and cartilage 30, 184–195.

Anraku, Y., Mizuta, H., Sei, A., Kudo, S., Nakamura, E., Senba, K., Takagi, K., Hiraki, Y., 2008. The chondrogenic repair response of undifferentiated mesenchymal cells in rat full thickness articular cartilage defects. Osteoarthritis and Cartilage 16, 961–964.

Bailón-Plaza, A., Vander Meulen, M., 2001. A mathematical framework to study the effects of growth factor influence on fracture healing. Journal of Theoretical Biology 212, 191–209.

Bentley, G., Biant, L., Carrington, R., Akmal, M., Goldberg, A., Williams, A., Skinner, J., Pringle, J., 2003. A prospective, randomised comparison of autologous chondrocyte implantation versus mossaicplasty for osteochondral defects in the knee. Journal of Bone and Joint Surgery 85, 223–230.

Biant, L., Bentley, G., Vijayan, S., Skinner, J., Carrington, R., 2014. Chondrocyte implantation in the knee for chronic chondral and osteochondral defects. The American Journal of Sports Medicine , 2178–2183.

Brittberg, M., 2008. Autologous chondrocyte implantation - technique and long-term follow up. Injury 39, 40–49.

Campbell, K., 2019. Mathematical modelling of cartilage and bone defect healing after cell implantation. Ph.D. thesis. Keele University.

Campbell, K., Naire, S., Kuiper, J., 2019a. A mathematical model of cartilage regeneration after chondrocyte and stem cell implantation - I: The effects of growth factors. Journal of Tissue Engineering 10, 2041731419827791.

Campbell, K., Naire, S., Kuiper, J., 2019b. A mathematical model of cartilage regeneration after chondrocyte and stem cell implantation - II: The effects of co-implantation. Journal of Tissue Engineering 10, 204173141982770.

Carlier, A., Brems, H., Ashbourn, J., Nica, I., Legius, E., Geris, L., 2016. Capturing the wide variety of impaired fracture healing phenotypes in neurofibromatosis type I with eight key factors: A computational study. Sci Rep. 7, 20010.

Chen, X., Macica, C., Nasiri, A., Broadus, A., 2008. Regulation of articular chondrocyte proliferation and differentiation by indian hedgehog and parathyroid hormone-related protein in mice. Arthritis and Rheumatism 58, 3788–3797.

Chu, C., Szczodry, M., Bruno, S., 2010. Animal models for cartilage regeneration and repair. Tissue Engineering Part B: Reviews 16, 105–115.

Dahmen, J., Lambers, K., Reilingh, M., van Bergen, C., Stufkens, S., Kerkhoffs, G., 2018. No superior treatment for primary osteochondral defects of the talus. Knee Surgery, Sports Traumatology, Arthroscopy 26, 2142–2157.

De Bari, C., Roelofs, A., 2018. Stem cell-based therapeutic strategies for cartilage defects and osteoarthritis. Current Opinion in Pharmacology 40, 74–80.

Einhorn, T., 1998. The cell and molecular biology of fracture healing. Clinical Orthopaedics and Medical Research 355, S7–S21.

Falah, M., Nierenberg, G., Soudry, M., Hayden, M., Volpin, G., 2010. Treatment of articular lesions of the knee. International Orthopaedics 34, 621–630.

Farmer, J., Martin, D., Boles, C., Curl, W., 2001. Chondral and osteochondral injuries. Clinics in Sports Medicine 20, 299–320.

Fasano, A., Herrero, M., López, J., Medina, F., 2010. On the dynamics of the growth plate in primary ossification. Journal of Theoretical Biology 265, 543–553.

Fontaine, M., Shih, H., Schäfer, R., Pittenger, M., 2016. Unraveling the mesenchymal stromal cells' paracrine immunomodulatory effects. Transfusion Medicine Reviews 30, 37–43.

Francis, K., Palsson, B.O., 1997. Effective intercellular communication distances are determined by the relative time constants for cyto/chemokine secretion and diffusion. Proceedings of the National Academy of Sciences 94, 12258–12262.

Garzón-Alvarado, D., García-Aznar, J., Doblaré, M., 2009. A reaction-diffusion model for long bones growth. Biomechanics and Modelling in Mechanobiology 8, 381–395.

Geris, L., Gerisch, A., Maes, C., Carmeliet, G., Weiner, R., Sloten, J., Oosterwyck, H., 2006. Mathematical modelling of fracture healing in mice: Comparison between experimental data and numerical simulation results. Medical and Biological Engineering and Computing 44, 280–289.

Geris, L., Gerisch, A., Sloten, J., Weiner, R., Oosterwyck, H., 2008. Angiogenesis in bone fracture healing: A bioregulatory model. Journal of Theoretical Biology 251, 137–158.

Getgood, A., Kew, S., Brooks, R., Aberman, H., Simon, T., Lynn, A., Rushton, N., 2012. Evaluation of early-stage osteochondral defect repair using a biphasic scaffold based on a collagen-glycosaminoglycan biopolymer in a caprine model. Knee 19, 422–430.

Gomoll, A., Filardo, G., Almqvist, F., Bugbee, W., Jelic, M., Monllau, J., Puddu, G., Rodkey, W., Verdonk, P., Verdonk, R., Zaffagnini, S., Marcacci, M., 2012. Surgical treatment for early osteoarthritis. part II. allografts and concurrent procedures. Knee Surgery, Sports Traumatology, Arthroscopy 20, 468–486.

Gotterbarm, T., Breusch, S., Schneider, U., Jung, M., 2008. The mini pig model for experimental chondral and osteochondral defect repair in tissue engineering: retrospective analysis of 180 defects. Laboratory Animals 42, 71–82.

Guo, X., Wang, C., Duan, C., Descamps, M., Zhao, Q., Dong, L., Lü, S., Ansleme, K., Lu, J., Song, Y., 2004. Repair of osteochondral defects with autologous chondrocytes seeded onto bioceramic scaffold in sheep. Tissue Engineering 10, 1830–1840.

Jackson, D., Lalor, P., Aberman, H., Simon, T., 2001. Spontaneous repair of full-thickness defects of articular cartilage in goat model: A preliminary study. Journal of Bone & Joint Surgery 83, 53–64.

Jiang, J., Leong, N., Mung, J., Hidaka, C., Lu, H., 2008. Interactions between zonal populations of articular chondrocytes suppresses chondrocyte mineralization and this process is mediated by pthrp. Osteoarthritis and Cartilage 16, 70–82.

Jung, M., Breusch, S., Daecke, W., Gotterbarm, T., 2009. The effect of defect localization on spontaneous repair of osteochondral defects in a gottingen minipig model: A retrospective analysis of the medial patellar groove versus the medial femoral condyle. Laboratory Animals 43, 191–197.

Jurgens, W., Kroeze, R., Zandieh-Doulabi, B., van Dijk, A., Renders, G., Smit, T., van Milligen, F., Ritt, M., Helder, M., 2013. One-step surgical procedure for the treatment of osteochondral defects with adipose-derived stem cells in a caprine knee defect: A pilot study. Bioresearch Open Access 2, 315–325.

Kelly, D., Prendergast, P., 2005. Mechano-regulation of stem cell differentiation and tissue regeneration in osteochondral defects. Journal of Biomechanics 38, 1413–1422.

Kelly, D., Prendergast, P., 2006. Predicting the optimal mechanical properties for a scaffold used in osteochondral defect repair. Tissue Engineering 12, 2509–2519.

Kerkhofs, J., Roberts, S., Luyten, F., van Oosterwyck, H., Geris, L., 2012. Relating the chondrocyte gene network to growth plate morphology: From genes to phenotype. PLoS ONE 7, 1–11.

Kiaer, T., Grønlund, J., Sørensen, K., 1989. Intraosseous pressure and partial pressures of oxygen and carbondioxide in osteoarthritis, in: Seminars in Arthritis and Rheumatism. Elsevier, pp. 57–60.

Kozhemyakina, E., Lassar, A., Zelzer, E., 2015. A pathway to bone: Signalling molecules and transcription factors involved in chondrocytes development and maturation. Development 142, 817–831.

Kronenberg, H., 2003. Developmental regulation of the growth plate. Nature 423, 332–336.

Lacroix, D., Prendergast, P., 2002. A mechano-regulation model for tissue differentiation during fracture healing: Analysis of gap size and loading. Journal of Biomechanics 35, 1163–1171.

Linero, I., Chaparro, O., 2014. Paracrine effect of mesenchymal stem cells derived from human adipose tissue in bone regeneration. PLoS ONE 9.

Lutianov, M., Naire, S., Kuiper, J., 2011. A mathematical model of cartilage regeneration after cell therapy. Journal of Theoretical Biology 289, 136–150.

Lydon, H., Getgood, A., Henson, F., 2019. Healing of osteochondral defects via endochondral ossification in an ovine model. Cartilage 10, 94–101.

Mackie, E., Tatarczuch, L., Mirams, M., 2011. The skeleton: a multi-functional complex organ. the growth pate chondrocyte and endochondral ossification. Journal of Endocrinology 211, 109–121.

Madry, H., van Dijk, C.N., Mueller-Gerbl, M., 2010. The basic science of the subchondral bone. Knee surgery, sports traumatology, arthroscopy 18, 419–433.

Madry, H., Grün, U., Knutsen, G., 2011. Cartilage repair and joint preservation: medical and surgical treatment options. Deutches Ärzteblatt International 108, 669–677.

Mariani, E., Pulsatelli, L., Facchini, A., 2014. Signaling pathways in cartilage repair. International journal of molecular sciences 15, 8667–8698.

Martin, R., Burr, D., 1984. Non-invasive measurement of lobg-bone cross-sectional moment of inertia by photon absorptiometry. Journal of Biomechanics 17, 195–201.

Moffitt, J.R., Lundberg, E., Heyn, H., 2022. The emerging landscape of spatial profiling technologies. Nature Reviews Genetics 23, 741–759.

Moyad, T., 2011. Cartilage injuries in adult knee: Evaluation and management. Cartilage 2, 226–236.

Munirah, S., Samsudin, O., Chen, H., Sharifah Salmah, S., Aminuddin, B., Ruszymah, B., 2007. Articular cartilage restoration in load-bearing osteochondral defects by implantation of autologous chondrocyte-fibrin constructs: An experimental study in sheep. Journal of Bone and Joint Repair - Series B 89, 1099–1109.

Niemeyer, P., Albrecht, D., Andereya, S., Angele, P., Ateschrang, A., Aurich, M., Baumann, M.and Bosch, U., Erggelet, C., Fickert, S.and Gebhard, H., Gelse, K., G¨unther, D., Hoburg, A., Kasten, P., Kolombe, T., Madry, H., Marlovits, S., Meenen, N., M¨uller, P., Nöth, U., Petersen, J., Pietschmann, M., Richter, W., Rolauffs, B., Rhunau, K., Schewe, B., Steinert, A., Steinwachs, M., Welsch, G., Zinser, W., Fritz, J., 2016. Autologous chondrocyte implantation (aci) for cartilage defects of the knee: A guideline by the working group. Clinical Tissue Regeneration" of the German Society of Orthopaedics and Trauma (DGOU). Knee 23, 426–435.

Nizak, R., Bekkers, J., de Jong, P., Witkamp, T., Luijkx, T., Saris, D., 2017. Osteochondral lesion depth on mri can help predict the need for a sandwich procedure. European journal of radiology 90, 245–249.

Obradovic, B., Meldon, J., Freed, L., Vunjak-Novakovic, G., 2000. Glycosaminoglycandeposition in engineered cartilage: Experiments and mathematical model. AIChE Journal 46, 1860–1871.

Okano, K., Tsukazaki, T., Ohtsuru, A., Namba, H., Osaki, M., Iwasaki, K., Yamashita, S., 1995. Parathyroid hormone-related peptide in synovial fluid and disease activity of rheumatoid arthritis. Rheumatology 35, 1056–1062.

Olsen, L., Sherratt, J., Maini, P., Arnold, F., 1997. A mathematical model for the capillary endothelial cell-extracellular matrix interactions in wound-healing angiogenesis. IMA Journal of Mathematics Applied in Medicine and Biology 14, 261–281.

Rayon, T., Stamataki, D., Perez-Carrasco, R., Garcia-Perez, L., Barrington, C., Melchionda, M., Exelby, K., Lazaro, J., Tybulewicz, V.L., Fisher, E.M., et al., 2020. Species-specific pace of development is associated with differences in protein stability. Science 369, eaba7667.

Rovensky, J., Kvetnansky, R., Radikova, Z., Imrich, R., Greguska, O., Vigas, M., Macho, L., 2005. Hormone concentrations in synovial fluid of patients with rheumatoid arthritis. Clin Exp Rheumatol 23, 292–6.

Shapiro, F., Koide, S., Glimcher, M., 1993. Cell origin and differentiation in the repair of full thickness defects of articular cartilage. Journal of Bone & Joint Surgery 75.

Wakitani, S., Goto, T., Pineda, S., Young, R.G. Mansour, J., Caplan, A., Goldberg, V., 1994. Mesenchymal cell-based repair of large, full-thickness defects of articular cartilage. Journal of Bone & Joint Surgery 76, 579–592.

Williams, J., Bush-Joseph, C., Bach, J., 1998. Osteochondritis dissecans of the knee. American Journal of Knee Surgery 11, 221–232.

Williams, R., Zipfel, W., Tinsley, M., Farnum, C., 2007. Solute transport in growth plate cartilage: In vitro and in vivo. Biophysical Journal 93, 1039–1050.

Wilsman, N., Farnum, C., Green, E., Lieferman, E., Clayton, M., 1996. Cell cycle analysis of proliferative zone chondrocytes in growth plates elongating at different rates. Journal of Orthopaedic Research 14, 562–572.

de Windt, T., Saris, D., 2014. Treatment algorithms for articular cartilage repair of the knee. towards patient profiling using evidence-based tools, in: Shetty, A., Kim, S., Nakamura, N., Brittberg, M. (Eds.), Techniques in Cartilage Repair Surgery. Springer, Berlin, Heidelberg, pp. 23–31.

Wong, M., Carter, D., 1990. A theoretical model of osteochondral ossification and bone architectural construction in long bone ontogeny. Anatomy and Embroyology 181, 523–532.

Wu, L., 2013. Mesenchymal stem cells as trophic mediators in cartilage regeneration. Ph.D. thesis. University of Twente.

Zhang, C., Wei, X., Chen, C., Cao, K., Li, Y., Jiao, Q., Ding, J., Zhou, J., Fleming, B.C., Chen, Q., et al., 2014. Indian hedgehog in synovial fluid is a novel marker for early cartilage lesions in human knee joint. International journal of molecular sciences 15, 7250–7265.

Zhang, Y., Wang, F., Tan, H., Chen, G., Guo, L., Yang, L., 2012. Analysis of the mineral composition of the human calcified cartilage zone. International Journal of Medical Sciences 9, 353–360.

Zhou, S., Cui, Z., Urban, J., 2004. Factors influencing the oxygen concentration gradient from the synovial surface of articular cartilage to the cartilage bone interface: A modelling study. Arthritis & Rheumatism 50, 3915–3924.